Studies of Protostars and Young Stellar Objects

A Thesis
submitted for the degree of
DOCTOR OF PHILOSOPHY

In
The Faculty of Science
Bangalore University
Bangalore

By
UMA GORTI

Indian Institute of Astrophysics
Bangalore 560 034
India

March 1996

Declaration

I hereby declare that the matter contained in this thesis is the result of the investigations carried out by me at the Indian Insitute of Astrophysics, Bangalore, under the supervision of Dr. H. C. Bhatt. This work has not been submitted for the award of any degree, diploma, associateship, fellowship, etc. of any university or institute.

Uma Gorti .

Uma Gorti

Candidate

H.C.Bhatt

H. C. Bhatt

Supervisor

Bangalore 560034
1996 March 26

Acknowledgments

I would like to thank my thesis supervisor, Dr. H. C. Bhatt for his guidance and support throughout the course of this work. He strongly encouraged me to think independently, and was always willing to discuss and clarify even my most trivial doubts. Working with him was a pleasure and has made my approach to a problem more objective.

Prof. Ram Sagar has been enormously kind and generous with counsel on all academic matters. I would like to take this opportunity to thank him for the keen interest he took in my work, and for the many stimulating discussions we have had.

Y.D. Mayya was a storehouse of information on a variety of subjects. He helped me start out in research, and I thank him for always being ready to explain whatever I did not understand. P. Bhaskaran initiated me into numerical computing and introduced me to some very good books. I would like to thank him for this and also for all his philosophical advice. I have also benefited greatly from discussions with Dr. S. Chatterjee.

I thank the Director, Indian Institute of Astrophysics, for all the facilities provided, which have made this research possible. The library staff at IIA have been very helpful, as have the computer personnel. I would especially like to thank Mr. J.S. Nathan for his patience and ready willingness to attend to any difficulties at the computer centre. I also thank Mr. B.A. Varghese for helping with the intricacies of LaTeX, and always answering those many Frequently Asked Questions.

I would also like to thank Prof. C.R. Rao of the Physics Department, Bangalore University, for all the help extended and for clearing all administrative formalities.

All of my friends at IIA have made working here an enjoyable experience, and I sincerely appreciate all that they have done. I would especially like to express my gratitude to my "batchmates"; they have contributed in their own ways towards making this thesis a reality. Annapurni Subramaniam, apart from being a good friend, was an excellent sounding board for many of my (sometimes wild) ideas. She and Eswar Reddy have been good critics, and have also borne the brunt of my ups and downs. I thank them both for this. Sujan Sengupta has helped greatly with bureaucratic and other matters, for which I am very grateful. Dipankar Banerjee has provided good company over the years. I have had many interesting discussions on academic and non-academic issues with Angom Dilip,

Sumit Banerjee and R. D. Prabhu. I thank them for relieving the tedium of work, and keeping my enthusiasm alive.

Nimisha Kantharia has been my good friend throughout and helped me through some rough patches. We've had some great times together. I have also had very stimulating discussions on "every topic under the sun" with Andal Narayanan, and a very free trade of books. Her infectious cheer and good humour have often lifted me out of a dark mood. C. Indrani has been a great friend, and is probably the most tolerant person that I've come across. I thank Nimisha, Jaya and Indrani — for everything.

Most of all, I would like to express my gratitude to my parents for their encouragement and support. The values they've inculcated in me, and their emphasis on the importance of "doing whatever you do, well" have been solely responsible for me getting this far. My brother, Srinivas, has been my guiding beacon through life, and I thank him, especially for the (long-distance) support these past few years. Lastly, I would like to thank my sister, Madhu, for all those innumerable things, including her critical reading of drafts of my thesis, and her own brand of wisdom.

Abstract

The star formation process in molecular clouds is an exceedingly complex phenomenon, with a strong radiative and dynamic coupling between the cloud gas and the forming stars at all stages. The focus of this thesis work is an investigation of star–cloud interactions, mainly on aspects pertaining to the influence of the star–forming environment on the early dynamical evolution of protostars and Young Stellar Objects (YSOs) embedded in molecular clouds. The study is conducted along the evolutionary sequence, from protostellar clumps to protostars and pre–main–sequence objects.

Molecular clouds are observed to have substructure within them, and to consist of dense condensations or clumps whose central cores eventually collapse to form stars. These high-density clumps are surrounded by a less dense interclump medium. The interclump gas can potentially retard the motion of the clumps in a cloud through drag caused by dynamical friction. The dynamics of an N–body system of protostellar clumps moving in the potential of the ambient gas and acted upon by dynamical friction is studied through numerical simulations. The clumps also accrete matter from the surrounding gas. The deceleration due to drag being mass–dependent, is greater for more massive objects which lose energy and angular momentum to settle in the central regions of the cloud. There is a clustering of high–mass clumps at the cloud centre and a radial mass segregation is established in the cloud. The timescale of the process (typically $\sim$ 1My) is governed by the cloud parameters, and is shorter for denser clouds. On postulating that the more massive protostellar clumps give rise to higher mass stars on collapse, it is suggested that the spatial segregation of mass seen in young protostar clusters is a result of the dynamics of the protostellar clumps from which they form. The dynamical evolution of a protostar cluster was also studied and it is found that dynamical friction acting on massive protostars themselves also leads to spatial mass segregation

on short timescales.

Star formation being an inherently inefficient process, only a small fraction of the cloud mass gets ultimately converted into stars. The dynamical evolution of an embedded protostar cluster is thus largely determined by the ambient gas and remnant clumps. The evolution of clumps and protostars is studied through N–body simulations. Mass segregation of the more massive clumps due to dynamical friction results in the formation of a dense central region, and the lower mass protostars are preferentially ejected out of the cloud via gravitational encounters. The protostellar cluster is found to expand gradually with time, forming an extended halo around the system. Halos of low–mass stars formed as a result of dynamical evolution, probably contribute significantly to the large halos of WTTS observed by the ROSAT all–sky survey around star–forming regions. The ejection of a significant fraction of protostars obtained in the numerical simulation is proposed as an explanation of isolated T Tauri stars, which are observed far from active star forming sites and in regions devoid of dense gas. The dynamical evolution of embedded protoclusters also holds interesting consequences for the star forming efficiency(SFE) of the clouds as the loss of low–mass protostars may imply a real SFE higher than that inferred from observations. On the other hand, the formation of a central concentration of the more massive protostars, may cause an increase in the "apparent" SFE and enable the formation of bound clusters, even if the overall SFE of the cloud is low.

The increasingly numerous discoveries of binary systems among pre–main–sequence stars have led to the inference that most stars form as binaries. The protostellar binaries remain embedded in the molecular cloud during the early phase of their evolution and suffer gas drag as they move relative to the cloud gas. The evolution of the orbital elements of the binary as a result of loss of angular momentum and energy, due to drag by ambient gas, is investigated by obtaining approximate analytical and numerical solutions of the relevant equa-

tions. Dissipation causes a decay of the orbit to smaller separations. Orbital decay thus provides a mechanism for forming close binaries from initally wide binaries. The observed frequency distributions with period for main–sequence and pre–main–sequence binaries are compared with statistically generated binary populations that are evolved in the presence of gas.

Stars that form from the protostellar clumps are surrounded by circumstellar disks of dust and gas, which absorb radiation of shorter wavelengths from the star, and re-radiate at longer wavelengths, predominantly in the infrared. The dust around the stars causes extinction and reddening of starlight and is an important tracer of the morphological features of the circumstellar environment. Some aspects of the circumstellar dust around the Herbig Ae/Be class of young, intermediate–mass stars, as inferred from photometric and infrared spectroscopic observations are studied. The photometric data in the UBVRI bands has been taken from the literature and the Low Resolution Spectra (LRS) obtained by the Infrared Astronomical Satellite are used where available. The photometric data are used to compute the colour excess ratios and thus study the wavelength dependence of extinction to these objects. The results imply the dominant presence of dust grains larger in size than the average dust grain in the interstellar medium. The dust spectral characteristics as revealed by the LRS, appear to depend on the spectral type of the central star and this is interpreted in terms of the chemical composition of the dust and the effects of stellar radiation. It is found that early type stars destroy the dust in their immediate environments.

The organisation of the thesis is as follows. A general overview of present–day star formation research—observations and theory, is presented in the first chapter. Chapter 2 describes the investigations carried out on the effects of gas drag on protostellar clumps in a cloud. Gas drag and the presence of clumps affect the dynamics of a young protocluster and the details of this investigation are given in Chater 3. The orbital evolution of pre–main–sequence binaries

in a cloud is discussed in chapter 4 and chapter 5 describes the work on the circumstellar dust around the pre–main–sequence Herbig Ae/Be stars. Finally, the conclusions of this thesis and scope for future research are presented in chapter 6.

Contents

Chapter 1

An overview of star formation

Stars are the major constituents of the visible universe. They form the basic structural units of galaxies and play a pivotal role in galactic evolution. Detailed studies, both observational and theoretical, have provided us with reasonable insight on the evolution of a star, the radiative and thermonuclear processes that go on in the stellar interior during various phases of its life, and the ultimate death of a star. The principal factor governing stellar evolution is now known to be the mass of a star. Higher mass-stars lead short, violent lives and enrich the interstellar medium with products of thermonuclear reactions. Lower mass stars undergo relatively quiescent stages of evolution over prolonged periods of time. Stellar masses are determined when they form, and the processes involved in the formation of stars have a direct bearing on further evolution of the star, the interstellar medium and the Galaxy itself. At the other extreme in scales, planetary system formation such as that of the sun, can be better understood by studying the formation and early evolution of stars. A study of star formation is, therefore, not only important in itself, but also essential because of the effects and consequences of the event. An understanding of the processes leading to the formation of stars is thus one of the fundamental problems of modern astrophysics.

The sites of star formation, at least in our Galaxy, appear to be huge clouds

of molecular hydrogen, the densest regions of which undergo gravitational collapse to form stars. Star formation is a complex physical phenomenon involving various processes such as gravity, turbulence and shocks, magnetic fields and other dynamical and radiative processes. The ranges of relevant physical parameters like density, mass and size, span many orders of magnitude with different processes gaining importance on different scales. The problem is further complicated by interactions of the newly-formed stars with their environment, through outflows, stellar winds and radiation. This affects subsequent star formation as the initial physical state of the system is altered. Star formation studies are also crucial in studying the evolution of the interstellar medium as associations of massive stars ionize the surrounding medium and finally even disrupt the parent molecular cloud. On the other hand, expanding shells driven by explosions of massive stars, may compress molecular gas and induce further star formation. Thus the star formation process is closely coupled to the formation and evolution of molecular clouds.

Stars form in a range of masses, with larger numbers of lower mass stars. High-mass and low-mass star-forming regions in the Galaxy appear to be spatially distinct, with both massive and low-mass stars being formed in the dense spiral arms and only low-mass stars being formed in clouds distributed throughout the galactic disk. This suggests a difference in formation processes involved in the two cases. The physical properties of the clouds which are capable of forming massive stars are known to be different from those of low-mass star-forming clouds. Recent observational studies indicate that massive-star forming clouds tend to produce stars in clusters or groups, whereas the low-mass star-forming clouds produce stars in relative isolation. Formation of massive stars in spiral arm regions which are denser has also led to the distinction between spontaneous and triggered star formation. Triggered star formation is induced in clouds which are rendered gravitationally unstable by external compression and hence collapse to form stars. On the other hand,

spontaneous star formation takes place without any external influence and is due to a dissipation of energy in the cloud, which ultimately collapses. An understanding of how stars form must thus essentially explain these different modes of star formation as well, apart from the basic processes that determine the collapse of the parent cloud. (*References on general reviews of star formation are listed at the end of the chapter, along with specific articles referred to in the course of the text*)

As stars form from the densest regions of molecular clouds and strongly interact with their natal environment, the formation and evolution of molecular clouds is central to a study of star formation.

1.1 Molecular Clouds

Molecular gas, predominantly made of hydrogen, constitutes about half the total mass of the interstellar medium in our Galaxy. The gas is concentrated in clouds and cloud complexes with masses upto more than 10^6 $M_\odot$. These cloud complexes are the most massive physical entities in the Galaxy. Most of the molecular cloud mass is confined to the spiral arm regions of the Galaxy, with a distribution of smaller, less massive clouds in the inter-arm regions. Molecular clouds are generally self-gravitating objects, i.e, they are bound by gravity. Observational studies indicate that the largest and most massive of these clouds are surrounded by extended envelopes of atomic hydrogen. As the hydrogen molecule does not possess a permanent electric dipole moment, it is not readily observed through its transitions. Observations of molecular clouds are generally made through collisional excitations of CO, the next most abundant molecule, with H_2. Other tracers of molecular gas include higher isotopes of CO, and molecules like NH_3, CS and HCN, which probe regions of differing physical conditions. Molecular clouds are highly structured objects and their masses, sizes and densities cover wide ranges in magnitude. All star

formation in our Galaxy takes place in the densest regions of molecular clouds. Reciprocally, most nearby molecular clouds harbour star-forming regions in their interior, though there appear to be a few clouds devoid of star-formation activity.

Giant Molecular Clouds and Dark Clouds Galactic molecular clouds are broadly classified as Giant Molecular Clouds (GMCs) and Dark Clouds (DCs). The two classes have different physical properties and occupy different spatial locations in the Galaxy. GMCs are typically warmer and more massive, with masses ranging from 10^5 to 10^6 $M_\odot$ and sizes of 20-60 pc. Examples of GMCs are the Orion Complex, W3 and M17. They are distributed along the spiral arms of the Galaxy and have typical lifetimes of about a few 10^7 years. The physical conditions in DCs are different from those in GMCs. They are less massive, with masses ranging from 10^3 to 10^4 $M_\odot$ and sizes of a few pc. They have lower temperatures and are distributed throughout the Galactic disk. Examples of Dark Cloud Complexes are the Taurus-Auriga Complex and the ρ Ophiuchus Complex. Star-formation activity in the two classes of clouds differs fundamentally in that the GMCs are *exclusive* sites of massive star formation. They also form low-mass stars prodigiously and all star-formation takes place in the dense core regions. Stars are formed in a clustered environment, i.e., groups of stars are formed in a star-forming event, rather than individually or in small numbers. In contrast, star formation in DCs is usually in loose associations or in an isolated mode. Moreover, DCs form *only low-mass* stars. These differences in the star-forming activity of GMCs and DCs are normally believed to reflect on the differing physical conditions prevalent in the clouds.

Cloud structure Observations indicate that molecular clouds are actually composite structures, composed of smaller units with masses 10^3 to 10^4 $M_\odot$. High-resolution observations of these sub-structures reveal further clumpiness on scales extending upto the smallest observable size. Thus it appears that

molecular clouds have substantial structure on scales from tens of parsecs to a few hundredths of a parsec, as seen from large scale maps of clouds with single dish telescopes and interferometric measurements. Gas distribution in molecular clouds is highly inhomogeneous, with clumps and filamentary structures on all scales (see Figure 1.1). For example, Orion A, a typical GMC, exhibits a complex structure extending over four orders of magnitude in scale. The gas is in dense clumps and filaments. Star formation activity in the cloud produces massive OB stars in associations which have strongly influenced the structure of the cloud, by creating cavities through outflows and winds. Thus there is structure from the largest to the smallest observable scale size. Dark clouds also exhibit a qualitatively similar hierarchical structure with denser sub-regions or clumps within the clouds. Star formation in DCs, produces low mass stars which are less destructive to their environment and these clouds are relatively less structured.

The presence of seemingly well-defined clumps in molecular clouds which contain a significant fraction of the total cloud mass, makes it imperative to understand the nature of these structures. One view holds that the clumps are stable physical entities which move in ballistic response to the other forces in the cloud. This is evidenced by observations of clouds, where the density enhancements are found well separated in position as well as velocity space, lending support to the notion that clumps are indeed individual objects. On the other hand, they may also be temporary fluctuations in a highly dynamic medium and part of an overall random fractal structure. The higher density regions are thus in pressure equilibrium with the environment. On the smallest scales, however, the high-density regions or cores are self-gravitating objects which may collapse to form stars.

Observations of CO lines in clouds show broad line wings which is often interpreted as due to the presence of a tenuous distributed component, called the inter-clump medium (ICM). The gas in the ICM is warmer and the clumps

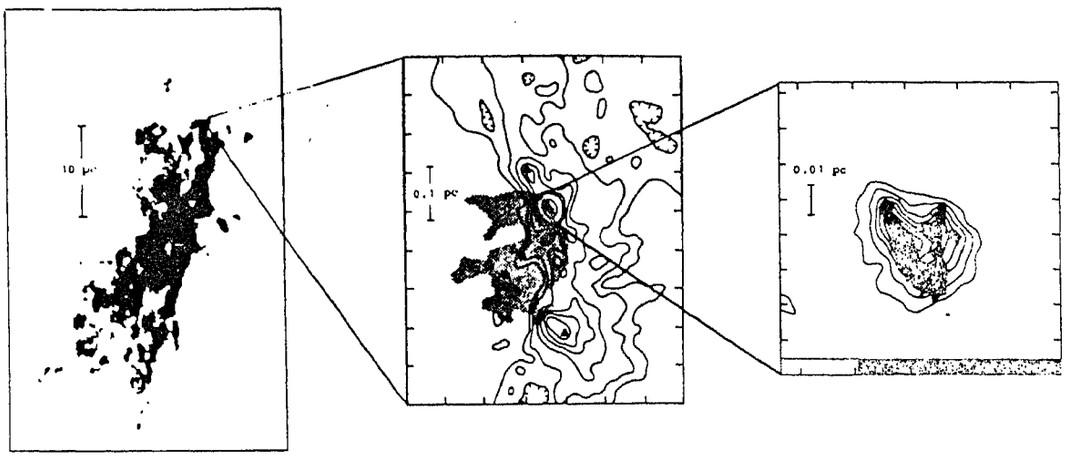

Figure 1.1: *Molecular line maps of Orion A over four orders of magnitude in spatial scale. The panel on the left is a ^{13}CO map of the cloud. The middle panel is a CS map of the OMC1 ridge. Asterisks mark the location of the Trapezium OB stars, and the shaded region is the the Orion A HII region. The panel on the right is a NH_3 map of the Orion-KL hot core. (adapted from Genzel 1991)*

are embedded in this medium. There is a large density contrast between the clumps and the ICM and ranges from $\sim$ 10 to $\sim$ 100 in most clouds. This contrast is larger for GMCs as compared to DCs. It also appears that most of the mass in GMCs is in the form of massive clumps, whereas the fraction of mass contained in the clumpy structures is lower in DCs.

Power-law relations and the mass spectrum of clouds The density of the cloud follows a power law distribution, with the central regions of the cloud being denser. The observed density distribution in clouds can be characterized by the relation $\rho(R) \propto R^{-1}$, on an average, for most clouds. R here

represents the linear extent, or, the size of the region being probed. The velocity dispersion of clouds ($\Delta\sigma$) as obtained from CO line observations is also correlated with the linear extent or size (R) of the cloud. This size-linewidth relation ($\Delta\sigma \propto R^{0.5}$) holds approximately well over a range of masses. The density and velocity dispersion scalings taken together, are often interpreted as a consequence of virial equilibrium of clouds. For clouds in virial equilibrium,

$$(\Delta\sigma)^2 \sim \frac{GM}{R} \sim \frac{G\rho(R)R^3}{R} \propto R,$$

which is the size-linewidth relation. Clouds and their constituent clumps (if considered self-gravitating) follow a power law spectrum in mass, with an exponent varying from 1.1 to 1.7. Thus the number of clouds/clumps within a mass interval is proportional to the power x of the mass, $dN(M)/dM \propto M^{-x}$. The exponent is found to have a typical value of $\sim$ 1.5, and holds over more than seven magnitudes of scale in mass, from the largest cloud complexes to the smallest cloud cores.

Stability of clouds Clouds and their constituent clumps are cold massive structures, which must lie on the verge of gravitational collapse. However, the star forming efficiency of clouds, or the fraction of total cloud mass that gets ultimately converted into stars, is found to be very small and of the order of a few % in the Galaxy. Also, though all Galactic star formation takes place in molecular clouds, all molecular clouds are not observed to contain star-forming regions. There is thus the problem of support of molecular clouds as, though their gravitational energy seems to exceed their thermal energy, they are not in free-fall collapse. Various mechanisms have been proposed for the support of clouds, which include magnetic fields, turbulence and rotation. Evidence for turbulence comes from the linewidths of CO lines, which indicate supersonic fluid motions within clouds. The velocities determined are approximately virial for measured masses and sizes of the clouds. The difficulty with supersonic turbulence is that in the absence of magnetic fields, it is highly

dissipative, because of the generation of shocks. The timescale for dissipation due to turbulence is short and of the order of the free-fall time or the collapse timescale. Thus, turbulent support of a cloud is not feasible unless it can be re-generated on a sufficiently short timescale. Clouds are observed to have sufficiently strong magnetic fields ($\sim$ 20 μG in GMCs) with a magnetic pressure comparable to the gravitational energy density. Interstellar polarization maps that trace the magnetic field structure in clouds, show that the field is relatively well ordered. Therefore, turbulence cannot be dominant over magnetic fields, as that would have led to a tangled configuration of field lines in the cloud. Magnetic fields are a possible attractive source of support for the cloud, as they appear to have the requisite energy and are not easily dissipated like turbulence. The observed broad CO line-wings can then be generated by non-linear Alfvenic waves. But however, magnetic fields cannot provide support *along* the direction of the field. Recent studies indicate that molecular clouds are in equipartition with approximately equal magnetic, kinetic and gravitational energies. It is now believed that a combination of magnetic, turbulent and rotational energies support molecular clouds against gravity.

Molecular clouds have substructure within them, and there is increasing evidence that the structure of clouds is hierarchical in nature, with the largest cloud complexes consisting of clouds with denser clumps and the constituent clumps further consisting of denser regions or cores and so on. The hierarchical structure is possibly due to a fragmentation process resulting from a gravitational instability. The densest of the cloud cores, formed from successive fragmentations, finally collapse to form stars.

1.2 Star formation in clouds

Observations of both GMCs and Dark Clouds indicate a spatial correlation between dense cloud cores and star formation sites, with young stars and star

clusters always being found in close proximity of the densest cloud regions. It is now well established that the collapse of the densest cloud cores leads to the formation of stars. The cloud core or clump is initially supported against gravity and collapses when it loses support through some dissipative mechanism. The condition for stability (of a thermally supported core of number density n and temperature T) is usually expressed in terms of a critical mass, called the Jeans mass, M_J, given by

$$M_J \approx 30\ M_\odot\ T^{3/2}\ n^{-1/2} \tag{1.1}$$

and represents a balance between thermal and gravitational energies. For masses greater than M_J, the cloud core is unstable to collapse. Similarly, a critical mass for cores supported by other means, such as rotation and/or magnetic fields can be obtained. The gravitational collapse of a core results in the formation of a young stellar object, which is ultimately supported by gas pressure. Clusters probably originate from the collapse of a single massive clump, which fragments during collapse to form a group of stars. The dichotomy in star formation between GMCs and DCs is presumed to arise from a difference in the initiation of collapse in the two cases. The star forming clumps or cores in GMCs are believed to be *supercritical*, i.e., far more massive than the critical mass described above. Collapse of massive clumps is thus rapid and fragmentation results in the formation of clusters and OB associations. Dark Cloud cores are significantly less massive and lose support against gravity rather gradually and on collapse, form low mass stars, either in isolation or in associations.

1.3 Protostar formation and evolution

As outlined above, the physical conditions of low-mass and high-mass star-forming regions differ and this has led to some distinctions between studies involving the formation and evolution of low and high mass stars. Massive

stars interact strongly with their environment through ionizing radiation and winds. They input enormous amounts of energy into their parent clouds affecting the local physical conditions, and hence affect subsequent star formation. Thermonuclear reactions begin in the central core region before the termination of the collapse phase, and the burning of hydrogen commences while the star is still enveloped in the parent cloud gas. They undergo rapid evolution, and the most massive stars explode as supernovae while within the cloud. Low mass stars, on the other hand, have longer evolutionary phases, and go through a distinct pre–main–sequence evolutionary phase, during which they are optically visible. They are more numerous, making them more amenable to observational studies.

1.3.1 Formation of low mass stars

The theory for the formation of a single low mass star has yielded a qualitative understanding of the different processes involved in the formation of an optically visible young star from the gravitational collapse of a cloud core (Shu et al 1987). Theoretical and observational studies indicate that the protostar passes through four distinct stages in its early evolution, summarized as follows. During the first stage, the cloud forms highly dense cores as it slowly loses support against gravity. The core then evolves into a gravitationally unstable object and collapses. Angular momentum is conserved during collapse and this results in the formation of a disk and a central condensation. The third stage is one of both accretion and outflow, as the central condensation or protostar grows in mass by accreting matter through the disk and at the same time also loses mass by ejecting matter out in the form of energetic bipolar outflows. The last stage reveals a protostar that radiates in the optical region. Accretion through the disk ceases and the end-product of star formation is a central young star with a circumstellar disk around it (see Figure 1.2). The term "protostars" is used to denote objects in the first two stages, whereas

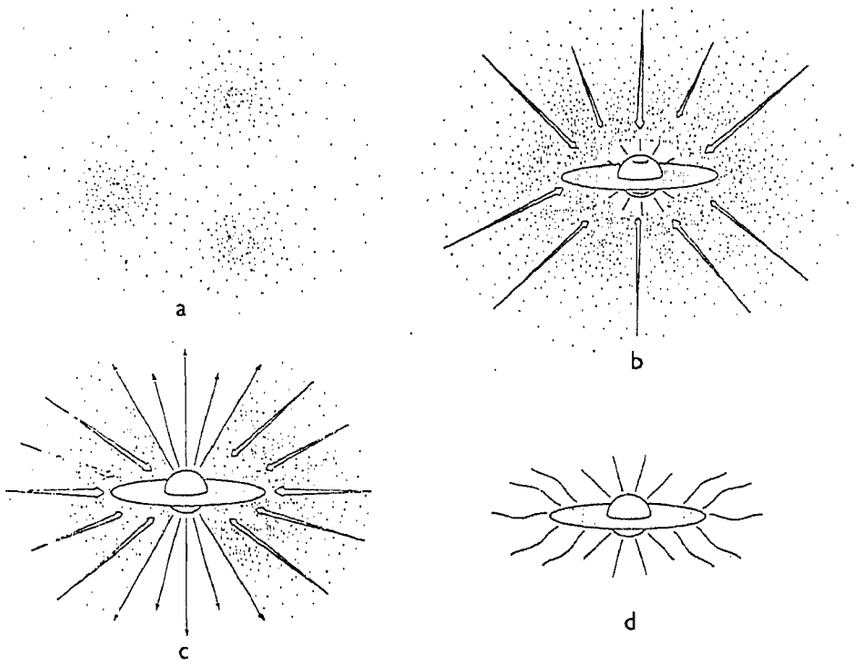

Figure 1.2: *The four stages in the formation of low-mass stars. (a) The cloud core formation. (b) The collapse of a core to form a central protostar and a disk. (c) The start of the outflow phase, during which the protostar also accretes through the disk. (d) The optically visible pre–main–sequence star with remnant disk. (Adapted from Shu et al 1987)*

those in the latter stages are usually termed as "young stellar objects" or YSOs. The latter group includes many classes of objects like T Tauri stars, Herbig Ae/Be stars, FU Ori stars and others.

Formation of dense cores For low-mass star-forming clouds, the predominant support mechanism which stabilizes the cloud against gravity is believed to be the magnetic field in the cloud. The primary component of the cloud is molecular hydrogen which is neutral and hence unaffected directly by the field.

The field affects the motion of only the charged particles, which are orders of magnitudes lower in number than the neutrals. Owing to the high densities in the cloud, collisional coupling between the ions and the neutrals is very effective and the field serves to constrain the motion of the neutral hydrogen molecules as well. Diffusion of the field over long timescales renders the cloud unstable to gravitational collapse and dense cores are formed. These cores now resemble isothermal singular spheres (with density profiles $\rho(r) \sim r^{-2}$) with only thermal pressure acting against gravity. For clumps with initial magnetic field energy densities exceeding the gravitational energy density (sub-critical clumps) diffusion of the field leads to the formation of a (slowly rotating) cloud core which gradually becomes denser and ultimately collapses. Clumps with higher gravitational energy, are unstable against collapse even in the presence of the field, and probably fragment in short timescales and form groups of stars.

Collapse of the dense core The dense core formed by dissipation as above, becomes dynamically unstable and collapes inside-out, i.e., the central region contracts faster than the envelope in a contraction wave that starts at the centre and moves outward as collapse progresses. The angular momentum of the cloud core which is conserved during infall, restricts collapse along the plane perpendicular to the rotation axis and this leads to the formation of a disk around the central condensation. The central regions of the core get denser as matter continues to fall inward both spherically and now primarily through viscous transport from the disk. The accretion disk is also substantially massive and both the central protostar and the disk emit strongly in the infrared region of the electromagnetic spectrum. Protostars in the late collapse phases are not visible in the optical region but are seen in the infrared largely due to re-radiation by dust in their envelopes. These are classified on the basis of their observed spectrum, as Class I protostars. The energy spectrum of Class I protostars is broader than a black-body spectrum and peaks in the far-infrared

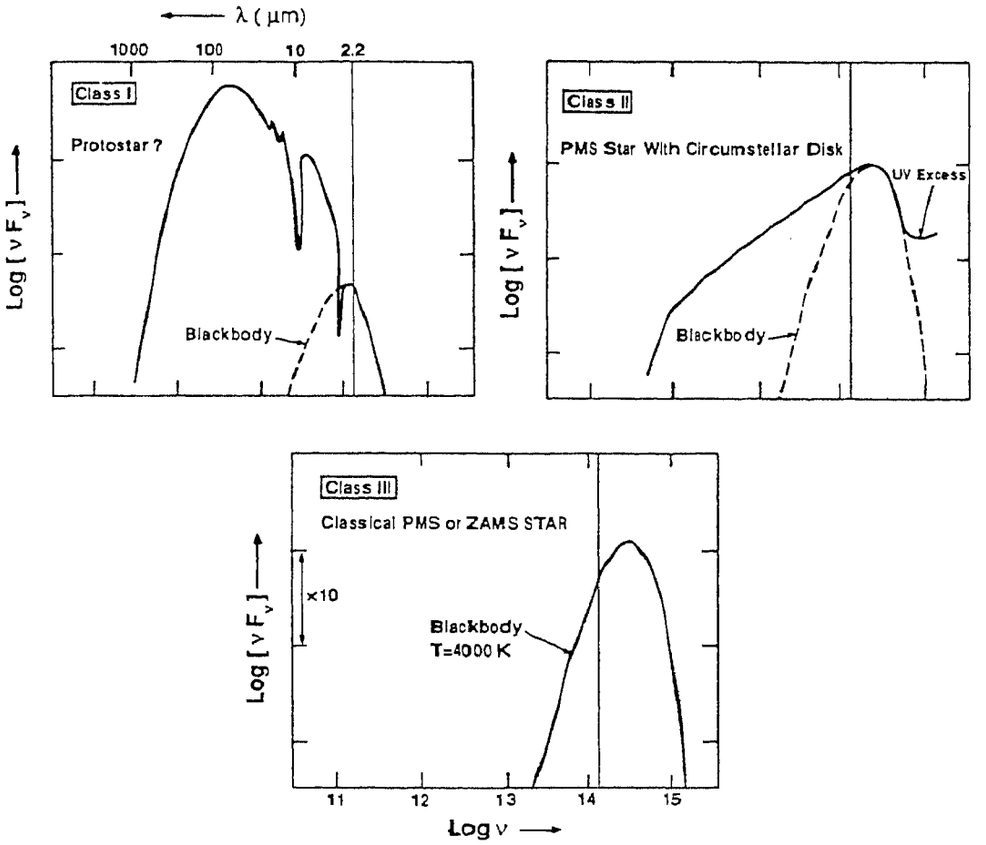

Figure 1.3: *The spectral energy distributions of different classes of low-mass protostars. (From Lada 1991)*

(Figure 1.3).

Outflow and accretion phase. The protostar gains mass via accretion through the disk and continues to collapse till the central region attains high enough temperatures to ignite thermo-nuclear reactions. Deuterium burning (in low-mass stars) starts at the centre and the overall contraction drives outflows and stellar winds which emanate from the disk and the protostar. During this phase, the star accretes mass from the disk and also loses mass through the outflows. The outflows are observed to be bipolar and are perpendicular to the disk, suggesting that they may be disk-driven. The outflow phase is

short-lived and typically lasts for about 10^4–10^5 years. The combined energy spectrum of the protostar and disk is again broader than the black-body spectrum and peaks now in the optical region. There is an excess of emission in the near-infrared and mid-infrared regions, and in some cases, a secondary peak in emission is seen. The protostar in this phase is classified observationally as a Class II object (Figure 1.3).

Pre–main–sequence star The bipolar outflow and stellar winds disperse the matter surrounding the star during the earlier stage. The outflow ceases and rate of accretion of mass through the disk decreases. Finally accretion stops and the disk re-radiates reprocessed light from the central protostar. The energy spectrum resembles that of a black body, with small excesses in the infra-red due to radiation from the circumstellar disk (Class III, Figure 1.3). The star now evolves along the pre-main–sequence, contracting slowly till it reaches the main-sequence and starts burning hydrogen in its centre.

1.3.2 Formation of massive stars

The clumps in a GMC fragment to form denser substructures with masses $\sim$ 3–100 $M_\odot$, which become gravitationally unstable. The individual fragments collapse to probably form a cluster of stars, with densities and temperatures changing over many orders of magnitude in $\sim$ a few 10^5 years. Theories of massive star formation identify three main evolutionary phases.

1. The first stage is the *isothermal collapse phase* during which the GMC core fragment undergoes free-fall collapse. The collapse is non-homologous, and the inner regions of the core have higher in-fall velocities. This leads to the formation of a central dense core in a few 10^5 years. The envelope is optically thin and the excess gravitational energy generated during contraction is radiated away. The central core is almost star-like with significant support from hydrostatic pressure, and increasingly becomes hotter

as it contracts. The temperature rises until thermal pressure becomes sufficiently high to temporarily halt collapse of the core.

2. The next phase is the *accretion phase.* Collapse of the central core ceases due to support from thermal pressure, whereas the envelope is still in free-fall collapse. The core now begins to accrete matter from the envelope and contracts as it grows in mass. The energy released via gravitational contraction continues to be radiated by the envelope. The contraction of the core takes place on timescales much longer than that of the outer regions, which are in free-fall. The core density and temperature continue to rise and are finally high enough to ignite hydrogen-burning. The processes that ultimately halt accretion are not well understood, and could be the onset of energetic stellar winds, radiation pressure on dust, etc.

3. The protostar probably reaches the main-sequence, i.e., begins burning hydrogen at the centre, before the termination of the accretion phase. The central star radiates strongly in the ultraviolet region of the spectrum and ionizes the gas surrounding it to form HII regions. During this early phase of evolution, the massive protostar is embedded deeply in the molecular cloud, and the ionized regions around them are much smaller and are termed Ultracompact (UC) HII regions. They have warm dust envelopes surrounding them and radiate predominantly in the far infra-red, with their spectra typically peaking around 100 μm.

These UC HII regions then expand later to form the classical HII regions seen around O and B type stars. The morphology of UC HII regions indicates the presence of bow shocks around most massive young stars. The circumstellar environment around a young massive star is depicted in Figure 1.4. An initially rotating cloud core must conserve angular momentum during collapse and this leads to the formation of circumstellar disks and associated outflows during the early evolution of the massive young star. Massive young stars, observed

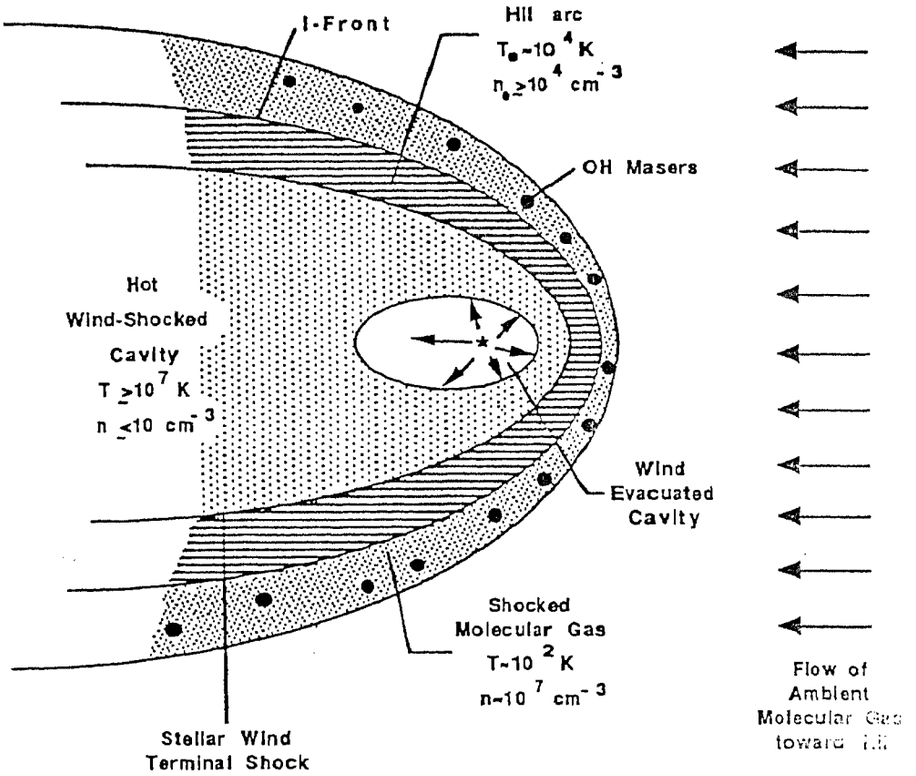

Figure 1.4: *A schematic diagram of the environment around a supersonically moving O star in a cloud, (from Churchwell 1991).*

usually as UC HII regions, are preferentially located in clusters and are to be found in the core regions of molecular clouds.

1.3.3 Formation of multiple systems and clusters

Star-forming regions in clouds are characterized by the presence of multiple systems or groups of stars. Young stars are always found densely packed in a clustered environment in GMCs. Star-forming regions in DCs like the Taurus-Auriga Complex, also appear to contain groups of stars in loose aggregates, which appear to be structured on larger scales. Isolated small dark clouds like

Bok globules, were earlier thought to contain single stars at their centres, but have now been found to harbour two or often more, low mass stars within them. Formation of groups or clusters of stars is now believed to be the outcome of collapse in all clouds, with single stars forming very rarely. This tendency for stars to form in associations appears to extend down to the smallest system of two stars – a binary. The ubiquitous discovery of binary systems among pre–main–sequence stars, with a frequency of occurence probably even larger than the $\sim 70\%$ found in main–sequence stars, stresses the importance of studying the formation of binaries in the parent cloud.

Binary formation A large fraction of stars, both young and old, are members of binary systems. Theories of binary formation aim to explain this basic observed datum, and others which include (a) the observed log-normal frequency distribution of orbital periods, (b) the mass ratios of binaries and (c) the distribution of eccentricities. The formation mechanism for binaries is not as well understood as that for single stars and various theories have been proposed. These include fragmentation of collapsing, rotating cloud cores to form multiple systems and gravitational instabilities of massive circumstellar disks which form companions. Fission of rapidly rotating protostars, tidal capture of a passing protostar induced via extended disks, and three-body captures are other mechanisms suggested for the formation of binaries (e.g., Bodenheimer 1992, Boss 1992, Mathieu 1994).

Cluster formation Formation of star clusters is generally attributed to fragmentation of the parent molecular cloud. Though this notion is widely accepted, the conditions in the cloud that induce fragmentation and other aspects of the process, such as, the masses of the stars formed and the star formation efficiency of the cloud are not well understood. The basic principle involved in fragmentation theories is a decrease in the Jeans mass (see Section 1. 2) once collapse has been initiated. A uniform density cloud is unstable to

perturbations on a lengthscale larger than a certain critical length

$$\lambda_J \sim M_J^{1/3} n^{-1/3} \sim T^{1/2} n^{-1/2},$$

and undergoes isothermal collapse. The increase in density (with temperature remaining constant) causes a decrease in the associated critical length and the collapsing cloud is unstable to successively smaller perturbations, leading to fragmentation. Recent refinements to fragmentation theory consider clouds with density profiles and effects of magnetic fields and rotation. The mass spectrum of open clusters is found to be similar to that for clouds, i.e., a power law with an index of ~ 1.5, lending support to the theory that clusters originate from the fragmentation of clouds or massive clumps.

The above sequence of events that lead to the formation of low mass stars and high mass stars is consistent with current observations and is generally accepted as a reasonable scenario for star formation. The details of the physical processes are however, not well known, and global aspects of star formation in the Galaxy are poorly understood. Most star formation, including the birth of low mass stars appears to take place in the clustered mode in massive-star forming GMCs, and a detailed picture of how stars form here is yet to emerge.

1.4 Cloud-star interactions

As stars form from molecular clouds, it is to be expected that the properties of the clouds themselves largely determine the nature of the star formation process as well as the nature of the stars themselves. The protostar remains embedded in the parent molecular cloud during its early evolutionary phase which typically lasts for a few 10^6 years. The star affects its environment through outflows, winds, and if massive, also through ionizing radiation and supernovae outbursts. Molecular outflows and stellar winds are believed to be

responsible for replenishing the turbulence in molecular cloud complexes on smaller scales. Associations of massive stars and clusters cause a large-scale expansion of the ambient gas through outflows and winds, and induce the formation of a range of structures, such as shells, tunnels, holes and filaments. Compression waves accumulate gas and form dense regions which in some cases may be unstable to gravitational collapse, thus leading to a triggered or induced star formation. Young stars inject energy and momentum affecting the structure and physical conditions of the cloud. Shock fronts driven into the gas ionize it and excite emission in globules, streamers, jets and emission knots called Herbig-Haro objects. Ultimately, the young stars disrupt the parent molecular cloud through their energetic evolutionary activity. Thus, star formation has a profound effect on the evolution of the cloud, eventually leading to its destruction.

Conversely, it is to be expected that *the presence of the gas will affect the evolution of the protostar* as well, through processes like accretion of matter and dynamical interactions. During the initial stages of collapse and during the wind and outflow phases, the protostar accretes matter from the surrounding gas and the accretion rate partly determines the mass of the star finally formed. The mass accretion rate is, in turn, dependent on the cloud conditions. The mode of star formation, clustered or isolated, triggered or spontaneous, and even the mass of the star appears to reflect the properties of the star-forming cloud as discussed in the beginning of this chapter. Further evolution of the protostar, once it has formed, is also expected to be affected by its surroundings. As the cloud is significantly more massive than the embedded protostar, one important source for interactions is the gravity of the cloud. Gravity plays an important role in the dynamics of the star-forming region and hence in the dynamical evolution of the protostars. This may, in fact, determine the most fundamental characteristic of a star, viz, its mass. The origin of stellar masses remains unknown, and a recent theory suggests that clump dynamics that re-

sult in the ejection of a protostar from its collapsing outer envelope may restrict the amount of matter accreted by it and hence its final mass (Podsiadlowski & Price 1995). Other possible gas-star interactions include collisions, ram pressure effects and gas drag (both hydrodynamical and due to dynamical friction) from the ambient medium. Furthermore, dynamical interactions between the protostars themselves and their disks are expected to significantly influence protostellar evolution. The physical conditions of the star-forming cloud and interactions with the environment thus largely determine the formation and early evolution of a young star.

This thesis considers some aspects of star-cloud interactions, with a view to understand the effects of the star-forming environment on the protostar in various stages of evolution. Interactions considered are mainly gravitational in origin.

References

Books:

- Physical processes in fragmentation and star formation, 1990, eds R. Capuzzo-Dolcetta, C. Chiosi & A. Di Fazio, Kluwer:Dordrecht
- Physics of star formation and early stellar evolution, 1991, eds. C.J. Lada & N.D. Kylafis, NATO ASI Series, Vol 342, Kluwer:Dordrecht
- Fragmentation of molecular clouds and star formation, 1991, eds E. Falgarone, F. Boulanger & J.L. Puget, Kluwer:Dordrecht
- Star formation in stellar systems, 1992, eds G. Tenorio-Tagle, M. Prieto & F. Sanchez, University of Cambridge Press:Cambridge
- Protostars and planets III, eds E.H. Levy & J.I. Lunine, 1993, University

of Arizona Press:Tucson

Articles:

Bodenheimer P., 1992, In "Star Formation in Stellar systems", eds G. Tenorio-Tagle, M. Prieto & F. Sanchez, University of Cambridge Press:Cambridge

Boss, A., 1992, In "Complementary approaches to double and multiple star research", IAU Coll. 135, p.195

Churchwell, E., 1991, In "Physics of star formation and early stellar evolution, eds C.J.Lada & N.D.Kylafis, Kluwer:Dordrecht

Genzel R., 1991, In "The Galactic Interstellar Medium", Saas-Fee Advanced Course 21, Springer-Verlag:Heidelberg

Henning Th., 1990, Fundamentals of Cosmic Physics, 9

Lada C.J., 1991, In "Physics of star formation and early stellar evolution, eds C.J.Lada & N.D.Kylafis, Kluwer:Dordrecht

Mathieu, R.D., 1994, Ann. Rev. of Astron. Astrophys., 32, 465

Shu F.H., Adams F.C., Lizano S., 1987, Ann. Rev. Astron. Astrophys., 25, 23

Podsiadlowski P, Price N.M., 1995, Mon. Not. Royal Astr. Soc., 273, 1041

Chapter 2

Protostellar clumps

2.1 Introduction

Molecular clouds form an important component of the interstellar medium in our Galaxy and account for a significant fraction of the total mass of interstellar gas. They cover a range of masses and sizes varying from the large Giant Molecular Cloud (GMC) complexes with masses of the order of 10^6 $M_\odot$ and sizes of 60 pc (e.g., W3, M17) to the smallest dark clouds of mass $\sim$ 10 $M_\odot$ and sizes of a few tenths of a parsec (e.g., TMC1, main core of B1). Observational studies of molecular clouds in the Galaxy and especially in the solar neighbourhood reveal a host of characteristic features, the most significant of which is that all star formation appears to take place in molecular clouds. Molecular clouds are gravitationally bound and their mass typically exceeds the Jeans mass by upto an order of magnitude. However all molecular clouds are not star-formation sites and even those that do form stars do not do so efficiently, converting only a small fraction of their mass into a stellar form. Any meaningful investigation of the star formation process must begin with an understanding of the molecular clouds, their structure, dynamics and evolution. It has been known since long that molecular clouds have substructure within them, as large scale maps and interferometric observations

in the radio and millimetre wave regions reveal clumpy structures within the clouds on all observable scale sizes, from a few hundredths of a parsec to tens of parsecs (see e.g. Wilson & Walmsley 1989). The gas distribution is highly non-uniform with spatially separated dense condensations in a ubiquitous less dense medium (e.g., Bally et al 1987). However, the exact physical nature of these "clumps" is as yet uncertain. They have been interpreted as temporary fluctuations in density caused by supersonic turbulence within the cloud (Falgarone & Phillips 1990, Scalo 1990). This view is supported by the apparent fractal nature of molecular clouds, which seem to show the same structure on smaller scales, traced by high density tracers and high resolution observations (Falgarone et al 1991). The other interpretation is that the clumps represent stable physical entities as they are well separated in position and velocity space as observed by molecular line spatial maps and velocity channel maps or position-velocity diagrams (see Blitz & Stark 1986, Stutzki & Gusten 1990). The large density contrast between the clumps and the medium in between them and the observations of the association of young stellar objects with dense clump cores (Beichman et al 1986, Tatematsu et al 1993), favours the notion of clumps being distinct physical objects. Here, we adopt the latter view that these clumpy structures are actual mass concentrations. The densest of these structures (the protostellar clumps), upon gravitational collapse, would in fact give rise to the formation of stars. The existence of an "interclump medium" or ICM is inferred from the broad linewings on CO maps. The interclump medium is believed to consist of both molecular and atomic hydrogen, as evidenced by the presence of HI envelopes around GMCs, in varying fractions in different clouds (e.g., Blitz 1991). However, the nature of the ICM is not clear, and may consist of a relatively homogeneous substrate or may also be clumpy with small density enhancements (Falgarone et al 1991). Here we assume that the ICM is homogeneous on length scales smaller than the clump size.

Observations of both the warm GMCs (e.g., Orion A,B) and the cold dark

clouds (e.g., Taurus) indicate that star forming regions are often found to be in the close vicinity of the dense cloud cores, suggesting that stars form in the most dense areas of molecular clouds (Myers 1987, Lada 1990). The density contrast between the clumps and the ambient interclump medium is found to vary from cloud to cloud. Clouds that form massive O and B type stars, i.e., the warm and dense clouds have a large clump to interclump density contrast while this is smaller for the low mass star-forming dark clouds (Blitz & Stark 1986, Falgarone & Puget 1988). Observations seem to imply a ratio of about 10 to 100 for most clouds and it appears that molecular clouds consist of self-gravitating clumps with a relatively large density compared to the surrounding medium. As clumps or possibly sub-structures within them seem to be the immediate precursors of stars, or at the least, active star-formation sites within the molecular clouds, a complete understanding of star formation and associated features like the initial mass function, rates and efficiency of star formation in galaxies, can be achieved only through a study of molecular clouds on all levels of hierarchy, from the huge complexes to the smallest cores, and the physical processes that determine their evolution. The dynamical evolution of the clumpy structures in molecular clouds is of special relevance to the spatial aspects of the star formation process, as stars presumably form here and are affected directly by the dynamical history of the clumps/cores from which they form.

The CO line widths in molecular clouds are invariably larger than the thermal line widths, implying supersonic velocities which are typically of the order of a few kms^{-1} (e.g. Blitz 1991). Observations indicate that clouds on large scales are in virial equilibrium and the larger clumps within them satisfy various scaling laws, such as mass-size ($M \propto R^2$), density-size ($\rho \propto R^{-1}$) and size-velocity dispersion ($\Delta v \propto R^{0.5}$) laws (e.g. Larson 1982, Elmegreen 1985). However the more dense protostellar clumps that are gravitationally bound would be more compact than these scaling laws indicate.

The motion of the clumps through the interclump medium has potentially interesting consequences brought about by the interaction of the dense condensations with the ambient gas. The clumps may accrete matter from the gas while moving through it, and also experience drag forces which decelerate them. The effect of drag due to dynamical friction on newly formed stars while still embedded in their parent clump(s) has been discussed qualitatively by Larson (Larson 1990) and Bally & Lada (Bally & Lada 1991). Larson (1990) discussed the possible effects of gas drag on embedded protostars in a cloud, and suggested that it may lead to a central concentration of massive stars in clouds. Bally and Lada (1991) suggested that in very dense massive cores of clouds, stars moving through the gas could cause 'cluster compactification' on a cloud crossing time scale, leading to locally greater concentration of mass in stars.

In the present work , we have carried out (Gorti & Bhatt 1995) a detailed numerical investigation of the effects of dynamical friction on the motion of dense protostellar clumps in molecular clouds. In addition to the frictional forces, the gravitational potential due to the gas and clump-clump interactions have been included. Physical parameters of molecular clouds such as size, mass, density, temperature etc. have been chosen to comply with observed values of these parameters. Dynamical friction acting on a clump causes a deceleration which depends on the mass of the clump, as the force arises from a second-order effect, and hence the dynamics of the clumps are likely to differ with their mass. Consequently, mass segregation is established in the cloud with a tendency for the more massive clumps to be located more centrally with respect to the cloud. The time evolution of such a cloud system will reflect in its physical properties and may also affect physical processes occuring in the cloud. The mass spectrum of clouds and clumps is observed to follow a power law ($dN/dM \propto M^{-x}$, where dN is the number of objects with mass between M and $M + dM$) over a range of masses spanning more than five

orders of magnitude, with the index x varying from about 1.1 to 1.7 in various cases (e.g., Bhatt et al 1984, for Dark Clouds; Sanders et al 1987, for GMCs; and also Genzel 1992). Protostellar clumps undergoing collapse and on their way to forming stars may have steeper mass spectra with a final stellar mass spectrum index of 2.35 (the Salpeter value). We have varied the power law exponent within this range and investigated any possible dependence of the dynamics of the system on the mass spectrum. Apart from dynamical effects, changes caused in the density distribution of the initial system are examined. Possible repercussions of the end state of the system on the star formation process are also discussed.

2.2 The physical model and analysis

In our study of the dynamics of clumps within molecular clouds, we adopt the following simplifying assumptions. A molecular cloud is presumed to consist of two distinct components, one being the high density clumps and the other the tenuous interclump medium (hereafter abbreviated as ICM). The volume filling fraction for clumps in a molecular cloud (the fraction of total cloud volume occupied by clumps), derived from the average densities of the clumps and the entire cloud, is generally of the order of a few % (e.g. Blitz & Thaddeus 1980, Perault et al 1985) or much less (Falgarone & Phillips 1991). In view of these observational facts, we believe that our assumption is not too unrealistic. The clumps have therefore been modeled as spherical particles moving through a fluid. This implies that the density falloff between the clumps and the ICM in our treatment is much sharper than what is observed.

The cloud is assigned spherical symmetry for simplicity and two states for the gas distribution are considered, one of uniform density and the other a Plummer density profile (cf Lada, Margulis & Dearborn 1984). For a Plummer distribution, the gravitational potential and the density are given by (Plummer

1911)

$$\Phi(r) = \frac{\Phi_o}{(1+(r/r_o)^2)^{1/2}} \quad , \quad \rho(r) = \frac{\rho_o}{(1+(r/r_o)^2)^{5/2}} \tag{2.1}$$

where r is the distance from the centre of the cloud and r_o the width of the distribution, (here chosen equal to the cloud radius). Apart from providing a source of gravitational potential, the ICM also retards the motion of a clump through gas drag due to dynamical friction.

2.2.1 Dynamical friction

The motion of a test particle through a gravitating medium is affected by interactions with the field particles constituting the medium. The test mass experiences an average force due to (many) long-range encounters and a fluctuating force due to the nearest particles. For a continuous medium, the average force is greater in magnitude and the test mass is subjected to collective effects of many small deflections from its original motion. The test particle moving through the medium gravitationally interacts with the field particles and deflects their orbits towards itself. The average density behind the test mass is thus slightly greater than along its direction of motion. This causes an excess gravitational force that acts to retard the motion of the test particle. This retardation is called *dynamical friction* (Chandrasekhar 1943). For a background medium with a Maxwellian distribution of velocities with dispersion σ, the dynamical friction force is given by (Binney & Tremaine 1987)

$$\mathbf{F}_{\rm DF}(r) = \frac{-4\pi\, ln\Lambda\, G^2\rho(r)M^2}{v^3}\left[erf(X) - \frac{2X}{\sqrt{\pi}}e^{-X^2}\right]\mathbf{v} \tag{2.2}$$

where v is the test particle velocity, G the gravitational constant, M the mass of the particle, ρ the density of the medium and ln Λ the Coulomb logarithm, where Λ is equal to the ratio of maximum to minimum impact parameters. X is a dimensionless parameter equal to $v/(\sqrt{2}\sigma)$. Figure 2.1 shows the force plotted against the parameter X. For small velocities, i.e., $v \ll \sigma$, dynamical friction increases proportional to the velocity. For large velocities, i.e., $v \gg \sigma$,

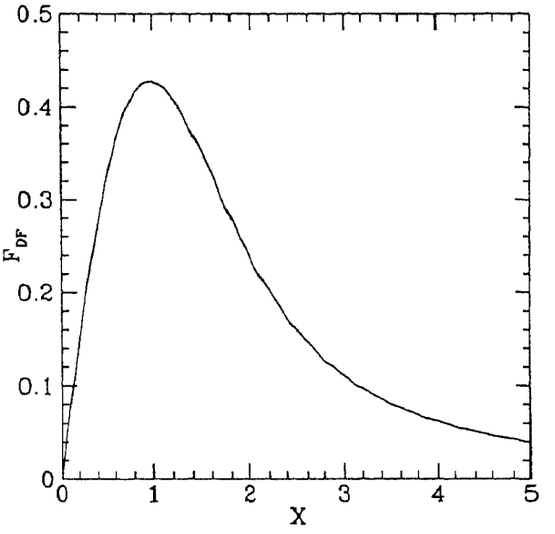

Figure 2.1: *The dynamical friction force is plotted against the dimensionless parameter* $X = v/(\sqrt{2}\sigma)$, *in scaled units.*

the dynamical friction decreases with velocity as relatively rapidly moving objects have fewer encounters and less time for perturbing the background. Dynamical friction acting on such objects causes their motion to be dragged over longer timescales. The drag timescale $\tau_{\rm drag}$ can be approximated as

$$\tau_{\rm drag} \sim \left|\frac{v}{dv/dt}\right| \simeq \frac{v^3}{4\pi ln\Lambda G^2 M\rho\,[erf(X) - 2Xe^{-X^2}/\sqrt{\pi}]} \qquad (2.3)$$

Deceleration is faster for more massive objects as $\tau_{\rm drag}$ is inversely proportional to mass. This is to be expected as dynamical friction is a second order effect arising from the gravitational pull of the density enhancement in the wake of the moving mass. More massive particles exert a stronger gravitational influence on the surroundings and hence cause larger density asymmetries leading to greater drag. The drag timescale also varies inversely with the density of the background. The drag timescale for typical molecular cloud parameters, can be estimated from equation 2.3. Consider a typical cloud of 10^3 $M_\odot$, and radius 1 pc, which has an average number density of $\sim 10^4$ cm^{-3}, and virial

velocity of 2.3 kms^{-1}. Assume that $v \sim \sigma \sim 2.3$ kms^{-1}, and $\ln \Lambda \sim 3$, and that the clump has a mass 50 $M_\odot$. The drag timescale for the clump is therefore 1.8×10^6 years . The time taken for the clump to traverse the cloud, or the crossing timescale, is the shortest dynamical timescale in the system, and is given by $2R/v$, which is seen to be 0.8×10^6 years. Thus, the drag timescale is only of the order of a few times the crossing timescale. This is also much shorter than the expected duration of the star formation phase in the cloud, ($\sim 10^7$ years), or the expected cloud lifetime ($\sim$ a few 10^7 years). Drag due to dynamical evolution is therefore expected to play a significant role in governing the dynamics of the clumps in the cloud.

Clumps moving in the ICM experience a dynamical friction force as detailed above. The ICM serves as the background medium through which the massive clumps move and get decelerated. The dynamics of the clumps are doubtless affected by other forces, notably the forces arising from the gravitational potential they are in, hydrodynamical drag and clump-clump interactions. As mentioned earlier, clumps constitute a significant fraction of the total cloud mass and realistic studies have to incorporate this basic feature. Considerable insight into the physics of the problem can be gained, however, by studying the simplest case of the motion of a single clump in the cloud gas.

2.2.2 Dynamics of a clump

We first consider a single clump moving through a spherical cloud of a given radius, and a density distribution $\rho(r)$. In the absence of dynamical friction, a clump with zero initial velocity, will oscillate about the cloud centre with a frequency determined by the density of the cloud. The inclusion of the drag force causes a deceleration of the clump which continually loses energy. The clump is expected to oscillate about the cloud centre with an ever-decreasing amplitude, and thus get dragged towards the cloud centre, on a timescale of the order of the drag timescale given by equation 2.3. For a clump with a

finite initial velocity at some angle with the radial direction, there is a loss of angular momentum as well, and the clump is expected to spiral in towards the centre of the cloud. We study the motion of a single clump moving through the cloud by writing down the equations of motion and solving them.

The forces considered acting on the clump are the gravitational force due to the cloud derived from the potential (determined by the density distribution) and the dynamical friction force given by equation 2.2, with the different parameters now pertaining to the cloud system. (The maximum impact parameter $b_{\rm max} \sim R$, the radius of the cloud; and the minimum impact parameter $b_{\rm min} = GM/v^2$, so that $\Lambda \sim Rv^2/GM$). There is an additional force due to accretion. The clump accretes mass from the surrounding medium while it moves with a relative velocity $\dot{v}$ through the gas, at a rate

$$\frac{dM}{dt} \simeq \pi {r_{\rm eff}}^2 \rho (v^2 + \sigma^2)^{1/2} \tag{2.4}$$

where $r_{\rm eff}$ is the effective radius of the clump, assumed here to be equal to its gravitational radius $r_g = 2GM/(v^2 + \sigma^2)$. Increase in mass due to accretion also causes a deceleration which is equivalent to a gas drag given as

$$\mathbf{F}_{\rm gas\ drag} \simeq -\mathrm{v}\frac{dM}{dt} \simeq -\pi {r_{\rm eff}}^2 \rho (v^2 + \sigma^2)^{1/2} \mathrm{v} \tag{2.5}$$

The velocity dispersion of the gas, is everywhere taken as equal to the virial velocity of the cloud ($\sigma^2 = GM_o/R$, where M_o is the cloud mass and R its radius). This drag has also been included in the equations of motion. The total force acting on a clump is thus

$$\mathbf{F}_{\rm tot} = \mathbf{F}_{\rm gas\ grav} + \mathbf{F}_{\rm DF} + \mathbf{F}_{\rm gas\ drag} \tag{2.6}$$

where $\mathbf{F}_{\rm gas\ grav}$ represents gravity due to the gas. From equations (2.1,2.2,2.4 and 2.5) the force acting on a clump of mass m is given by

$$\mathbf{F}_{\rm tot} = \ - \ \frac{m\,\Phi_0}{r_0^2} \frac{\vec{r}}{(1 + r^2/r_0^2)^{3/2}}$$

$$- \frac{4\pi\, ln\Lambda\, G^2\rho(r)m^2}{v^3}\left[erf(X) - \frac{2X}{\sqrt{\pi}}e^{-X^2}\right]\vec{v}$$
$$- \frac{4\pi\, G^2\rho(r)m^2}{(v^2+\sigma^2)^{3/2}}\vec{v} \qquad (2.7)$$

where $\Phi_0 = GM/r_o$, and M is the mass of the cloud. The equations of motion are thus given by

$$\frac{d\vec{v}}{dt} = - \frac{4\pi G\rho_0}{3}\frac{\vec{r}}{(1+r^2/r_0^2)^{3/2}}$$
$$- \frac{4\pi\, ln\Lambda\, G^2\rho_0 m}{v^3(1+r^2/r_0^2)^{5/2}}\left[erf(X) - \frac{2X}{\sqrt{\pi}}e^{-X^2}\right]\vec{v}$$
$$- \frac{4\pi\, G^2\rho_0 m}{(1+r^2/r_0^2)^{5/2}}\frac{\vec{v}}{(v^2+\sigma^2)^{3/2}} \qquad (2.8)$$

which are to be solved simultaneously with the rate of change of mass of the clump due to accretion, given by equation 2.4. The equations are solved consistently in three dimensions using a fourth order Runge-Kutta method with adaptive step size control. An initially eccentric orbit was chosen for the clump, which was given the appropriate position and velocity. Figure 2.2 shows the evolution of the (eccentric) orbit with time, where the quantities are plotted in appropriately scaled units. (The radial distance r, is expressed as a fraction of its initial value, and time is in units where $4\pi\, ln\Lambda\, G^2\rho = 1$, which is about 10^6 years for a number density of 10^5 cm^{-3}). Panel 2.2(a) shows the radial distance from the cloud with time for two clumps with differing masses. The radial distance, r, is found to decrease with time as is expected. The oscillations seen superposed on the decay of r, are due to the eccentric nature of the initial orbit. In the absence of drag, r remains bounded between the pericentric and apocentric distances. It can be seen that the more massive clump decays faster than the lower mass clump, which is to be expected, as $\tau_{\rm drag}$ is inversely proportional to the mass of the clump (see equation 2.3). Panel 2.2(b) shows the trajectory of the less massive clump in the plane of its orbit. The clump loses both energy and angular momentum and spirals in towards the centre of the cloud.

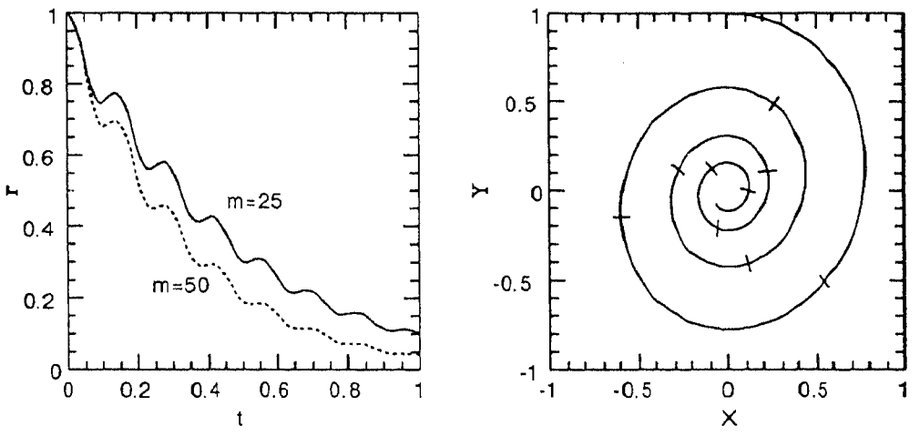

Figure 2.2: *The variation of the average radial distance from the centre of the cloud with time is shown in panel a. Panel b shows the trajectory of the clump along the plane of the orbit. Time has been marked at intervals of 0.1 along the orbit.*

2.2.3 Formulation for the N-clumps cloud

The motion of a single clump in a cloud gives us a qualitative understanding of the effects of dynamical friction due to the ICM. Molecular clouds, however, are better modelled by a description in which a significant fraction of the cloud mass is contained in many discrete clumps. We therefore consider a model where the cloud consists of many clumps embedded in the ICM. The ratio of mass contained in the clumps and ICM is varied (from 10% to 50%) in different cases, though in general it is assumed that a significant amount of the cloud mass is contained in the interclump gas.

For the clumps within molecular clouds the mass spectrum is generally a power law with the power law exponent x, which is observationally found to vary from 1.1 to 1.7, but is typically about 1.5 (e.g., Loren 1989, Stutzki & Gusten 1990). For clumps in the collapse phase and forming stars, the spectrum may be closer to the Salpeter mass function (Salpeter 1955) with an

index of 2.35. We have adopted a power law mass spectrum for the clumps with an index of 2.35 for all our cloud systems and have varied x for one such system to study any dependencies on the form of the mass function assumed. The upper and lower cut-offs of the mass spectrum have been appropriately chosen for clouds of different total masses.

Massive clumps suffer greater drag (or equivalently, get dragged on shorter time-scales) as compared to less massive clumps. Given an ensemble of clumps evolving in a cloud for a certain period of time, *a spatial mass segregation of clumps* is thus expected. As the system evolves, the more massive clumps are dragged down faster than their lower-mass companions and occupy positions closer to the centre of the cloud. To investigate the segregation phenomenon in greater detail, the dynamics of an N-clump cloud is studied. The forces acting on each clump now have an additional component from the N-body gravitational force due to the presence of other clumps in the system. Thus,

$$\mathbf{F}_{\mathrm{clump},i} = -Gm_i \sum_{j,j\neq i}^{N} \frac{m_j \vec{r}_{ij}}{(r_{ij}^2 + \epsilon^2)^{3/2}} \tag{2.9}$$

where the symbols have their usual meaning. The potential is softened by a softening parameter ϵ. This is done to smoothen out very close encounters which could lead to a large increase in the N-body force. The inclusion of a softening parameter can be physically interpreted as the force between two finite sized "clouds" of radius ϵ. At distances much larger than ϵ, the N-body force reduces to the usual $1/r^2$ form, and for distances shorter than ϵ, it varies as $\sim r/\epsilon^3$, which corresponds to the gravitational force between two constant density gas spheres. The softening parameter has been chosen here to be equal to the characteristic size of a clump.

The equations of motion have again been set up and the forces acting on an individual clump considered are the gravitational force due to the cloud gas, clump-clump gravitational interactions and a dynamical drag force due to the ambient gas along with an increase in mass of the clump because of

accretion. In the earlier discussion on the motion of a single clump in a cloud, the clump was represented by a point-like particle for simplicity. In a realistic case, clumps are finite-sized and they have in fact now been "assigned" a characteristic radius. The expression for dynamical friction (equation 2.2) was derived for point particles, but is nevertheless found to be a reasonably good approximation for extended objects as well, if $r_c \lesssim b_{max}/\sqrt{\Lambda}$, where r_c is the radius of the object (Binney & Tremaine 1987, p.426). The mass accretion rate is proportional to the square of the effective radius, r_{eff} (equation 2.4). For a clump with its gravitational cross-section larger than its physical cross-section, r_{eff} is given by its gravitational radius $r_g = 2GM/(v^2+\sigma^2)$. For larger clumps,

$$r_{eff}{}^2 = r_c{}^2 \left[1 + \frac{r_g}{r_c}\right] \tag{2.10}$$

with r_c being the physical radius of the clump. Clumps that are in virial equilibrium or those that are pressure confined in GMC Complexes and GMCs usually have relatively large radii ($r_c \geq r_g$) and r_{eff} is given by equation 2.8. The actual accretion process is, however, ill–understood, as the supersonic motion of the clumps through the ambient medium causes the formation of bow shocks which may prevent any real accretion (Pumphrey & Scalo 1983). Further, any matter impinging on the surface of the clump may cause ablation of the clump rather than get accreted (Scalo & Struck-Marcell 1984). There is however transfer of momentum, and the clumps suffer a hydrodynamical drag given by equation 2.5. From equations 2.2 and 2.5, for typical velocities $v \sim \sigma$ the ratio between dynamical friction F_d, and hydrodynamical drag $F_{\text{gas drag}}$, is $\sim 0.8 ln\Lambda (r_g/r_c)^2/(1+(r_g/r_c))$. Thus $F_{\text{gas drag}} > F_d$ for clumps with $r_c/r_g \gtrsim 0.9\sqrt{\ln\Lambda} \gtrsim 2$ for $ln\Lambda \sim 5$. The dynamics of such clumps in molecular clouds is dominated by hydrodynamical drag and clump-clump collisions (Scalo & Pumphrey 1982, Elmegreen 1985). Protostellar clumps and protostars are denser objects with $r_c < r_g$ and the accretion rate is given by (cf. Hoyle &

Lyttleton 1939)

$$\frac{dM}{dt} = \frac{4\pi G^2 \rho(r) M^2}{(v^2 + \sigma^2)^{3/2}} \tag{2.11}$$

We restrict our analysis to protostellar clumps, whose physical radii are smaller than their gravitational radii.

Typically, about 100 clumps are considered and are initially (at $t = 0$) given random positions so that the total configuration corresponds to that of a uniform number density distribution of clumps in the cloud. The initial velocities for the clumps have their virial values and are given random orientations. The equations are solved consistently in three dimensions using a fourth order Runge-Kutta method with adaptive step size control. Integration times are typically of the order of the cloud lifetime, which is about 50 Myr (1 Myr=10^6 years) for molecular clouds in the Galaxy.

The model is first evolved in the absence of the dynamical friction force, so that the effects of N-body evolution can be studied in isolation. Two-body relaxation in N-body systems also causes a mass segregation over timescales of the order of the relaxation time. The relaxation time can be defined as the time over which, the nett change in velocity due to two-body encounters becomes as large as the velocity itself, i.e., $\delta v \sim v$. This timescale, τ_R, is approximately given by

$$\tau_R \sim \frac{N}{\ln N} \tau_{\rm cross},$$

for a self-gravitating system of N particles, where $\tau_{\rm cross}$ is the typical time taken for a particle to cross the system. The system evolves towards an equipartition state, with the kinetic energy of all clumps approaching the same value. This clearly implies that more massive clumps have lower velocities, while less massive clumps gain velocity on an average during encounters. Higher mass clumps thus settle towards the centre of the cloud and lower mass clumps orbit at larger distances, leading to a spatial mass segregation, on timescales of the order τ_R. Dynamical friction is also expected to lead to mass segregation as discussed earlier. For typical cloud conditions, mass segregation due to dy-

namical friction is estimated to take place on shorter timescales than required by N-body relaxation effects. The analysis is repeated, including the frictional force, to assess the relative effects of the two processes. The results of the analysis are discussed in the following section, where the effects of changing various parameters in the model are also studied.

It should be noted that we have not considered the effects of magnetic fields or collisions between clumps, for simplicity.

2.3 Results and discussion

The formulation described above has been used to obtain the temporal evolution of the protostellar clumps in molecular clouds for a range of parameters. The densities, masses, sizes etc are taken to be similar to those observed for the systems under consideration. The densities and fraction of mass contained in the clumpy form have been varied along with a change in mass spectrum of clumps. In all, thirteen cases were run and in each individual case the spatial positions and velocities of the constituent clumpy particles have been followed at different epochs of time as the system evolves. Depending on the prevailing physical conditions the cloud evolutionary properties change, as is to be expected. The effects of dynamical relaxation of the clumps in a cloud in the presence of a constant gas potential have been looked at first and it is found that mass segregation due to N-body relaxation takes a long time to be established. The inclusion of the dynamical drag on the clumps significantly alters the dynamics in all the interstellar cloud systems considered, and mass segregation is established on a much shorter time. (The two cases are compared in Figure 2.6 and discussed at the end of this section). The dynamical drag acting on a clump is dependent on its mass, and thus clumps of different masses have in general different retardations. The most massive clumps suffer the maximum decelerating effects and their orbits get closer to the cloud

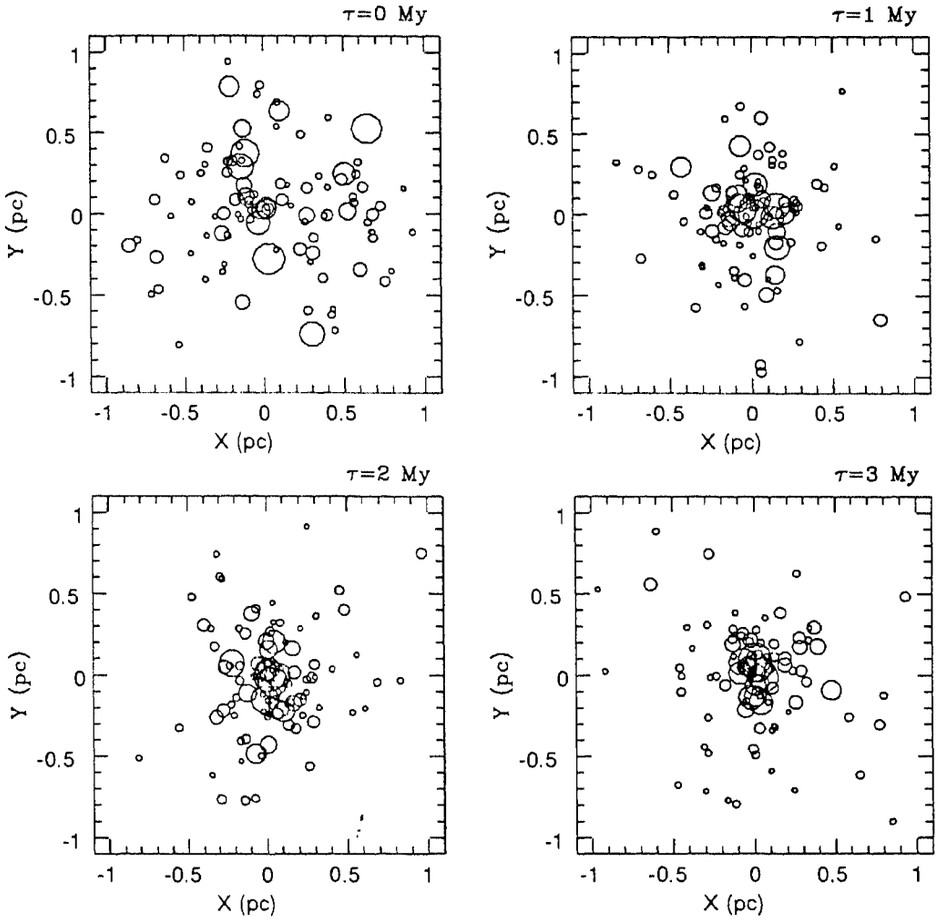

Figure 2.3: *The projected spatial positions of clumps at different epochs. The size of the symbols denotes the mass of the clumps as indicated.*

centre. The "in-fall" timescales over which the clump falls to the centre of the cloud, is different for clumps of different masses. The more massive clumps settle to the centre in a shorter time than the lower mass clumps. A spatial plot of the system projected along the x–y–z planes is shown in Figure 2.3 at different epochs. The size of the circles in the plot is indicative of the mass of the clumps. There is a clustering of the clumps towards the centre of the

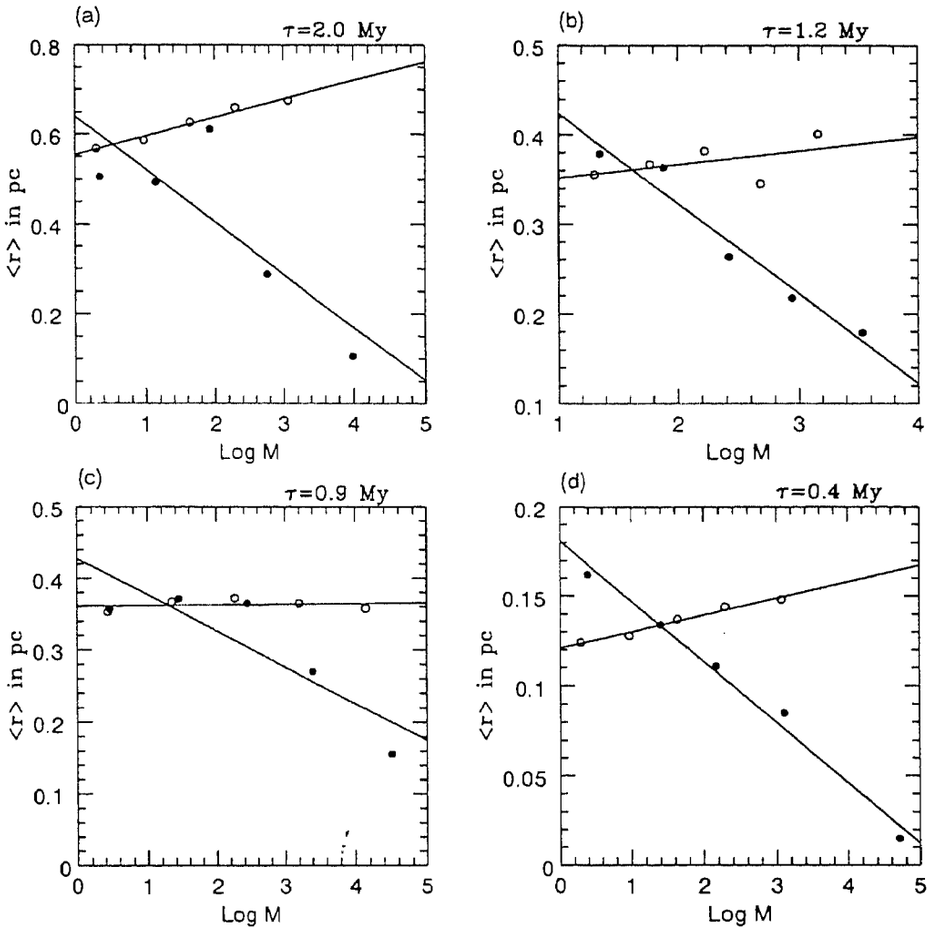

Figure 2.4: *Average positions of clumps which have been divided into logarithmic mass bins have been plotted against the mean mass of each bin. The open circles correspond to the initial distribution of the clumps and the filled circles to the distribution after a time τ indicated in the upper right corner of each plot. Least square fits have been drawn to the points. Panels a, b, c and d correspond to clouds with increasing average densities of* 10^4, 1.2×10^5, 4×10^5 *and* 10^6 cm^{-3} *respectively.*

cloud, and a radial segregation of mass is established in the cloud. This can be seen from the plots in Figure 2.4. The clump mass spectrum is divided into logarithmic mass intervals and the masses of the clumps in each such bin

are averaged over to obtain a mean mass of the bin. The positions (radial positions) of the clumps with respect to the cloud centre for each mass bin have similarly been averaged to get an average position $< r >$, which is plotted against the mean logarithmic mass of the bin. The open and filled circles in the figure correspond to the times t=0 and a later time at which the cloud shows evidence of mass segregation. The lines are least square fits drawn to the points. Initially, the clumps are distributed over the cloud randomly and hence are all equally probable to lie anywhere in the cloud, independent of their mass. At later times, the more massive clumps suffer greater drag due to dynamical friction and move toward the centre of the cloud. The least massive clumps which are not significantly impeded by the drag force move in orbits that could be all over the cloud and thus have an average radial position further from the cloud centre than the high mass clumps. This results in a gradual steepening of the slope in the log m – $< r >$ plots with time. The timescale of the process is governed by the cloud parameters, and is shorter for denser clouds. We define a mass segregation time $\tau_{\rm ms}$ in the following manner. The ratio η of the average radial distance $< r_h >$ of the most massive clumps (in number, 10% of the total population) to that of the least massive clumps $< r_l >$ has been computed at various times, (where $\eta = < r_h > / < r_l >$). At t=0, η is roughly equal to one, and $\tau_{\rm ms}$ has been considered as the time at which $\eta \simeq$ 0.5. It is found that the segregation timescale $\tau_{\rm ms}$ is typically of the order of a few times the cloud crossing timescale $\tau_{\rm cross}$ ($\tau_{\rm cross} \sim 2R/\sigma$, where R is the radius of the cloud and σ the velocity dispersion). The lifetime of the molecular cloud is typically about a few 10^7 years, and the estimated duration of the star formation phase is also of similar order. The mass segregation timescale is of the order of a few 10^6 years, and is thus short enough to be of relevance to the dynamical evolution of protostellar clusters, as they probably spend much longer periods of time embedded in molecular clouds. Figure 2.4 shows the mass-radius plots for the various systems. As the system further evolves, i.e.,

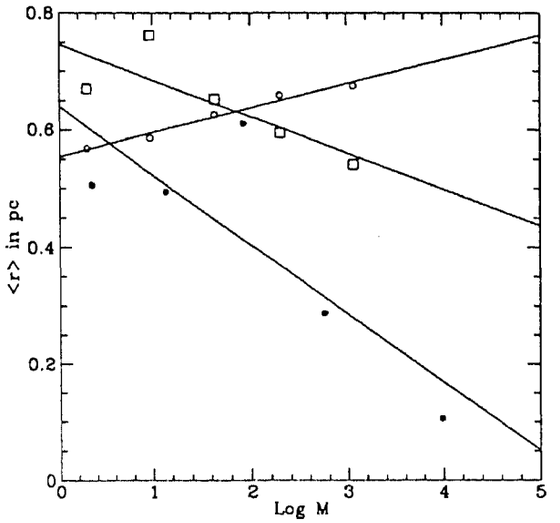

Figure 2.5: *The same conventions as earlier, where the open circles correspond to the initial positions, the filled circles to the case with drag included, and the squares to the case with no drag, after 2 Myr.*

at times t > τ_{ms}, there is an expansion of the system, as N-body interactions take some of the low mass clumps into orbits with radial distances larger than their original radii, and mass segregation is enhanced. As was discussed earlier, ordinary N-body relaxation also causes a spatial mass segregation to be established in the system, and to assess the effects of inclusion of the drag force, a cloud system was evolved with and without drag. Figure 2.5 shows the log m - $< r >$ plot for the two cases. The initial conditions were identical for both runs, and the open circles in the figure denote the initial positions. The filled circles denote the average positions for the case with drag included, after a time 2 Myr, and mass segregation has been clearly established in the system. The squares denote the N-body relaxation case, without drag, at the same epoch. N-body relaxation is also seen to cause a mass segregation in the system, though the timescales involved in this process are much longer than that for dynamical friction (τ_{ms}, as defined earlier, is $\sim$ 11 Myr for segregation

due to N-body relaxation, and $\sim$ 2.4 Myr for segregation due to drag). The extent of mass segregation is thus seen to be clearly enhanced by the inclusion of the drag forces, and now takes place on much shorter timescales.

As dynamical friction depends on the cloud parameters, τ_{ms} is expected to vary for different physical conditions in the cloud. Changes in the dynamical evolution of the protostellar clumps with change in cloud density, mass fraction in the form of clumps, clump mass spectra, and density profile of the inter-clump medium are studied by varying these parameters individually, keeping all others fixed. These cases are discussed below in detail.

2.3.1 Effect of change in density

Molecular clouds are observed to have a range of densities, from the less dense warm GMCs to the cool, dense dark clouds, with the star-forming ρ Oph cloud core being a prototypical example of the latter. The effects of a change in the average density of a cloud on the dynamics of its constituent clumps is studied. Four different cases identified as Clouds I, II, III and IV are considered with average densities ranging from 10^4 to 10^6 cm^{-3}. Cloud I has a mass of 10^3 M$_\odot$ and a size of 1.6 pc (velocity dispersion σ_v = 2.3 kms^{-1}). The average density of the cloud is 10^4 cm^{-3}, and has 42% of its mass distributed in 150 clumps whose masses range from 1 to 30 M$_\odot$. The ordinary N-body dynamical relaxation time for all four cases is greater than 10 Myr. The spatial mass segregation timescale is found to be 2.4 Myr, which is far shorter than the ordinary N-body relaxation time. Cloud II has a mass of 3×10^3 M$_\odot$, size 1.0 pc, σ_v = 5.1 kms^{-1} and an average density of 1.2×10^5 cm^{-3}. 185 clumps form 40 % of its mass and have masses from 3 to 30 M$_\odot$. Mass segregation takes place on a slightly shorter timescale of 1.2 Myr. Cloud III (M = 10^4 M$_\odot$, R = 1 pc, σ_v = 9.3 kms^{-1}), has an average density of 4×10^5 cm^{-3} and has a segregation time nearly the same as that of Cloud II, 0.9 Myr. Cloud IV has the highest average density of 10^6 cm^{-3}. All cloud parameters are the same as

that of Cloud I, except for its size which is 0.25 pc ($\sigma_v = 4.9$ kms^{-1}). The mass segregation timescale is only 0.4 Myr. The mass-radius plots for all four cases are shown in Figure 2.4. It is to be noted that a density increase by a factor of 100 from Cloud I to Cloud IV, causes a decrease in segregation timescale by a factor of 6. There is also some expansion of the initial system as can be seen from Figure 2.4. Thus $\tau_{\rm ms}$ is shorter for denser clouds and segregation effects are expected to be enhanced in the densest star-forming molecular clouds. It may very well be probable that the mass segregation observed in young star clusters in star-forming regions (e.g. NGC 2071,NGC 2024; Lada 1991), is a result of the dynamics of the protostellar clumps from which they form.

In all of the above systems, the physical radius of the protostellar clump r_c is assumed to be small compared to its gravitational radius, r_g. The N-body gravitational force is softened using a parmaeter ϵ equal to 10^{-3} R, (3×10^{15} cm for R=1pc) for all the clumps. For computational convenience, ϵ is chosen such that it is larger than the clump radius, but should be small enough to allow close clump-clump encounters. For stars, protostars and protostellar clumps that have developed high density cores that contain most of their mass, our choice of ϵ is satisfactory. But protostellar clumps that have just begun to collapse, may have r_c as large as r_g. We have therefore run the simulation for a case where ϵ is set equal to r_g. Though, the segregation time $\tau_{\rm ms}$ does not change, and is 2.4 Myr for both cases, there is however still a qualitative difference in the subsequent evolution of the system. There is no expansion of this system with smaller clumps moving out to radii larger than their initial positions, as all clump-clump encounters are highly softened. It can be seen from Figure 2.6 that the protostellar clumps form a more compact system after dynamical evolution. When the clumps collapse to form stars, the resulting cluster in such a case would have a higher 'apparent' star forming efficiency (SFE) which may eventually form a bound system. (cf. Bally & Lada 1991)

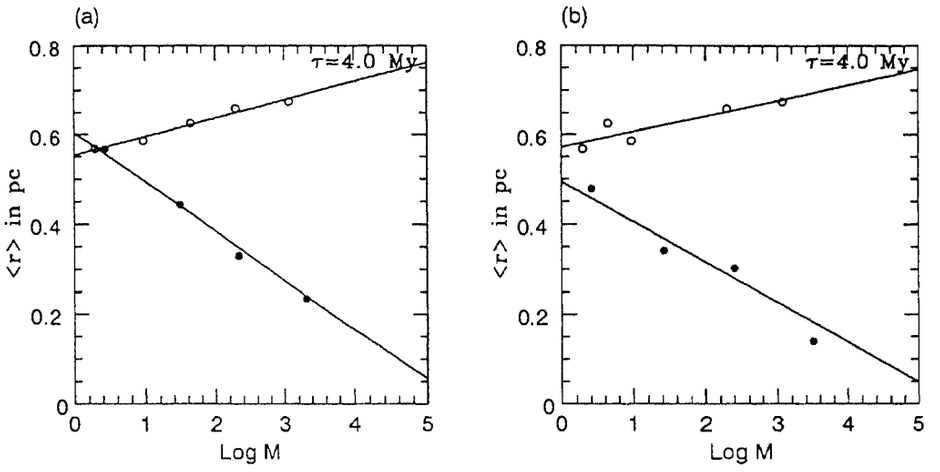

Figure 2.6: *The radial positions against mass for Cloud I (see text), with different softening, at 4 Myr. Panel a shows the plot when a small physical cross-section is assumed for the clumps, and panel b when their size is set equal to their gravitational radius.*

2.3.2 Effect of change in mass fraction in clumps

The total fraction f_c, of mass contained in the clumps is varied for Cloud I from 10% to 50%. The number of clumps was modified accordingly with the same power-law spectrum and upper and lower cutoffs. There is no significant difference in mass segregation timescales. Figure 2.7 shows the mass-radius plots for the clouds at the same epoch. The segregation time for the different cases is: $f_c = 0.1, \tau_{\rm ms} = 2.0 Myr$; $f_c = 0.2, \tau_{\rm ms} = 1.8 Myr$; $f_c = 0.3, \tau_{\rm ms} = 2.4 Myr$ and $f_c = 0.5, \tau_{\rm ms} = 2.0 Myr$. Clouds with lower clump mass fractions, have more gas in the ICM which is also denser, as the total mass and radius of the cloud is kept constant. This ensures that the velocity dispersion of the gas, which is assumed to be the virial value for the cloud, is also a constant. The clumps have the same mass range, differing only in number to make up the fraction f_c of the total cloud mass. Clouds with small f_c, have clumps that move in denser gas which are thus expected to segregate faster. No

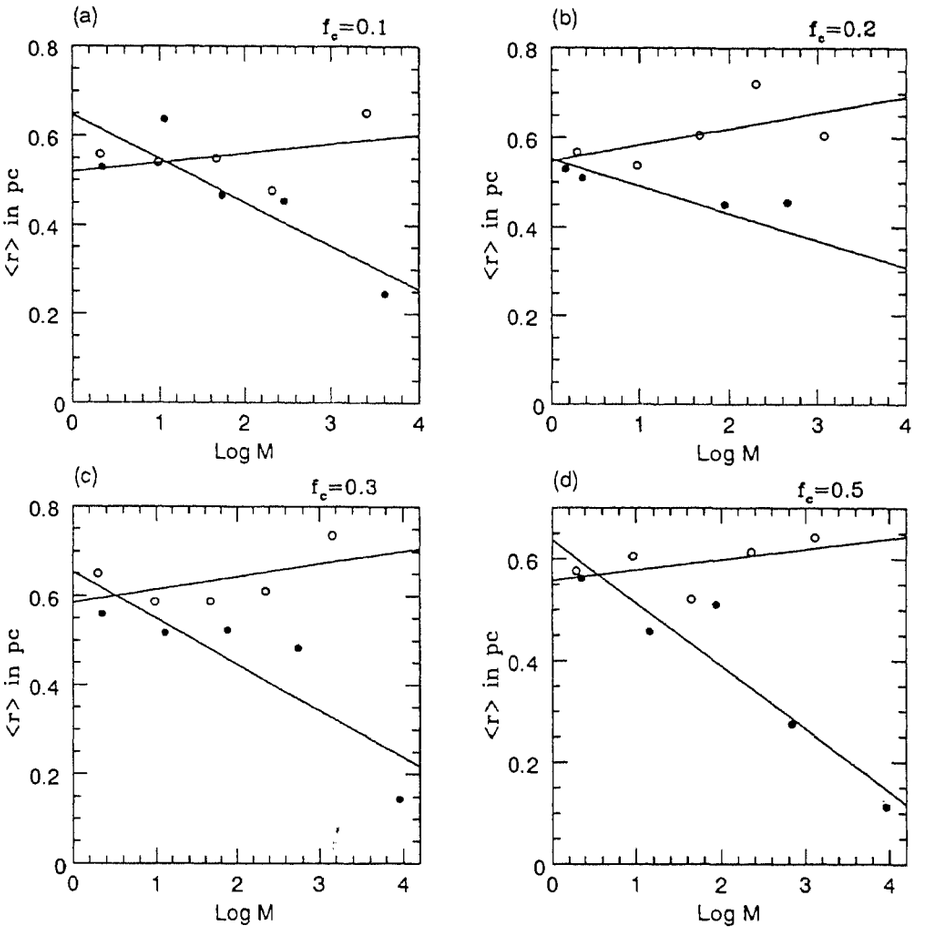

Figure 2.7: *The same conventions as Figure 2.4 with the plots corresponding to varying mass fraction of clumps in the cloud (at 2 Myr). Panels a, b, c and d have clump mass fractions of 10%, 20%, 30% and 50% respectively.*

such trend is apparent from the study, probably indicating that the density change from $f_c = 0.1$ to $f_c = 0.5$ is not large enough to noticeably affect the segregation timescales. (As was seen above, an increase by a factor of 100 in the density, causes a change in the mass segregation timescale only by a factor of 6). The lack of any systematic trend in $\tau_{\rm ms}$ with varying f_c in our

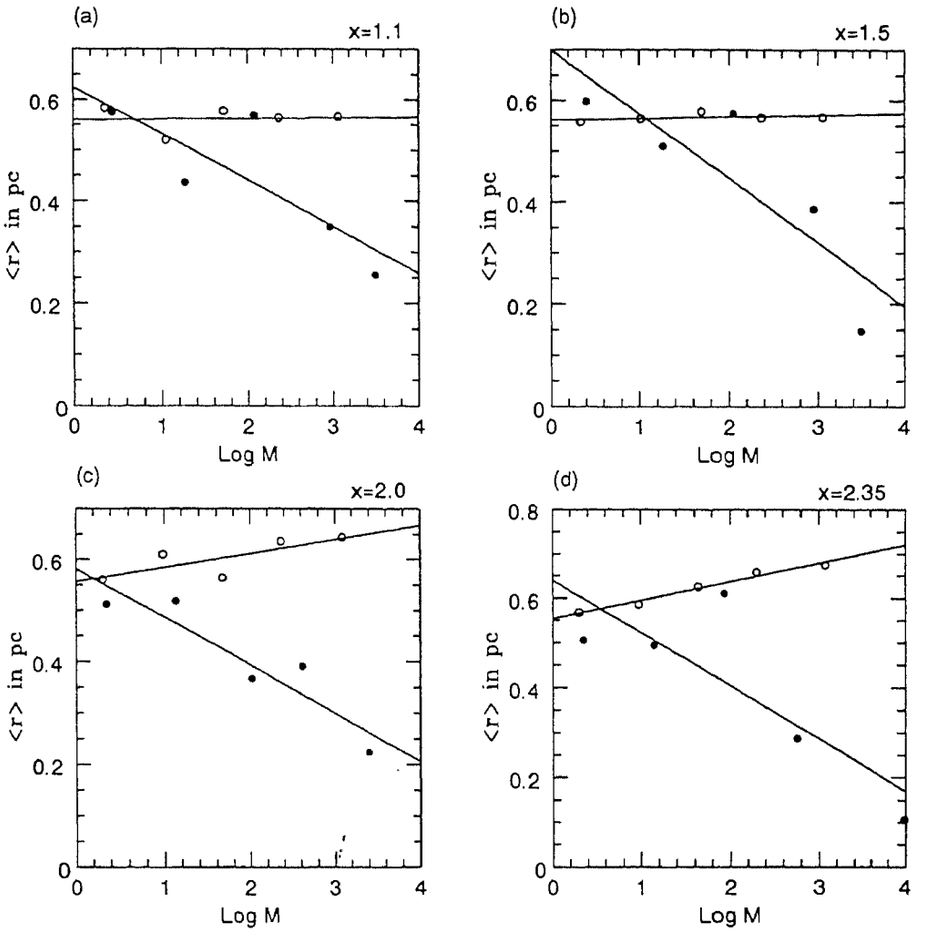

Figure 2.8: *These plots show average positions against mass for clouds with the same parameters, but different mass spectra for the clumps. They are all at the same epoch (2 Myr) and the mass spectrum power law exponent is denoted by x, in the upper right corner for each case.*

simulations is probably a result of poor statistics along with different initial clump conditions (clump positions and velocities at t=0), especially for low f_c values. For clouds with a large fraction of mass in clumps, the effects of N-body relaxation probably augment the segregation process due to drag, causing a

decrease in the overall segregation timescale, τ_{ms}, for the cloud.

2.3.3 Effect of change in mass spectrum index

A change in the exponent of the power law mass spectrum has only a minor effect on the dynamics of the protostellar clumps. In order to investigate the effect of variation in the mass spectrum index, one of the above cases (Cloud I) has been run for x=1.1,1.5,2.0 and the stellar mass spectrum index of 2.35. A variation in the power law exponent for the clumps does not seem to have very pronounced effect on the final state of the system. (x=1.1, τ_{ms} = 2.4 Myr; x=1.5, τ_{ms} = 2 Myr; x=2.0, τ_{ms} = 2 Myr; x=2.35, τ_{ms} = 2.4 Myr) In each case, the fraction of the mass contained in the clumps (40%) has been kept constant by suitably adjusting the number of clumps, so that the gravitational potential does not appreciably change. Figure 2.8 shows that the extent of segregation (at the same epoch of 2 Myr) is little affected by change in mass spectrum. As the clumps accrete gas from the ambient medium at a rate dependent on their mass, the mass spectrum of the clumps could also be potentially altered. However such changes are found to be almost negligible, as the accretion rates are not high enough to significantly change the power law index, in any of the cases considered. The power law exponent after segregation x_f, was computed for the two extreme cases. For x=1.1, x_f=1.15 and x=2.35, x_f was found to be 2.31.

2.3.4 Effect of change in density distribution of ICM

The density distribution of the gas, i.e, the interclump medium in all of the above clouds is given by the Plummer distribution (equation (1)). The analysis for Cloud I has been repeated for a constant density or a uniform gas distribution, to study any alterations brought about by variations in the gas density profile. The same initial conditions were imposed and it is found that the mass segregation timescale increases (Figures 2.9a and 2.9b) marginally.

A steepening in the density profile of the cloud due to mass segregation is also found as is to be expected, especially when the clumps form a significant fraction of the total mass. Due to the drag forces acting on the clumps, there is a spatial mass segregation established in the molecular cloud clumps. The velocity distribution is also affected. The protostars are acted upon by dynamical friction as they move through the cloud. They are decelerated and their orbits get closer to the cloud centre. They tend to approach local virial velocities at their new positions. Decay of the orbits of the most massive protostars also modifies the density structure in the inner regions of the cloud which in turn causes a change in the virial velocities here. For a power law density profile of the form $\rho(\mathrm{r}) \propto \mathrm{r}^{-\alpha}$, the virial velocity is given by $v(r) \propto r^{(-\alpha+2)/2}$. Thus the velocity dispersion increases with increasing radius for a cloud with a density profile less steep than $\alpha = 2$. Such clouds are expected to show a velocity segregation with mass along with the spatial mass segregation, i.e., the more massive clumps are more centrally located and also have lower velocites on an average than the lower mass clumps. On the other hand, clouds with steeper density profiles are likely to show an increase in velocity dispersion towards the centre of the cloud. This increase could to some extent compensate the loss due to drag, thus decreasing the extent of segregation of mass with respect to velocity. Figures 2.9(c) and 2.9(d) show the velocity dispersion against log m for the constant and Plummer density models, respectively. Velocity segregation with respect to mass is more apparent for the constant density model than for the Plummer model. Thus, mass segregation appears to be an inevitable consequence of clump dynamics in most interstellar clouds. For a thorough analysis of the cloud-clump systems, all the forces acting on the clumps have to be included, in particular clump-clump collisions and magnetic field effects. Collisions are expected to be important especially after a central clustering of clumps has occured, if not at an earlier stage. The outcome of a collision depends on the parameters of the encounter, and in general could lead to either

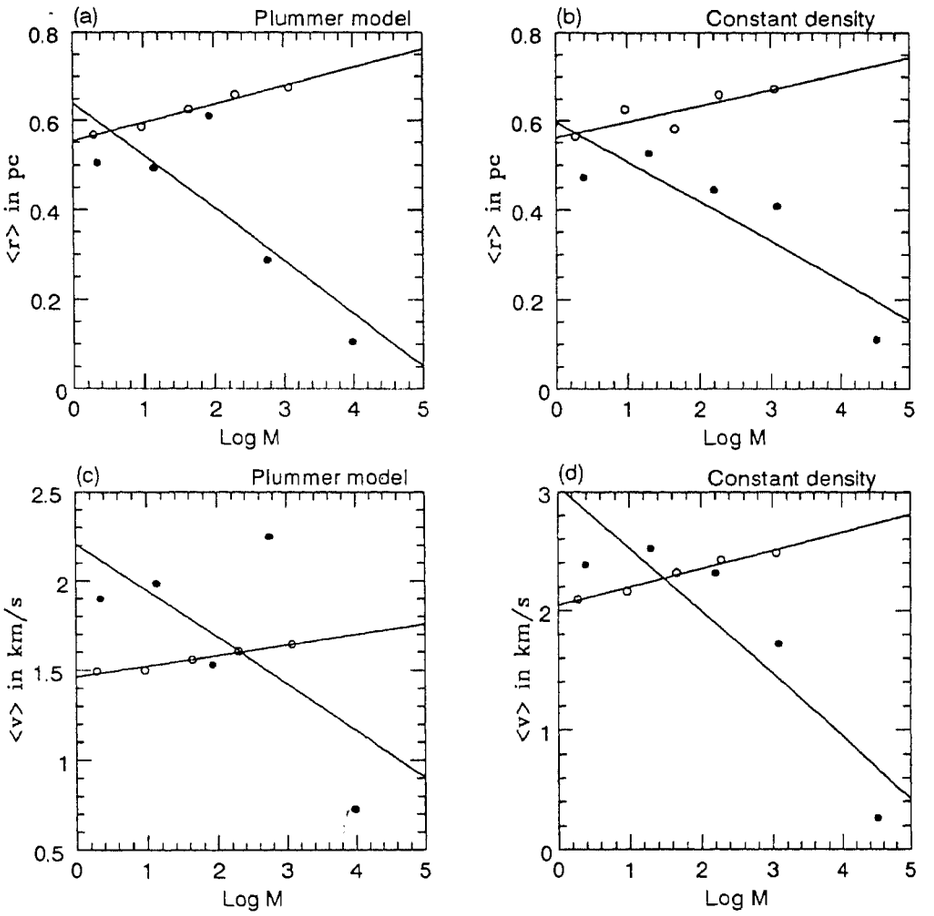

Figure 2.9: *Variations in extent of mass segregation with respect to the density profile of the interclump gas. A constant density cloud and a Plummer model are considered. Panels a and b show the extent of spatial mass segregation and c and d, the velocity dispersion against the mean logarithmic mass of each bin. The open circles and fitted lines correspond to the initial times and the filled circles to a time of 2 Myr.*

a coalescence of the clumps forming a larger clump or a fragmentation into smaller clumps. If it is assumed that collisions cause clumps to coalesce, the massive clumps thereby formed would lose momentum and sink to the center

of the cloud. This would also lead to spatial segregation of mass in the cloud. We make simple estimates of the time scales involved in collision and drag processes for comparison as follows. The timescale at which dynamical friction causes deceleration can be obtained from equation (3) for the drag force and can be written as

$$\tau_{\rm drag} \simeq \frac{v^3}{4\pi ln\Lambda G^2 M\rho\,[erf(X) - 2Xe^{-X^2}/\sqrt{\pi}]} \tag{2.12}$$

The time scale for deceleration of a clump due to clump-clump collisions, would be of the order of the time scale for the growth of the clump mass due to accretion of clump masses, following collisions that result in coalescence. The rate of change of mass of a clump due to collisions and subsequent coalescence can be approximated as an effective cross-sectional area times a mass flux

$$\frac{dM}{dt} \simeq \pi {r_{\rm eff}}^2 < \rho_c > v_{\rm rel} \tag{2.13}$$

where $r_{\rm eff}$ is given by equation (6) and ρ_c is the mass density in the form of clumps, averaged over the volume of the cloud. The relative velocity of the encounter is denoted by $v_{\rm rel}$, which is of order $\sqrt{2}v$. The collisional timescale $\tau_{\rm coll}$ is given by $M/(dM/dt)$ and the ratio of the two timescales can be written as

$$\frac{\tau_{\rm drag}}{\tau_{\rm coll}} \simeq 1.3\,\frac{\rho_c}{\rho ln\Lambda}\left(\frac{r_{\rm eff}}{r_g}\right)^2 \tag{2.14}$$

Thus, collisional drag dominates dynamical friction (i.e., $\tau_{\rm coll} < \tau_{\rm drag}$) only when

$$\frac{r_c}{r_g} \gtrsim 0.9\,\sqrt{\frac{\rho}{<\rho_c>}\ln\Lambda} \tag{2.15}$$

Typically, $\rho \sim \rho_c$ and $ln\Lambda \sim 5$. Thus, for the situations under consideration here with $r_c < r_g$ ($r_{\rm eff} = r_g$), the drag time is much shorter than the collision time and mass segregation due to drag dominates that due to collisions, by a factor of $\sim 0.9 ln\Lambda$. But collisions may considerably affect the dynamics at the center of the cloud where the number density is enhanced by drag effects. If the outcome of a collision is fragmentation rather than a coalescence, the

evolution may be quite different. For a more realistic picture, a detailed model of the collision process has to be made and included with the gas drag to study the motions of the clumps within the cloud.
The magnetic field in clouds is an important contributor to the overall energy density of the cloud, and doubtless has an important role to play in governing the dynamics of the clumps, more so if the principal mode of support in the cloud against gravitational collapse is magnetic pressure. The subject of the inclusion of magnetic fields is however beyond the scope of the present work. Though the consequences of the drag force acting on the clumpy constituent of the molecular cloud seem to hold an interesting variety of possibilities, it should be noted that the present treatment is very simplistic and that for a more realistic analysis, collisions and magnetic fields have to be taken into account.

Mass segregation in star-forming regions The spatial segregation of mass among protostellar clumps is found to be significant for a range of cloud parameters, within reasonably short timescales. Mass segregation due to dynamical friction typically takes place in about 1–2 Myr, which is much shorter than, the duration of the star formation phase ($\sim$ 10–30 Myr), typical cloud lifetimes ($\sim$ 30–40 Myr), or the N-body relaxation time for the cluster($\sim$ 40 Myr). Dynamical evolution of clumps prior to the onset of gravitational instability and star formation in clouds, thus determines mass segregation in the protocluster. If massive stars form from the collapse of the most massive clumps, as is highly probable, they are expected to lie closer to the centre of the cloud. Mass segregation in young open clusters and in embedded clusters in star-forming regions is observed to be a common feature (e.g., Trapezium, NGC 2024, NGC 2071; McCaughrean et al 1991, Lada 1991). The radial distribution of HII regions in GMCs show an increased concentration at the centres of clouds (Waller et al 1987, Scoville et al 1987), indicating a preferential location for massive stars at the cloud centres. Mass segregation of young

stars could thus be explained as a consequence of the effects of dynamical drag at the protostellar clump stage of evolution in clouds.

The effects of gas drag due to dynamical friction, also hold implications for the star–forming efficiency(SFE) of the cloud. If the protostellar clumps are extended objects with a physical extent as large as their gravitational radii, it was seen that they form a compact system on evolution. On collapse to form a protostellar cluster, the cluster would have dynamically evolved to occupy a limited spatial region at the centre of the cloud. In such an event, the apparent or local SFE of the cloud would be enhanced, with important consequences for the formation of bound clusters. The SFE and implications for cluster formation are discussed in greater detail in the next chapter.

2.4 Conclusions

Protostellar clumps moving in molecular clouds through an ambient interclump medium are acted upon by the decelerating forces of dynamical drag due to the gas, lose momentum and fall towards the centre of the cloud. Since the forces are mass dependent, the more massive clumps suffer greater deceleration and settle towards the centre on shorter timescales. This causes a radial segregation with respect to mass of the clumps in the cloud. This segregation induced by dynamical friction is found to be significant for protostellar clumps in interstellar clouds as the timescale involved is much shorter than the typical cloud lifetime and the N-body relaxation time. The segregation is more pronounced and quicker in denser clouds. Variations in clump mass spectra and density profile of interclump gas have little effect on the dynamics, and do not affect the timescale of segregation in the cloud system very much. The fraction of mass contained in the clumpy and tenuous forms to some extent influences the dynamics of the system, but the segregation timescales are not significantly altered. There is also some velocity segregation with respect to

mass, with the more massive clumps tending to have lower velocities. This is not, however, as pronounced as the radial segregation. The most massive star-forming clumps are thus expected to be closer to the centre of the parent cloud. It is suggested that (Gorti & Bhatt 1995) subsequent star formation in these clumps can then explain the mass segregation observed in many young clusters of pre-main sequence stars and YSOs.

References

Bally, J., Lada, E., 1991, in The Formation and Evolution of Star Clusters, A.S.P. Conference Series, No 11, ed K.A.Janes, 38

Bally, J., Langer, W.D., Stark, A.A., Wilson, R.W., 1987, Astrophys. J. 312, L45

Beichman, C.A., Myers, P.C., Emerson, J.P., Harris, S., Mathieu, R., Benson, P.J., Jennings R.E., 1988, ApJ, 307, 337

Bhatt H.C., Rowse D.P., Wiliams I.P., 1984, MNRAS, 209, 69

Binney, J., Tremaine, S., 1987, Galactic Dynamics (Princeton Univ. Press)

Blitz, L., 1991, in The Physics of Star Formation and Early Stellar Evolution, eds C.J. Lada, N.D. Kylafis, 3

Blitz, L.,Stark, A.A., 1986, ApJ, 300, L89

Blitz, L., Thaddeus, P., 1980, ApJ, 238, 148

Hoyle, F., Lyttleton, R.A., 1939, Proc.Camb.Phil.Soc., 35

Chandrasekhar, S., 1943, ApJ, 97,255

Elmegreen, B.G., 1985, ApJ, 299, 196

Elmegreen, B.G. and Clemens, C., 1985, ApJ, 294, 523

Elmegreen, B.G., Elmegreen, D.M., 1987, ApJ, 320, 182

Falgarone, E., Phillips, T.G., 1990, ApJ, 359, 344

Falgarone, E., Phillips, T.G., Walker, C., 1991, ApJ, 378, 196

Falgarone, E., Phillips, T.G, 1991, in Fragmentation of Molecular Clouds and Star Formation, eds E. Falgarone, F. Boulanger, and G. Duvert (Kluwer, Dordrecht), 119

Falgarone, E., Puget, J.L., 1988, in Galactic and Extragalactic star forming regions, eds R.Pudritz, M.Fich ,195

Genzel, R., 1991, in The Physics of Star Formation and Early Stellar Evolution, eds C.J.Lada, N.D. Kylafis, 230

Genzel, R., 1992, in The Galactic Interstellar Medium, by W.B.Burton, B.G.Elmegreen, R.Genzel, 353

Goldsmith, P.F., 1987, in Interstellar Processes, eds D.J.Hollenbach, H.A.Thronson Jr. (Dordrecht, Reidel), 51

Gorti U., Bhatt H.C., 1995, MNRAS, 272, 61

Guelin, M., Cernicharo, J., 1987, in Molecular Clouds in the Milky Way and External Galaxies, eds R.L.Dickman, R.L.Snell, J.S.Young, 200

Lada, E., 1990, Ph.D Thesis, Univ. of Texas

Lada, C.J., 1991, in The Physics of Star Formation and Early Stellar Evolution, eds C.J. Lada, N.D. Kylafis, 339

Lada, C.J., Margulis, M., Dearborn, D., 1984 ApJ, 285, 141

Larson, R.B., 1982, MNRAS, 200, 159

Larson, R.B., 1990, In "Physical Processes in fragmentation and star formation", eds. Capuzzo-Dolcetta R., Chiosi C., Di Fazio A., p390 (Kluwer, Dordrecht)

Loren, R.B., 1989, ApJ, 338, 902

Myers, P., 1987,in Star Forming Regions. eds M.Peimbert, J.Jugaku, 33

Perault,M., Falgarone, E., Puget, J.L., 1985, A&A 152, 371

Plummer, H.C., 1911, MNRAS, 71, 460

Pumphrey, W.A., Scalo, J., 1982, ApJ, 269, 531

Salpeter E.E. 1955, ApJ, 121, 161

Sanders, D.B., Scoville,N.Z., Solomon, P.M., 1985, ApJ, 289, 373

Scalo, J., 1990, in Physical Processes in Fragmentation and Star Formation, eds R.Capuzzo-Dolcetta, C.Chiosi, A. deFazio (Kluwer, Dordrecht), 151

Scalo, J., Pumphrey, W.A., 1982, ApJ, 258, L29

Scalo, J., Struck-Marcell, C., 1984, ApJ, 276, 60

Scoville, N.Z.,Yun, M.S., Clemens, D.P., Sanders. D.B., Waller W.H., 1987, ApJSS, 63, 821

Stutzki, J., Gusten, R., 1990, ApJ, 356, 513

Tatematsu, K., Umemoto, T., Kameya, O., Hirano, N., Hasegawa, T., Hayashi, M., Iwata, T., Kaifu, N., Mikami, H., Murata, Y., Nakano, T., Ohashi, N., Sunada, K., Takaba, H., Yamamoto, S., 1993, ApJ, 404, 643

Waller, W.H., Clemens, D.P.,Sanders, B., Scoville, N.Z., 1987, ApJ, 314, 397

Wilson, T.L., Walmsley, C.M., 1989, A&AR, 1,141

Chapter 3

Protostellar clusters

3.1 Introduction

Observations of star-forming regions indicate that stars form either in clusters (e.g. Trapezium, ρ Oph, etc) or associations (e.g. Taurus), or even in relative isolation (e.g. star formation in Bok globules). Isolated star formation is, however, not as prevalent, with most Galactic molecular clouds forming clusters or loose associations. The cluster mode appears to be dominant, – a significant fraction of the high and low mass stars in both the warm GMCs and the dark clouds are found in dense compact clusters (e.g., the Trapezium cluster and the ρ Oph cluster). Stars also form in loosely bound groups or associations, like the OB associations and the T-associations of low mass stars. These groups are perhaps hierarchically organised structures with sub-groups of stars and clustered on larger scales (see Larson 1995). Thus the mode of formation is apparently determined by the pre-natal environment of the cloud and reflects on the physical properties of the clouds.

Though most star formation is in an aggregated mode, few such clusters eventually survive the disruption of the molecular cloud to remain bound, as only about 10% of stars in the Galaxy are found in bound open clusters (Elmegreen & Clemens 1985). The early dynamical evolution of a protostel-

lar cluster has been studied in some detail both analytically and numerically by various authors, the main emphasis of most of these works being on the gas removal process (e.g., Elmegreen 1983, Matheiu 1983, Lada, Margulis and Dearborn 1984, Verscheuren 1990, etc). The dynamical evolution of an embedded star cluster as it begins to disperse the molecular material surrounding it, was studied numerically by Lada, Margulis & Dearborn (Lada, Margulis & Dearborn 1984). They found that the stellar winds from the cluster members and other disruptive radiative effects of the young stars, serve to weaken the central gravitational potential of the cloud via gas dispersal, which causes a decrease in the binding energy of the cluster. The cluster thus gradually expands and if the loss in gravitational potential is high enough the cluster becomes unbound. Therefore the formation of a bound cluster is determined by the amount of mass contained in the stars. The latter is usually expressed in terms of a quantity called the star formation efficiency (SFE) η, of a cloud and is the fraction of the total core mass converted into stars during the star formation process. A qualitative estimate of the SFE can be made by making certain simplifying assumptions. For the star cluster to remain bound, the total energy after gas removal must be negative. For a cloud initially in virial equilibrium, the total energy E_0, is equal to one-half its potential energy and hence equal to

$$E_0 \sim \frac{GM_T{}^2}{2R} \qquad \text{where} \qquad M_T = M_\star + M_G$$

is the total mass and $M_\star$ and M_G represent the stellar and gas masses. Assuming that gas dispersal is instantaneous, the energy lost by the system via gas dispersal is equal to the binding energy of the gas and thus the condition for a bound state of the final system is

$$-\frac{GM_T{}^2}{2R} + \frac{GM_TM_G}{R} \leq 0 \quad \text{which reduces to} \qquad M_G \leq \frac{M_T}{2}$$

Expressed in terms of the SFE, η,

$$\eta = \frac{M_\star}{M_\star + M_G} \geq 0.5$$

The formation of a bound cluster therefore requires a SFE of at least 50%. The required SFE is lower for a gradual removal of gas, that allows the system to evolve quasi-virially. In their numerical analysis, Lada, Margulis & Dearborn considered different gas dispersal mechanisms, and the SFE needed to form a bound cluster was found to lie between 30% to 50%. Inclusion of magnetic fields leads to a lower SFE ($\sim$ 20–25%) for the emergence of a bound cluster (Elmegreen & Clemens 1985, Verscheuren 1990).

Most of these studies, however, consider the evolution of the embedded protocluster subsequent to star formation, as a cluster of stars in a homogeneous medium. Molecular clouds are known to be highly inhomogeneous structures consisting of dense concentrations of gas or cores, which could influence the dynamics of the embedded protostars, even prior to gas dispersal. The formation of a star cluster involves the gravitational collapse and subsequent fragmentation of a dense core region in a molecular cloud. Since star formation is not a very efficient process with a relatively small fraction of the cloud mass being converted into stars (e.g. Lada 1991), the collapse phase culminates in a young star cluster embedded in gas and those clumps which do not undergo collapse to form stars. Alternatively, stars may drift out of their parent core fragments, and the dynamics of the protocluster is also affected by these remnant clumps. (e.g. the spatial offset of IRAS sources from the CS peak intensity positions in star-forming regions, McCaughrean et al 1991). This has also been theoretically suggested by Price and Podsiadlowski (1995) who propose that encounters between protostellar clumps, and those between clumps and protostars could lead to removal of the embedded protostar from its parent clump. In the early stages of protocluster evolution, it is thus very likely that the system consists of protostars and clumps embedded in molecular gas. Clumps being relatively more massive than the stars they form, are expected to significantly influence the motion of stars through gravitational encounters. The dynamics of the clumps themselves influences the

initial stages of the evolution of a protocluster.

It is thus important to study the evolution of the clumps, to assess their role in the early dynamical evolution of the protostar cluster. The dynamics of protostellar clumps in molecular clouds was discussed in the previous chapter and it was found that dynamical drag due to the interclump gas causes a spatial segregation of mass along with a central clustering of the highest mass clumps. This chapter describes the effects of gas drag and the dynamics of the clumps and protostars in a young protocluster through numerical simulations, the main aim being the dynamical evolution of the protostellar system. It is found that the presence of massive clumps and their dynamics in the cluster-forming region strongly affects the motion of the lower mass protostars. The protostar-cluster expands in the course of its dynamical evolution and a few of the lowest mass objects get ejected out of the cloud via gravitational encounters. This may explain the observations of the so-called "isolated" T-Tauri stars seen in surveys of star-forming clouds, which appear to be located far from active star-forming sites (e.g., Scalo 1990, Alcala et al 1995, Neuhäuser et al 1995). These stars apart from their spatial separation are found to be in low-density regions contrary to expectations of star-formation theories which require association with dense gas (de La Reza 1989). They are also found to be too young to have drifted to their present positions from a neighbouring star cluster, assuming drift velocities of the order of the internal stellar velocity dispersion in the cluster which is typically $\lesssim$ 1 kms^{-1}. We propose (Gorti & Bhatt 1996) that these stars have been ejected from their formation sites in dense regions by N-body interactions with other clumps and stars in the cloud. Encounters between clumps and protostars lead to the formation of a halo of low-mass protostars around the system. Large halos of weak-lined T Tauri stars have been observed around star-forming regions by the ROSAT all-sky survey and it is suggested that these halos are formed by the processes discussed in this chapter (Alcala et al 1995, Sterzik et al 1995). The implications of the results

on the apparent SFE of the cloud and further evolution of the protocluster are discussed briefly.

3.2 Embedded protocluster

Mathematical model In our analysis, we adopt a simplified model for the molecular cloud and the embedded protocluster. A molecular cloud is presumed to consist of two distinct components, the high-density clumps and interclump medium (hereafter abbreviated as ICM), as earlier. The clumps are modelled as spherical particles that move through the smoothly distributed ICM. The ICM is treated as a homogeneous substrate of gas distributed according to a Plummer density profile given by

$$\rho(r) = \rho_0 \left(1 + \frac{r^2}{{r_0}^2}\right)^{-5/2}$$

where r_0 is a scalelength, chosen here to be equal to half the cloud radius, and r is the distance from the centre of the cloud. ρ_0 denotes the density in the central regions of the cloud and is determined by

$$\rho_0 = \frac{3\ M}{4\ \pi\ {r_0}^3}$$

where M is the mass of the cloud. The cloud density distribution is truncated beyond the assigned cloud radius. The velocity dispersion of the ICM is equal to the virial velocity of the entire cloud. About $\sim$ 50% of the total cloud mass is assumed to be contained in the ICM. The quantity ρ_0 is determined from the assigned cloud parameters given in Table 3.1. The parameters are chosen so that they represent the conditions in a typical star-forming cloud. The clumps follow a power law distribution in mass. Thus, $dN/dM \propto M^{-x}$ where dN is the number of objects with mass between M and $M + dM$ and $x = 1.5$ as determined from observations (e.g. Genzel 1992). The cloud also contains the embedded protocluster which forms a small fraction of the total

Table 3.1:

Cloud mass ($M_\odot$)	10^4	Number of stars	105
Cloud size (pc)	3.2	Number of clumps	105
Average density (cm^{-3})	1600	Maximum mass of clumps ($M_\odot$)	200.0
Total mass in clumps ($M_\odot$)	4612	Minimum mass of clumps ($M_\odot$)	10.0
Total mass in stars ($M_\odot$)	128	Maximum mass of stars ($M_\odot$)	10.0
Mass spectrum index of stars	2.35	Minimum mass of stars ($M_\odot$)	0.5
Mass spectrum index of clumps	1.5		

mass of the cloud. The protostar masses are also distributed according to a power law whose index x has the Salpeter value of 2.35. The details of the mass distribution are again given in Table 3.1.

Initial conditions The clumps are distributed randomly in position within the cloud radius, such that the average density of clumps in the cloud is approximately a constant. The overall distribution of molecular material in the form of uniformly distributed clumps and a gas substrate with a Plummer density profile, results in an approximate $1/r$ profile for the total density of the cloud, in accordance with observations. The velocities of the clumps are randomly drawn from a Gaussian distribution with a mean equal to the virial velocity for the entire cloud. An upper cut-off in velocities is imposed at the escape velocity of the cloud at the cloud radius, so that there is no initial escape of clumps from the cloud. The velocity vector is randomly oriented in space with its magnitude as determined above. The positions and velocities for the protostars are also determined in a similar manner.

Forces and softening The system (clumps and stars) evolves under the influence of the gravitional forces due to the various components and the dynamical friction drag due to the ICM. The ICM is considered static and only provides a source of gravitational potential. The potential arising from the gas

is derived from the Plummer density distribution, and the corresponding force obtained. Thus

$$\vec{F}_{gas}(r) = -\vec{\nabla}\Phi = -\vec{\nabla}\frac{\Phi_0}{[1+(r/r_0)^2]^{1/2}} \tag{3.1}$$

where the symbols have their usual meaning. The gravitational force acting on a clump or star due to the other objects is obtained from a simple summing of the individual contributions

$$\vec{F}^k_{N-body} = -Gm_k \sum_{i,i\neq k}^{N} \frac{m_i \vec{r}_{ij}}{(r_{ij}^2+\epsilon^2)^{3/2}} \tag{3.2}$$

where the summation is over both clumps and stars and ϵ is the softening parameter. The use of the softening parameter was briefly described in the previous chapter, in section 2.2.3. Inclusion of the softening parameter modifies the force expression, so that the force does not tend to infinity for a zero separation, as is the case for interactions of point masses. The resulting interaction is characteristic of two penetrable spheres of radius ϵ. This prevents variables of the equations from attaining extremely large values which may render the time integrations inaccurate. The choice of ϵ is critical to the nature of the present problem as the dynamics of protostars in the presence of massive clumps is being investigated. Encounters between stars and clumps are to be modelled with care and therefore are best treated exactly. This requires a model for the clumps which are assumed to be constant density gas spheres, with sizes determined by their masses. In order to keep the force evaluation as accurate as possible, the softening parameter is varied according to the nature of the encounter and is different for stars and clumps. A variable softening length is used for the clumps where ϵ is scaled with the clump mass. It is assumed that the clumps all have a constant density ($\sim 10^6$ cm^{-3}) and ϵ_c is set equal to the clump radius. For clump-clump encounters, the smaller of the softening lengths is used. Star-star encounters are modelled with a fixed softening length, ϵ_s. The mean separation between stars distributed uniformly within the cloud, is given by $R^{1/3}/N$, which for the parameters chosen, is ~ 5

10^{-3} pc. ϵ_s is chosen such that it is much smaller than the mean separation, and is assigned a value 10^{-4} pc. Star-clump encounters are treated exactly within the above model for the clump. *No softening is used for separations larger than* ϵ_c. Since the clumps and stars are chosen to have non-overlapping mass spectra, clumps are always more massive than stars and the force acting on the clump due to a star-clump encounter is softened with the constant softening parameter, ϵ_s.

As discussed in Chapter 2, the clumps and stars are also acted upon by a dyamical friction force due to the ICM given by (Chandrasekhar 1943, Binney & Tremaine 1987)

$$\vec{F}_{drag}(r) = \frac{4\pi \ln\Lambda G^2 \rho(r) M^2}{v^3}\left[erf(X) - \frac{2X}{\sqrt{\pi}}exp(-X^2)\right]\vec{v} \qquad (3.3)$$

where $\vec{v}$ is the velocity of the clump, G is the gravitational constant, M is the mass of the clump, ρ is the density of the gas and $\ln\Lambda$ is the Coulomb logarithm, Λ being equal to the ratio of maximum to minimum impact parameters. (The maximum impact parameter $b_{max} \sim R$, the radius of the cloud, and the minimum impact parameter $b_{min} = GM/v^2$, so that $\Lambda \sim Rv^2/GM$.) the gas velocity distribution is assumed to follow a Maxwellian distribution with a dispersion σ (the virial velocity for the cloud), and X is a dimensionless parameter equal to $v/(\sqrt{2}\sigma)$. The equations are integrated in time using a fourth order Runge-Kutta method.

It should be noted here that no accretion processes are considered here and the masses of the protostars/clumps do not change with time. This simplification is not expected to affect the results as the mass accreted (within timescales of interest) here is very low (see Chapter 2). Effects of magnetic fields and collisions between clumps are beyond the scope of this work and have not been included.

3.3 Dynamical evolution of protoclusters

The dynamics of the embedded protocluster is determined by the potential due to the gas, encounters with the massive clumps, and effects of gas drag on the clumps and the protostellar members themselves. A better insight into the evolution of the protocluster can be obtained by studying the different factors governing protocluster dynamics separately. We consider three different initial configurations. In the first run, the system consists of the ICM, the clumpy constituent and the protostars as described earlier. We also study cases in which the gas distribution is smooth with no clumps and another where there is no drag due to dynamical friction acting on the clumps and the stars.

Clumpy gas distribution The system was evolved numerically for a few cloud crossing times (the crossing time is given by the ratio of the spatial extent of the system to the average velocity and is thus $\sim R/\sigma \approx 10^6 years$). It is found that there is an overall expansion of the protostar/clump system with the formation of a centrally dense region. There is a mass segregation established in the cloud with the more massive objects concentrated towards the centre of the cloud and the lower mass objects moving on orbits which take them far from the cloud centre. Figure 3.1 shows spatial plots of the system at different times, where protostars are denoted by asterisks and clumps by open circles. The large circle is drawn at twice the cloud radius (i.e., at 2R, where R, the radius of the cloud is defined as twice the scalelength r_0, of the density distribution). The protostar system continuously expands with time and a few objects move in large orbits which take them out of the cloud system. In about 5 Myr (1 Myr=10^6 years), about 10% of the protostars are at distances greater than twice the cloud radius. It is also seen that a few clumps (2 out of 105 in number) also lie outside this boundary. The average positions of clumps and stars at different instances of time are plotted in Figure 3.2 where open circles denote the average radial distance from the cloud centre, <r>, for clumps, and

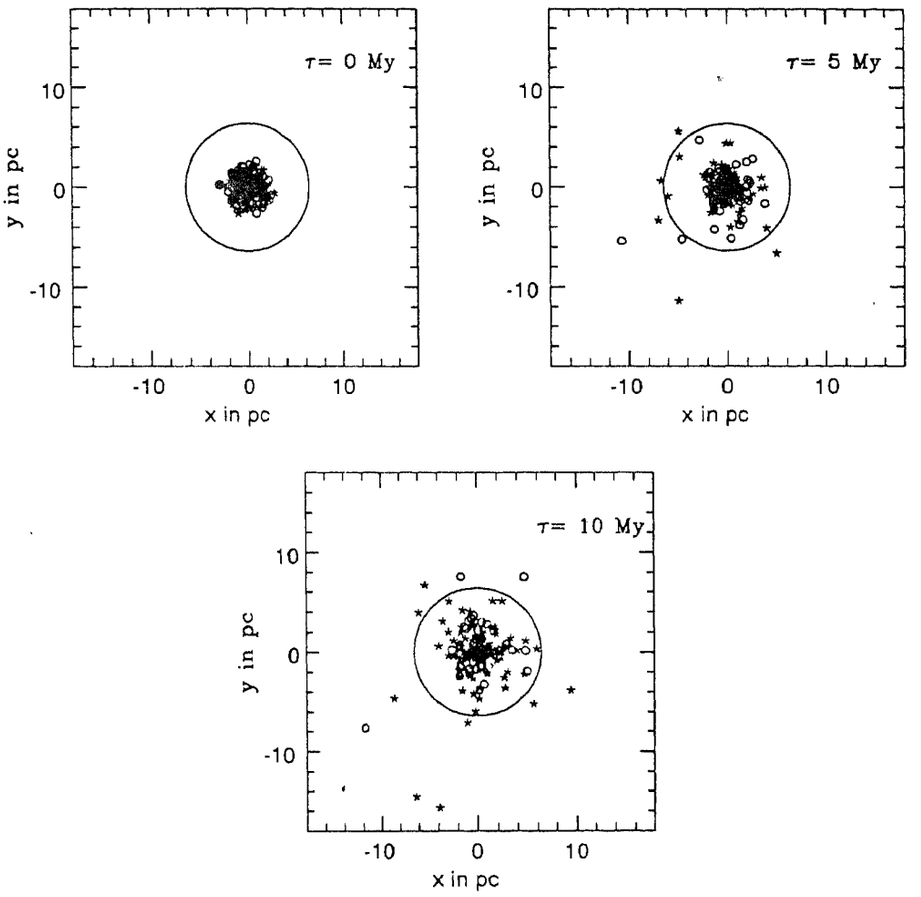

Figure 3.1: *The plots show the projected spatial positions of the clumps (denoted by open circles) and stars (denoted by asterisks) at three different epochs. The large circle is drawn at twice the assigned cloud radius.*

asterisks that for the stars. The protostar system expands considerably with time as can be seen from the figure, as compared to the clump system. The average radial position of the clumps, <r>, remains approximately constant in 10 Myr, whereas <r> for the protostars steadily increases to almost twice its initial value.

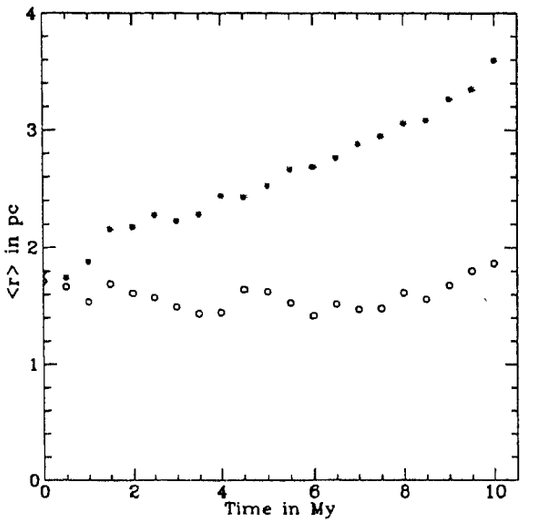

Figure 3.2: *The figure shows the average radial distance for the stars (asterisks) and clumps (open circles) at different times as the system evolves. This figure corresponds to the case with a clumpy gas distribution with dynamical drag included.*

Clumpy gas distribution with no gas drag The system was also evolved under only gravitational forces, excluding the gas drag. The clumps and stars thus move under the influence of the gas potential and the N-body forces. The plot of average positions for the two components against time is shown in Figure 3.3. The protostellar and clump systems are both seen to expand slightly with time, with no significant difference in their evolution. The protostellar system expansion is marginally more than that of the clump system.

Smooth gas distribution Though molecular clouds are known to be clumpy in nature, with a large fraction of their mass in high density clumps, we study here a hypothetical case where the gas is smoothly distributed throughout the cloud. This is done so that the the dynamical influence of clumps on an embedded protocluster can be studied, by comparison with the earlier simulation.

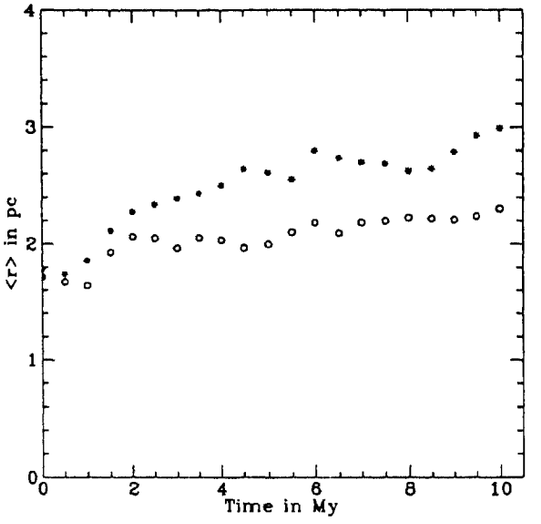

Figure 3.3: *Same as Figure 3.2 for a clumpy gas distribution and no dynamical drag*

In order to study the effect of the gas distribution on the dynamics of the protocluster, an equivalent mass of gas as was contained in clumps earlier, was distributed uniformly over the cloud. Thus the cloud gas consists of the ICM distributed according to a Plummer density profile and some gas distributed uniformly through the cloud. This is done so that the overall potential as seen by the stars remains unaltered and the timescales of the system do not change. The average of the radial positions of the stars is plotted against time in Figure 3.4 and on comparing with Figure 3.2, it is evident that there is relatively little expansion of the protocluster system.

3.4 Discussion

Embedded protostar clusters in molecular clouds appear to be dynamically influenced by the presence of clumps in the cloud cores. The three cases

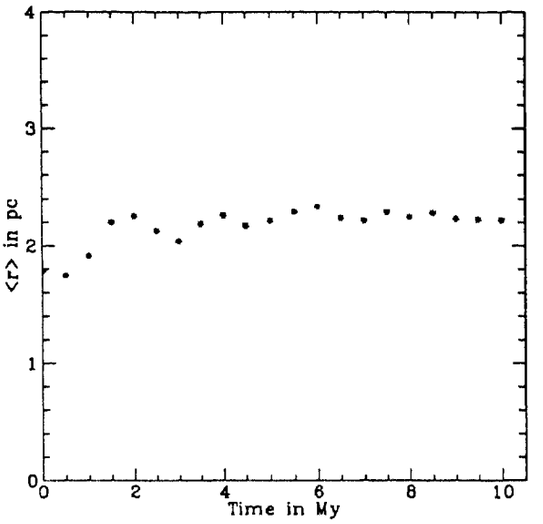

Figure 3.4: *Same as Figure 3.2 for a smooth gas distribution and dynamical drag included.*

considered above, clearly demonstrate that the combined effects of gas drag and encounters with clumps in the cloud, largely determine the evolution of the protostars. This is to be expected, as the clumps are more massive than the protostars, and contribute significantly to the gravitational potential of the cloud. The dynamical evolution of the clumps thus plays an important role in governing the dynamics of the protostellar cluster.

3.4.1 Drag and relaxation of the protocluster

The effect of dynamical friction on clumps is to cause a spatial mass segregation in the cloud. As the frictional force is mass dependent, the more massive clumps are dragged down preferentially with respect to the low mass objects and settle towards the centre of the cloud. This deepening of the gravitational potential well at the centre of the cloud affects the dynamics of the lower mass protostars/clumps which gain kinetic energy via three(few)-body encounters

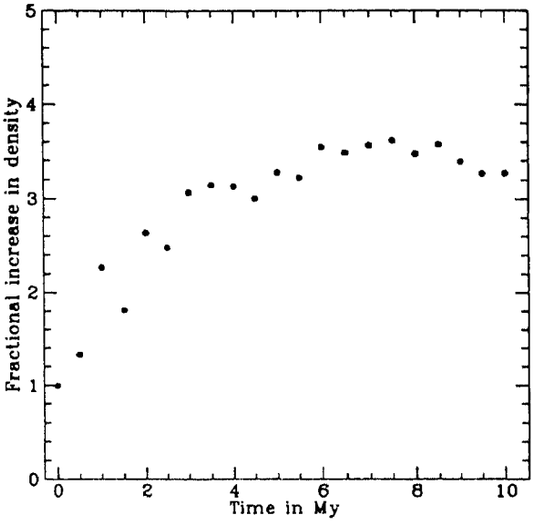

Figure 3.5: *The ratio of the central core density ($r_0/2$) at a given epoch, normalized to its initial value, against time*

during the passage through the cloud interior. The density at the centre of the cloud increases due to mass segregation. This can be seen from Figure 3.5, where the fractional increase of density in the central core of the system is plotted against time. The core has been defined as the region within half the scalelength ($r_0/2$). The density of the core is computed by adding the masses of all objects that lie within $r_0/2$ from the cloud centre, and the gas mass in the core. The fractional increase of density at a time t, is the ratio of the initial core density to that at time t. The density of the core is thus seen to increase by more than a factor of 3 within 10 Myr. The accumulation of massive clumps at the centre forms binaries or few-body systems, which influence the subsequent evolution of the protocluster. Encounters of a passing object with the central core, result in an exchange of kinetic energy. In most cases, the object gains energy and for low-mass protostars, the energy gained takes them to distant orbits and in some cases they may gain sufficient energy

to escape from the system. The formation of a dense nucleus in the system also causes scattering of the halo orbits and results in an exchange of energy. This causes low mass protostars/clumps to move in larger and larger orbits with successive interactions, and a gradual expansion of the halo. Thus the system tends towards a state where the dense central region continues to lose energy and becomes increasingly bound. This is accompanied by the formation of an extended halo, by the low-mass objects that gain kinetic energy during the process.

Equipartition of energy due to gravitational two-body encounters also leads to mass segregation in an N-body system, as seen in section 2.3 of the previous chapter, and re-iterated here. Cumulative effects of multiple gravitational encounters cause velocity deflections, which over a period of time, are as large as the typical velocity, v, of the system. The timescale over which the change in velocity $\Delta v \sim v$, is called the relaxation time of the system and is approximately the time taken for equipartition of energy. Successive encounters ultimately bring about a redistribution of kinetic energy, and equipartition. Massive objects hence lose their velocity and sink to the centre of the system, whereas lower mass objects gain energy which takes them to higher orbits. Thus mass segregation is established. This can be seen from Figure 3.3, for the run with no dynamical friction included. The higher mass clumps occupy a slightly lower average radial position than the protostars and the difference in evolution indicates mass segregation due to equipartition. Figure 3.2 shows the combined effects of mass segregation due to both equipartition of energy and dynamical friction. Dynamical friction is more pronounced on the higher mass clumps and is a decisive factor governing their dynamical evolution. The gas drag, being smaller for lower mass objects, does not significantly affect their motion directly but causes an "accelerated relaxation" of the system in relatively short timescales, through encounters or scattering by the massive clumps.

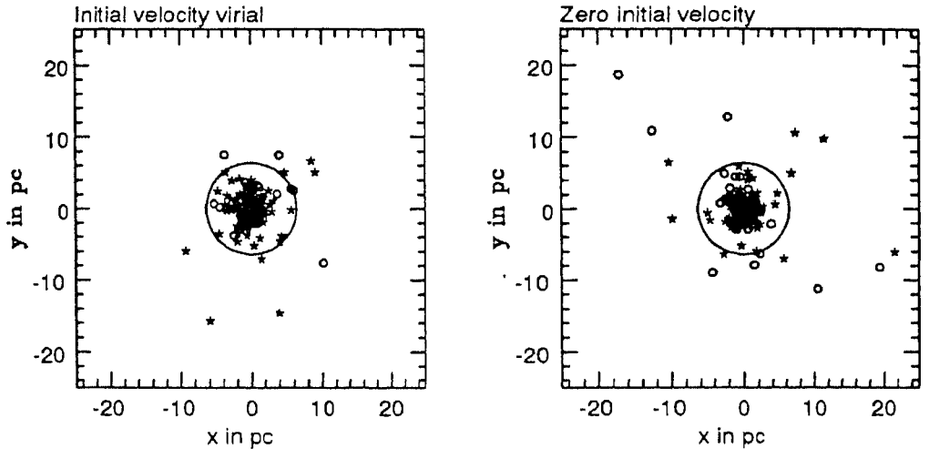

Figure 3.6: *Spatial positions for two different initial conditions are shown in the two panels. The notations used are the same as that for Figure 3.1.*

It should be noted that the timescale is dependent to some extent on the initial conditions, especially the initial velocity distribution. If the stars that form after fragmentation have a velocity distribution that is subvirial, the cluster goes through a collapse phase and stabilizes after a few oscillations. The protocluster undergoes violent relaxation, which is due to the collective scattering by groups of objects rather than individual encounters. Equipartition is achieved, not of energy, but of energy per unit mass. This relaxation does not lead to mass segregation but there is an ejection of cluster members as the cluster attempts to gain stability. Ordinary two-body relaxation also goes on simultaneously and takes over after the initial stages of evolution. The change in dynamical evolution caused by considering different initial velocity distributions was studied through simulations. The spatial positions of the clumps and stars for two cases, after 10Myr, are indicated in Figure 3.6. The two panels correspond to a case where the initial velocities of the objects were drawn from a Gaussian distribution with a mean at the virial velocity of the system, and the other to a case where the the particles were given zero initial

velocities. The latter condition causes a violent relaxation of the system, as desribed earlier. It is seen that a greater fraction of objects get ejected from the system, and that they also move to greater distances. Further, a significant fraction of *clumps* are also thrown out to large distances, as expected during violent relaxation.

3.4.2 Ejection of low-mass protostars

As can be seen from Figure 3.1, a few objects are ejected out on very short timescales. There is thus a gradual evaporation of stars from the cluster with time, with some of the protostars thrown out to very large distances. The loss of low-mass protostars from the embedded cluster takes place in typically a few cloud crossing timescales or about a few 10^6 years. The clusters remain embedded in the parent cloud material for about 10^7 years which is the typical duration of the star formation phase. The presence of isolated T Tauri stars far from active star-forming regions and with no associated dense gas can thus probably be explained by the dynamics of the protostar cluster/cloud it formed from. Harder encounters than ones considered here, such as those involving protostellar binary systems, may lead to further rapid ejection of protostars (Kroupa 1995). It might appear from Figure 3.2 that the stars are perhaps expanding in an *unbound* halo. This is not so, however, as the fraction of stars that escape from the system ($\sim$ 6 % in 10 Myr), is found to be small, even for evolution times longer than 10 Myr.

The cloud here is considered an isolated system and in more complex environments, other forces could affect the dynamics of the protostars and clumps in the outer regions of the cloud. Molecular clouds usually have multiple star-forming sites within them, an example of which is the Orion A cloud, with the Trapezium cluster and the star cluster associated with the Kleinman-Low nebula (e.g. Genzel 1992). The presence of nearby protostar clusters could perturb the motion of protostars in the outer regions. Other forces include

nearby molecular clouds themselves, and larger scale forces such as the Galactic tidal field. These external forces act to disrupt the cluster and *the fraction of unbound stars in such realistic situations would in fact be larger than that obtained in this analysis.*

3.4.3 Formation of a halo

Another implication of the dynamical evolution of the system is the preferential loss of low mass objects. If protostar clusters lose their low mass members in the initial stages of evolution, the real star formation efficiency of the cloud could be very different from that deduced by observations. Observed protostar clusters could very well be systems in an evolved dynamical state which have lost many of their low mass stars and have formed a dense nuclear region containing the higher mass objects. Observations of star-forming regions around clouds reveal the presence of large numbers of low-mass stars distributed in extended spatial regions. The discovery of these T Tauri stars was made through the ROSAT all-sky X-ray survey around the Chameleon and Orion star-forming regions (Alcala et al 1995, Sterzik et al 1995). It has been proposed that the halo arises from a contribution by high-velocity stars produced during close encounters in young multiple ($N \sim 5$) systems (Sterzik & Durisen 1995). The multiple system is the outcome of the fragmentation of a rotating (elongated) core during isothermal collapse, and the protostars formed evolve under their mutual gravitational interactions, resulting in the ejection and escape of some members. The large numbers of stars observed in the halos suggests that this mechanism is probably supplemented to a considerable extent by that suggested in this chapter. It is to be noted that the combined effects of dynamical friction and the presence of remnant clumps result in a halo that is likely to contain a few higher mass stars as well, as the detailed outcome is dependent on specific encounters during evolution. Our model is general and not contingent on any particular fragmentation process.

It thus applies equally well to conditions in GMCs and DCs. Production of a halo of low mass stars is also possible through close three-body encounters in dense stellar systems, resulting in the ejection of 5–10% of members (Kroupa 1995), which then populate the halo.

The ejection and loss of low-mass stars also holds implications for the SFE of a cloud. The apparent SFE of the cloud is then underestimated as the mass contained in ejected protostars is not accounted for. The increased binding energy of the remaining members of the cluster reduces the size of the system and raises the local SFE of the cloud. It should be noted that in the present simulation, the stars form a very small fraction of the total cloud mass and hence we do not address the issue of SFE and survival of bound clusters here. Young protostar clusters with high stellar densities like the Trapezium, however, evolve in similar physical conditions and the general results are probably still applicable.

It is to be noted here that the present calculation may lead to an enhanced ejection of stars, as they are initially scattered throughout the cluster. Different results may be obtained if the stars were originally in a self-gravitating subsystem, as might result from the fragmentation of one of the clumps. The internal dynamics of a forming star cluster while it is still embedded in its parent cloud may thus play a significant role in determining whether the group of protostars emerges as a bound cluster after gas dispersal or is disrupted. In this work, the cloud was treated as an isolated system which contains embedded protostars and clumps with a range of masses. Star-forming molecular clouds are not, however, isolated systems and many of them have multiple star-forming sites. Examples are the Orion A cloud with the Trapezium cluster and the BN-KL cluster, the Orion B Cloud and the dark cloud complexes like the Taurus complex which have many groups of stars (e.g., Lada 1991, McCaughrean 1991, Larson 1995). The presence of nearby clusters/clumps can affect the motion of objects which lie on orbits which take them far from the

centre of the cloud. These stars may never re-enter the cluster and could get captured by other systems or drift away once they reach the cloud boundaries.

3.5 Conclusions

The evolution of an embedded protostar cluster in a molecular cloud is studied by numerical simulations. Massive clumps in the cloud strongly affect the dynamics of the embedded protostars. Mass segregation of clumps due to dynamical drag by the interclump gas results in the formation of a dense central region and the lower mass protostars get preferentially ejected out of the cloud via gravitational encounters. This explains observations of T Tauri stars which appear to be isolated from active star-forming sites and are in regions devoid of dense gas. The loss of low mass protostars in the initial stages of evolution indicates that the real SFE of a cloud is higher than inferred from observations. Embedded protostar clusters are probably dynamically evolved systems with large halos of low mass protostars. Multiple star formation sites in clouds being common, outer members are subject to velocity perturbations due to massive clumps and other clusters, possibly leading to a faster removal of objects.

References

Alcala J.M., Krautter J., Schmitt J.H.M.M., Covino E., Wichmann R., Mundt R., 1995, A&A Suppl. Ser., in press

Binney J., Tremaine S., 1987, Galactic Dynamics. Princeton Univ. Press, Princeton, NJ

Chandrasekhar S., 1943, ApJ, 97, 255

de La Reza et al, 1989, ApJL, 343, L61

Elmegreen B.G., 1983, MNRAS, 203, 1011

Elmegreen B.G., Clemens C., 1985, ApJ, 294, 523

Genzel R., 1992, in Burton W.B., Elmegreen B.G., Genzel R., eds, The Galactic Interstelar Medium. Springer-Verlag, Berlin

Gorti U., Bhatt H.C., 1996, MNRAS, 278, 611

Kroupa P., 1995, MNRAS, in press

Lada C.J., Margulis M., Dearborn D., 1984, ApJ, 285, 141

Lada C.J., 1991, in Physics of star formation and early stellar evolution, eds Lada C.J. and Kylafis, N.

Larson R.B., 1990, in Physical Processes in fragmentation and star formation, eds Capuzzo-Dolcetta R., Chioisi C., Di Fazio A., p390 (Kluwer,Dordrecht)

Larson R.B., 1995, MNRAS, 347, 340

Mathieu R.D., 1983, ApJL, 267, 97

McCaughrean M., 1991, ApJL, 371, L34

Neuhäuser R., Sterzik M.F., Torres G., Martin E.L., 1995, A&A, 299, L13

Scalo J., 1990, in Physical Processes in fragmentation and star formation, eds Capuzzo-Dolcetta R., Chioisi C., Di Fazio A., p163 (Kluwer,Dordrecht)

Sterzik M.F., Alcala J.M., Neuhäuser R., Schmitt J.H.M.M., 1995, A&A, 297, 418

Sterzik M.F., Durisen, R.H., 1995, A&A, 304, L9

Verscheuren W. 1990, A&A, 234, 156

Wilking B., Lada. C.J., 1989, in Protostars and Planets II, eds Black & Matthews, p297 (Univ. Of Arizona Press, Tucson)

Chapter 4

Orbital decay of binaries

4.1 Introduction

Studies of star formation and early stellar evolution have, in the past, mainly concentrated on the processes involved in the formation of a single star. These have yielded a plausible sequence of events that lead to the formation of an optically visible young star from the gravitational collapse of a dense molecular cloud core (e.g., Shu et al 1987). Observations of main-sequence stars and of present-day star formation sites, however, indicate that binary and multiple systems of stars are more common and also that most star formation activity produces groups of stars rather than individual objects. Recent discoveries of large numbers of pre-main-sequence (PMS) binary systems, in both high-mass and low-mass star-forming regions, indicate that binaries are formed very early in the star formation process, probably even during the collapse phase itself. The formation of binaries thus appears to involve processes differing from or additional to those for a single star. Observational studies of main-sequence binaries of F and G type dwarfs in the solar neighbourhood (Abt 1983, Duquennoy and Mayor 1991) indicate certain characteristic features, which are summarized below.

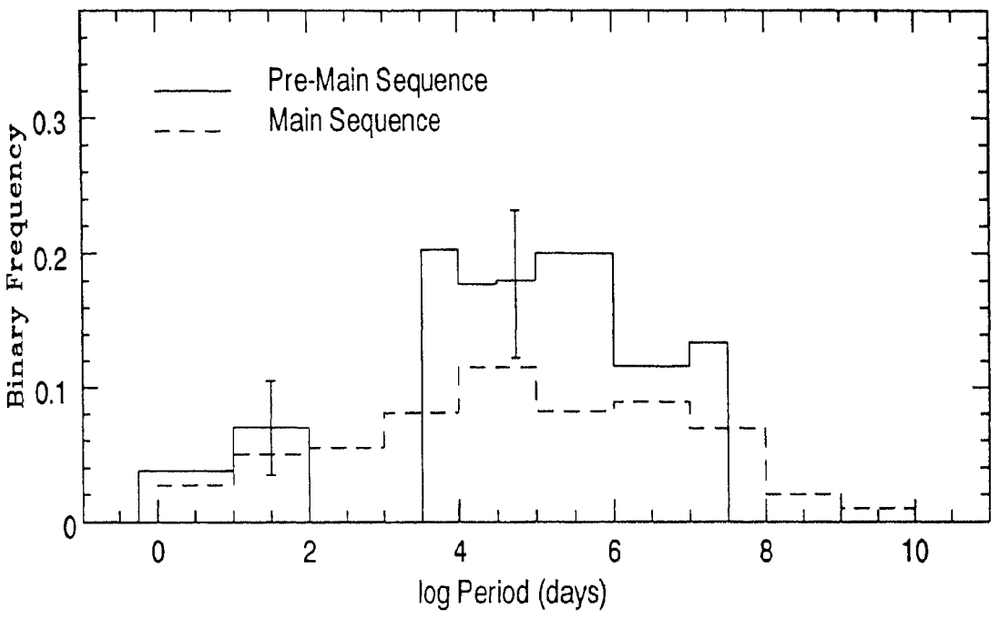

Figure 4.1: *The frequency distribution with period of main-sequence and pre-main-sequence stars. (From Mathieu 1994)*

- A high fraction ($\sim$ 70%) of stars are members of binary systems
- The frequency distribution of periods of binaries follows a log–normal distribution and has has a single peak at about 180 years
- There appears to be a period–eccentricity relation, with the a tendency for the closest binaries (with periods of the order of a few days) to move on circular orbits
- The masses of the primary and secondary may be correlated, though the mass ratios observed are consistent with random pairing from an initial mass function.

These observations have provided constraints on theories of binary formation, which in recent times have been made more stringent by observations of PMS binaries themselves. The frequency distribution with period of PMS binaries appears also to have a single peak, but with seemingly a larger fraction of stars in binaries, as compared to the MS stars (see Figure 4.1). There is a distinct peak in the frequency distribution at around 180 years for the MS binaries, and the number of binaries decreases towards longer and shorter periods (and separations). The peak for the PMS binaries is less well-defined and appears at approximately the same period as that for the MS binaries. PMS binaries also exhibit a wide range of eccentricities and periods and are coeval. For a recent detailed review of PMS binary stars, refer Mathieu (1994). (Also see reviews by Reipurth & Zinnecker 1993, Leinert et al 1993, Bodenheimer 1992 and for theoretical aspects of binary formation, Pringle 1991, Boss 1992). Theories for binary formation, thus in addition, must also explain the above observed characteristics of the binary population. There have been various mechanisms proposed to form binaries, which include (a) capture of individual stars by dissipation through tides, disks or residual gas, (b) fission of a collapsing rotating cloud core into two nuclei, (c) formation of a binary during hierarchical fragmentation of a collapsing cloud core and (d) instabilities in circumstellar disks. The observed smooth distribution of frequency with period for MS binaries with a single peak, suggests the presence of a characteristic lengthscale and perhaps a single dominant mode for binary formation, if there were no further evolution of the binary orbit. Alternately, different formation mechanisms acting on different lengthscales could all be equally important and would be expected to produce multiple peaks in the frequency distribution of periods. The observed smooth distribution may then be due to an evolutionary process subsequent to formation that changes the binary orbital parameters. As binaries form as condensations out of a molecular cloud, it is possible that their general properties depend on the physical properties of the parent molec-

ular cloud/core. This is especially so, if the dominant formation mechanism is one of fragmentation, (e.g, Pringle 1991, Bodenheimer et al 1992, Boss 1992) where the properties of the fragments themselves are largely determined by the initial conditions in the collapsing cloud (e.g., Bodenheimer 1980, Boss 1992). In fact, observations of PMS binaries in different star-forming regions do appear to indicate some differences in their features; the frequency of binaries may be lower in high-mass star-forming regions (binary-surveys of the Trapezium cluster region, Prosser et al 1994) and there appears to be an excess of short-period binaries in the Ophiuchus-Scorpius region as compared to the Taurus-Auriga region, (Mathieu 1992). Apart from an intrinsic difference in the nature of the protostellar cores formed subsequent to fragmentation, these objects probably undergo further dynamical evolution leading to an evolution of the binary properties as well. The protostellar binary is formed embedded in massive amounts of distributed molecular cloud gas. Detection of binaries among protostars as young as 10^5 years, and the fact that the observed frequency of PMS binaries appears to be as high as MS binaries, indicates that most binaries are formed during the early collapse phase. This suggests that a binary remains embedded in the cloud during much of its initial evolutionary period. Interactions with the residual gas in the cloud through various effects, can cause an orbital evolution of the protostellar binary. In this chapter, (also Gorti & Bhatt 1996) we study the influence of gas drag due to dynamical friction (Chandrasekhar 1943) on the binary, and the time evolution of its orbital parameters. The effects of introducing the dissipative drag force are investigated both analytically and numerically. Dynamical friction may be regarded as arising from a density asymmetry of the surrounding medium in the wake of a moving object which tends to retard its motion by exerting a gravitational pull on the object (Binney & Tremaine 1987, also refer Chapter 2 of this thesis). Drag due to dynamical friction depends on the density and velocity dispersion of the ambient medium, and hence orbital evolution under

different cloud conditions is considered. The evolution is also dependent on the binary parameters, such as the masses of the components, initial separation and eccentricity of the orbit. Statistically generated samples of binaries with a range of initial parameters are evolved in time to study changes in gross features of the binary population due to dissipative drag forces. Approximate analytical results are presented in Section 4.2, the numerical methods are described in Section 4.3, and Section 4.4 contains a discussion of the results obtained. Section 4.5 discusses a statistical study of PMS binaries. Sections 4.6 and 4.7 contain a discussion on the implications of the results obtained for binary formation and the main conclusions, respectively.

4.2 Equations of motion

We consider a spherical cloud of uniform density, in which the protostellar binary system is embedded. The forces considered to be acting on each component of the binary system are (i) the gravity of the cloud, (ii) the gravitational force due to the other member and (iii) the dynamical friction force due to the ambient gas. All other forces are neglected. Thus the equations of motion in a coordinate frame centered on the cloud are ,

$$\frac{d^2\vec{r}_1}{dt^2} = -4\pi G\rho\vec{r}_1 - \frac{Gm_2\vec{r}_{12}}{|\vec{r}_{12}|^3} - 4\pi \ln\Lambda_1 G^2 m_1 \rho \left(erf(X_1) - \frac{2X_1 e^{-X_1^2}}{\sqrt{\pi}} \right) \frac{\vec{v}_1}{|\vec{v}_1|^3} \tag{4.1}$$

$$\frac{d^2\vec{r}_2}{dt^2} = -4\pi G\rho\vec{r}_2 + \frac{Gm_1\vec{r}_{12}}{|\vec{r}_{12}|^3} - 4\pi \ln\Lambda_2 G^2 m_2 \rho \left(erf(X_2) - \frac{2X_2 e^{-X_2^2}}{\sqrt{\pi}} \right) \frac{\vec{v}_2}{|\vec{v}_2|^3} \tag{4.2}$$

where the last term in each of the above equations is the dynamical friction force. Here, m denotes the mass of the protostar, ρ is the density of the cloud and $\ln\Lambda$ denotes the Coulomb logarithm and is the ratio of maximum to minimum impact parameters. X is a dimensionless parameter equal to $v/\sqrt{2}\sigma$, where σ is the velocity dispersion of the cloud. The subscripts 1 and 2 in each

case refer to the corresponding quantities for the two protostars, and $\vec{r}_{12}$ the relative position coordinate $\vec{r}_1 - \vec{r}_2$.

The equations are a set of coupled non-linear differential equations and an exact solution of which cannot be obtained. Since our interest is in the evolution of the binary, the orbital evolution can be equivalently described by the evolution of the angular momentum and energy of the system. These equations are also not easily solved for the general case. However they may be approximately solved in the two limiting cases of (i) $v \ll \sigma$ where the dynamical friction term is proportional to the velocity v and (ii) $v \gg \sigma$ when the drag is proportional to $1/v^2$. The equations can then be described in terms of the reduced mass of the system.

Case (i): $v \ll \sigma$

The velocities of the two masses can be expressed in terms of the relative motion, v, and the centre of mass motion V. Thus,

$$v_1 = \frac{m_2\vec{v}}{m_1+m_2} + \vec{V}; \qquad v_2 = \frac{-m_1\vec{v}}{m_1+m_2} + \vec{V} \tag{4.3}$$

From equations 4.1,4.2 and 4.3, with the dynamical friction term now given by $-\eta m_i \vec{v}_i$ for each particle, we get

$$\frac{d^2\vec{r}}{dt^2} = -4\pi G\rho\vec{r} - \frac{G(m_1+m_2)\vec{r}}{|\vec{r}|^3} - \eta\frac{m_1m_2}{m_1+m_2}2\vec{v} - \eta(m_1-m_2)\vec{V} \tag{4.4}$$

where $\eta = 16\pi^2G^2\ln\Lambda\rho/(3(2\pi\sigma^2)^{3/2})$. On neglecting the last term, the rate of change of angular momentum can then be written as

$$\frac{d\vec{L}}{dt} = \mu\vec{r}\times\frac{d\vec{v}}{dt} = -2\mu\eta\vec{L} \tag{4.5}$$

where $\mu = m_1m_2/(m_1+m_2)$, and is the reduced mass. Therefore,

$$\vec{L} = \vec{L}_0 e^{-2\mu\eta t} \tag{4.6}$$

The time rate of change of energy and angular momentum of the orbit can be obtained in a more general manner by rewriting the equations in a Lagrangian

formulation. The generalized co-ordinates are the three–dimensional velocities and positions. The dissipative drag force can be expressed as the velocity gradient of a "dissipation function", $\mathcal{F}$, (in the limit $v \ll \sigma$) given by

$$\mathcal{F} = \eta\mu^2 v^2 \tag{4.7}$$

The rate of change of angular momentum is obtained from one of the Lagrange equations, and is equal to $-2\mu\eta L$, as was already obtained in equation 4.5. The rate of change of energy is related to the dissipation function and given by (refer e.g, Goldstein 1977)

$$\frac{dE}{dt} = -\sum_j \frac{\partial \mathcal{F}}{\partial \dot{q}_j}\dot{q}_j = -2\eta\mu^2 v^2 \tag{4.8}$$

where $\dot{q}_j$ represent the generalized velocities. It can be assumed that the system evolves quasi-virially, such that the virial theorem always holds during the motion. The binding energy of the orbit, E, is thus equal to one-half the kinetic energy and for a circular orbit, the velocity can be expressed in terms of the binding energy as $v^2 = -2E/\mu$. Thus,

$$\frac{dE}{dt} = 4\eta\mu E \qquad \text{and} \qquad E = E_0 e^{4\eta\mu t} \tag{4.9}$$

The binding energy thus increases exponentially with time. Figure 4.2 shows the time evolution of energy, semi-major axis and angular momentum of the binary system. The binary loses energy and the components move on orbits of lower energy, i.e., become more bound. The semi-major axis of the system thus decreases with time. The binary also loses angular momentum with time, and the rates of energy and angular momentum loss are such that the eccentricity of the orbit remains constant, and in this case, the orbit is always quasi-circular. The equations have also been numerically solved (see Section 3) and a comparison with the analytical solutions (equations 4.5 and 4.8) shows that though the equations have been solved for the circular orbit, they approximate reasonably well for higher-eccentricity orbits. The rate of change of eccentricity with time cannot, however, be obtained from the present solutions,

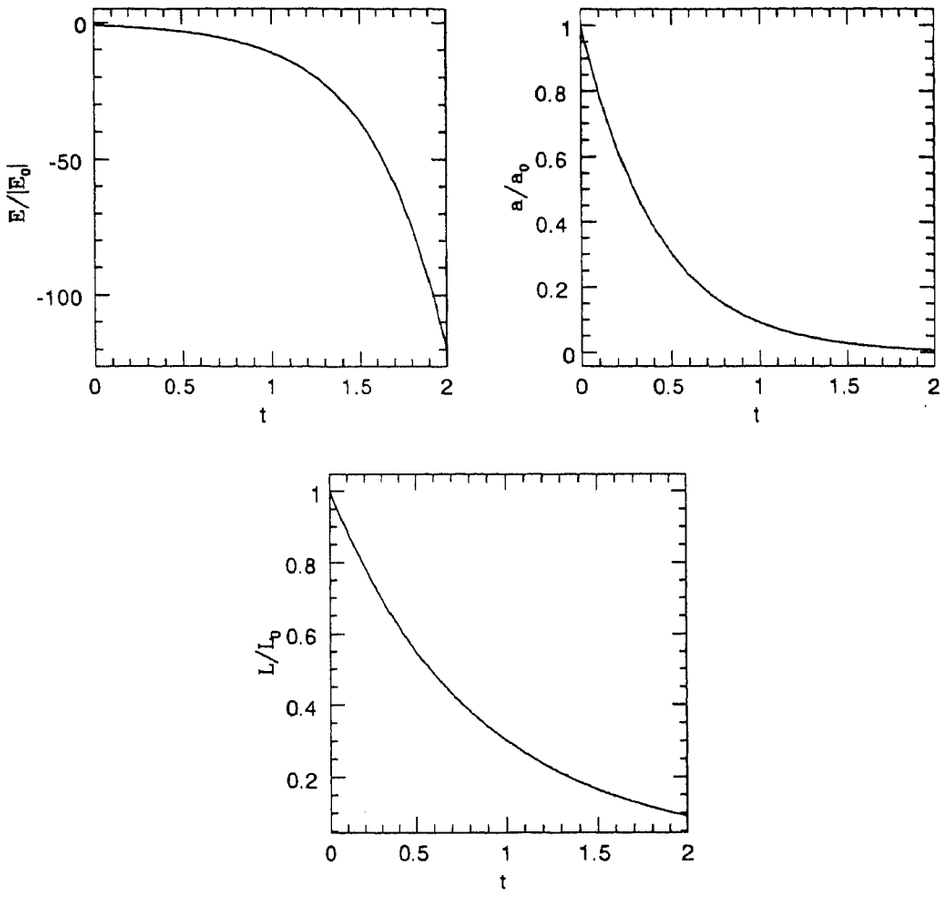

Figure 4.2: *The energy, semi-major axis and angular momentum are plotted against time, scaled by their corresponding initial values. Time is in units where* $\eta = 1$. *(Case 1:* $v \ll \sigma$*)*

as the orbit always remains circular.

Case (ii): $v \gg \sigma$

For velocities large compared to the local velocity dispersion of the background, the dynamical friction force is proportional to $1/v^2$ and the equations of motion are

$$\frac{d^2\vec{r}}{dt^2} = -4\pi G\rho\vec{r} - \frac{G(m_1+m_2)\vec{r}}{|\vec{r}|^3} - \tilde{\eta}\left(\frac{m_1\vec{v}_1}{|\vec{v}_1|^3} - \frac{m_2\vec{v}_2}{|\vec{v}_2|^3}\right), \qquad (4.10)$$

where $\tilde{\eta} = 4\pi \ln \Lambda G^2\rho$. For simplicity, it is assumed that the two masses are equal and ${v_1}^3 = {v_2}^3 \approx (v^2/4 + V^2)^{3/2}$ so that equation 4.10 reduces to

$$\frac{d^2\vec{r}}{dt^2} = -4\pi G\rho\vec{r} - \frac{2Gm\vec{r}}{|\vec{r}|^3} - \frac{\tilde{\eta}m\vec{v}}{(v^2/4 + V^2)^{3/2}} \qquad (4.11)$$

where m represents the mass of the protostars. The dissipation function $\mathcal{F}$ is thus

$$\mathcal{F} = -\frac{2\tilde{\eta}m^2}{(v^2/4 + V^{\,2})^{1/2}} \qquad (4.12)$$

The rate of change of energy is again given by equation 4.8, and assuming that the orbit is circular. Therefore,

$$\frac{dE}{dt} = \frac{2\tilde{\eta}m^{5/2}E}{(E + mV^2)^{3/2}} \qquad (4.13)$$

which is integrated by assuming that the velocity of the center of mass is a constant, and that virial equilibrium always holds. Therefore,

$$\frac{2}{3}\sqrt{E_k - E}(4E_k - E) + {E_k}^{3/2} \ln \frac{\sqrt{E_k - E} - \sqrt{E_k}}{\sqrt{E_k - E} + \sqrt{E_k}} = 2\eta m^{5/2}t + c \qquad (4.14)$$

where E_k is equal to $mV^{\,2}$ and c is the constant of integration, to be determined from the initial conditions. The equation of motion for a particle circularly orbiting a central point mass was studied by Hoffer (1985) who developed approximate expressions for the evolution of the semi-major axis of the orbit. He found that the energy of the orbit is proportional to the (2/3) power of time. It can be easily shown that the above equation corresponds to Hoffer's solution in the limit of vanishing E_k. The angular momentum equation can be obtained as earlier,

$$\frac{d\vec{L}}{dt} = -\frac{\tilde{\eta}m\vec{L}}{(v^2/4 + V^{\,2})^{3/2}} \qquad (4.15)$$

For a circular orbit, the condition for virial equilibrium gives $\mu v^2 = k/r$, where $k = Gm^2$, and hence the angular momentum

$$L = |\vec{L}| = \mu|\vec{r} \times \vec{v}| = \mu r v = \frac{k}{v} \qquad (4.16)$$

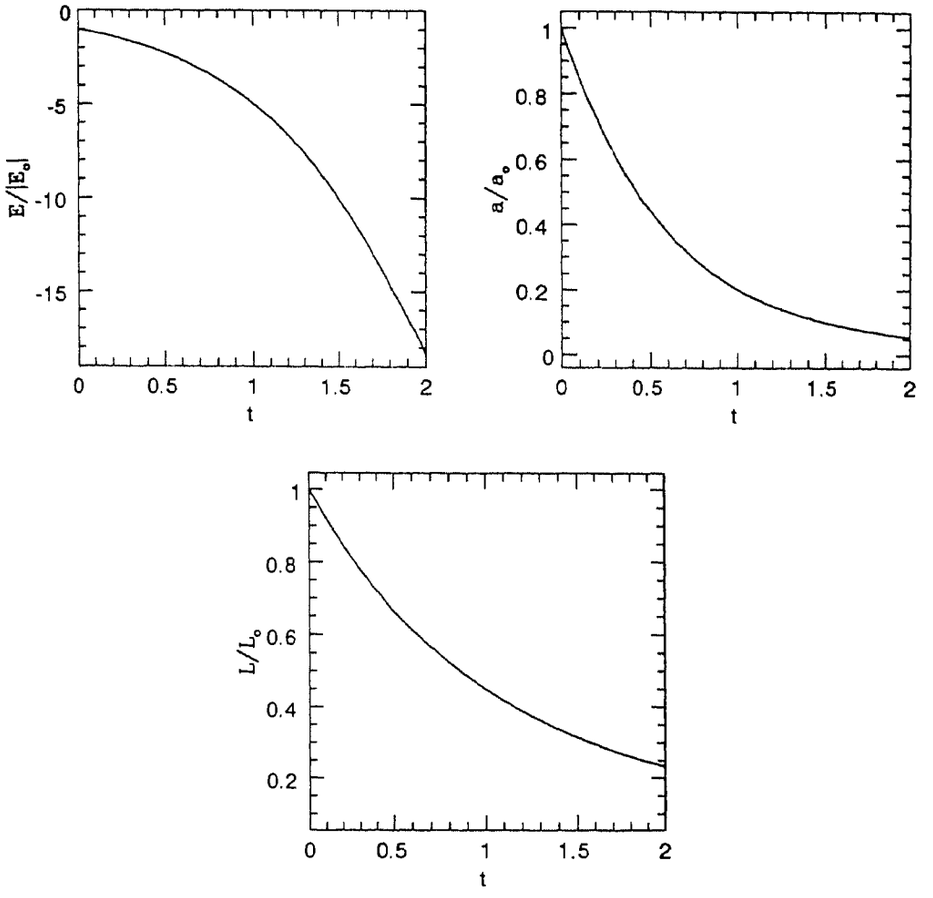

Figure 4.3: *The energy, semi-major axis and angular momentum are plotted against time, scaled by their corresponding initial values. Time is in units where* $\tilde{\eta} = 1$. *(Case 1:* $v \gg \sigma$*)*

Therefore,

$$\frac{d\vec{L}}{dt} = -\frac{\tilde{\eta} m \vec{L}}{(k^2/(4L^2) + V^2)^{3/2}} \tag{4.17}$$

This can be integrated for a circular orbit to give the evolution of angular momentum

$$\left(-\frac{4V^2}{3} - \frac{k^2}{12L^2}\right)\left(\frac{k^2}{4L^2} + V^2\right)^{1/2} +$$

$$V^3 \ln \left[V^2 L + LV \left(\frac{k^2}{4L^2} + V^2 \right)^{1/2} \right] = -\tilde{\eta} m t + c \tag{4.18}$$

where k is equal to Gm^2 and c is a constant to be determined from the initial conditions. The equations 4.13 and 4.15 are transcendental in nature and the energy and angular momentum cannot be easily expressed as explicit functions of time. The nature of the evolution can, however, be inferred. Initially, both energy and angular momentum are exponential functions of time with a timescale of the order $2\tilde{\eta}m/V^3$ and $\tilde{\eta}m/V^3$ respectively. For typical cloud conditions surrounding a protostar, with densities $\sim 10^6$ cm^{-3} (e.g., ρ Oph), these timescales are of the order of a few 10^5 years. As the binary loses kinetic energy, the protostars fall in and become more tightly bound. The relative velocity of the binary thereby increases and change in energy and angular momentum of the binary is no longer exponential, but slower. At later times (when the relative velocity $v \ll V$, the center of mass velocity), the binding energy increases as $\approx t^{2/3}$ and angular momentum decreases as $\approx t^{-1/3}$. Figure 4.3 shows the variation of energy, angular momentum and semi-major axis of the binary system with time.

4.3 Numerical Solutions

The equations governing the motion of the binary can be solved only in the limiting cases, where the dynamical friction term reduces to a simple form, and by making certain approximations. To study the complete evolution of the binary system, and to check the validity of the above derived expressions, equations 4.1 and 4.2 have been solved exactly using numerical methods. Also, the above expressions do not yield the variation of eccentricity with time, as it has been assumed that the orbit is always circular. The eccentricity of the orbit increases or decreases with time, depending on the relative rates of change of energy and angular momentum. Though dissipative forces are

in general believed to circularise orbits, this is not necessarily so, one such exception being the drag due to dynamical friction (e.g., Hoffer 1985). This can be qualitatively understood by considering an eccentric orbit, that evolves such that the drag force is always in the regime where it is proportional to $1/v^2$. At apastron the orbital velocity is at its minimum. Dynamical friction being at its maximum causes a shrinking of the orbit towards the centre of mass. As the (reduced) mass approaches the periastron, the drag decreases due to the increase in velocity and the mass reaches the shortening periastron with a larger velocity and hence the orbit becomes more eccentric with time. The numerical solutions allow a study of the eccentricity variation with time and also a more exact investigation of the other orbital parameters.

4.3.1 Integration scheme

The problem essentially involves two very different timescales, one being the period of the binary, which may be of the order of years, and the other the drag timescale which can be estimated to be of the order of $\sim 10^{5-6}$ years, for usual protostellar cloud parameters. Thus the orbit has to be typically integrated over a few 10^6 periods. In order to check the accuracy of the integration scheme to be adopted, the binary is first evolved in the absence of drag for about 10^6 years. This should yield a constant energy orbit with time, and the extent to which energy is conserved denotes the accuracy attained. Energy conservation is normally achieved by using a constant time-step in the integration, as this leaves the equations of motion time-symmetric and hence conserves energy. Desired accuracy levels are maintained by reducing the time-step appropriately. For the problem to be solved here, ensuring energy conservation by choosing a constant time-step criterion (and thus a time-symmetric integrator) turns out to be prohibitively expensive. Hut, Makino and McMillan (1995) have devised an integration scheme that allows the use of a variable energy time-step criterion that preserves time-symmetry of the equations and hence conserves energy

excellently. We adopt their prescription for a time-symmetrized leapfrog with a variable time-step. The leapfrog scheme is a standard method of integrating equations and is symplectic in nature, i.e., the positions and velocities are evaluated at alternate instances of time and are hence interleaved.

$$\begin{aligned} r(t_1) &= r(t_0) + v(t_{1/2})\delta t \\ v(t_{3/2}) &= v(t_{1/2}) + a(t_1)\delta t \end{aligned} \tag{4.19}$$

where r,v, and a represent the intantaneous position, velocity and acceleration. δt is the timestep and $t_{1/2} = t + \frac{1}{2}\delta t$, and so on. As the displacement of v is time-symmetric with respect to r and a, there is no systematic build-up of an error in energy. These equations can be transformed into a set where the positions and velocities are specified at the same instant of time:

$$\begin{aligned} r(t_1) &= r(t_0) + v(t_0)\delta t + \frac{1}{2}a(t_0)(\delta t)^2 \\ v(t_1) &= v(t_0) + \frac{1}{2}(a(t_0) + a(t_1))\delta t \end{aligned} \tag{4.20}$$

The equations are integrated over time from the initial conditions (r, v, a) at t_0, by first computing $r(t_1)$, then the acceleration $a(r_1, t_1)$, and finally the velocity $v(t_1)$. Though, energy conservation is ensured by the leapfrog, the use of a constant time-step is highly impractical. The central idea behind the new approach is the use of a variable time-step and a time-symmetrization of the equations, that involves iterative procedures to solve an implicit time-step criterion. The implicit form for the leap-frog integrator is thus

$$\xi(t_1) = f(\xi(t_0), \delta t)\delta t = \frac{1}{2}\left(h(\xi(t_0)) + h(\xi(t_1))\right) \tag{4.21}$$

The quantity ξ represents the vectors (r, v) and which are evaluated through equations (4.16-4.17). A time-step h is specified by an appropriate criterion that may depend explicitly on instantaneous position and velocity. (For the binary problem, we have taken $h = P(t)/1000$, where $P(t) = r(t)/v(t)$). The same criterion is used to compute the new time-step size at t_0 and t_1. Then δt

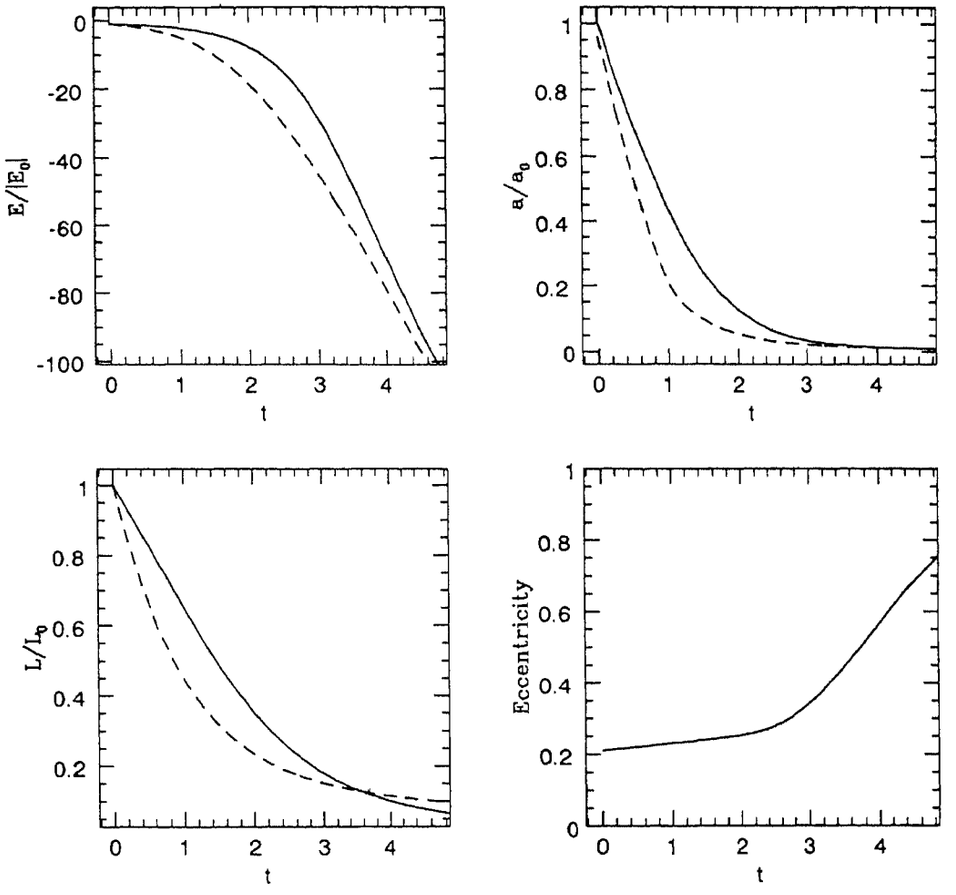

Figure 4.4: *The energy, semi-major axis and angular momentum and eccentricity are plotted against time. The solid lines correspond to the numerical result and the dashed lines to the analytical approximation. Time is in units where* $\tilde{\eta} = 1$.

is re-defined as the mean of these two values, and the state $\xi(t_1)$ is re-evaluated. The equations are iteratively solved to reach convergence. The system is thus integrated over time. The leap-frog is a second order method, and Hut, Makino and McMillan have also extended this scheme to a fourth-order integrator. The

second order method has been chosen over the fourth-order Hermite integrator as the latter has proved less economical for the present problem. Convergence is reached after typically 3 or 4 iterations, and 1000 points have been chosen along the orbit to meet requirements of accuracy. Therefore about 3 10^9 force evaluations are needed to integrate the equations over 10^6 years. Having ensured accuracy and stability of the integration scheme, the orbits are then integrated including the drag term in the forces.

Figure 4.4 shows the variation in time of energy, angular momentum, eccentricity and semi-major axis. Also shown superposed on these plots are the corresponding analytical solutions (for the case $v \gg \sigma$). The orbit of the binary is initially not circular, but slightly eccentric, with an eccentricity of 0.2. The analytical solutions shown superposed, are however, those for a circular orbit with the same energy. It is seen that there is reasonable agreement between the analytic and numerical solutions, even though the orbit is not circular.

4.4 Evolution of a binary in a cloud

As seen above, the predominant effect of the drag force on the binary is to shrink the orbit to smaller separations. The extent to which the orbit shrinks in a given period of time depends on the initial separation of the binary components. The initial semi-major axis of the binary determines the initial relative velocity, and hence the magnitude of the drag term in the force initially. As the masses lose energy and angular momentum and spiral in, their orbital separation decreases and there is an increase in the magnitude of their relative velocity. If the initial velocity is less than the gas velocity dispersion σ, then the drag force increases in magnitude in the beginning as v and decreases later as $1/v^2$. Thus, there is an initial rapid decay of the orbit and as the relative velocity increases, drag decreases and the decay is slower. Figure 4.5 shows the evolution of semi-major axis for different initial separations during a fixed

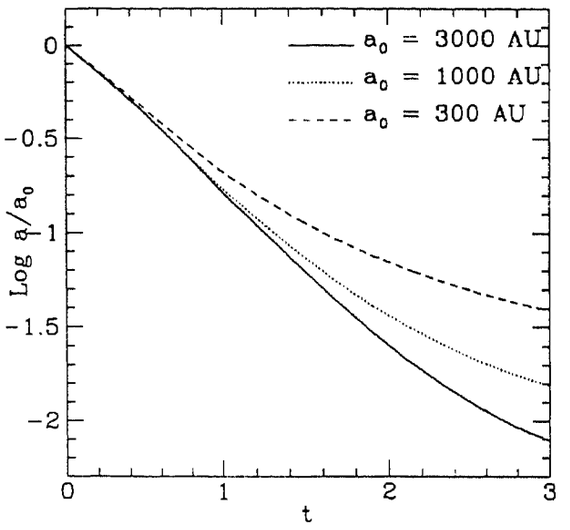

Figure 4.5: *Evolution of semi-major axis for different separations. Time is plotted in units of* 10^6 *years.*

interval of time. The cloud in which the protostellar binary is embedded is assumed to be of constant number density (10^6 cm^{-3}) and with a velocity dispersion of 2.3 kms^{-1}. These parameters are typical of the environment of protostars and have been chosen to comply with observations of the prototypical star-forming cloud core, ρ Ophiuchus. It is seen that the timescale for a decrease in the semi-major axis by a factor of two, $t_{1/2}$, is about a few 10^5 years. A distinct feature of drag due to dynamical friction, is that orbits get increasingly more eccentric with time. This implies that the fractional loss of angular momentum exceeds that of energy. The eccentricity increases with time and asymptotically tends towards one. We have studied eccentricity variations for differing initial eccentricity and Figure 4.6 shows the initial and final eccentricity for an orbit with the same initial separation, after 10^6 years. Also shown are the changes in angular momentum and energy with time. As is to be expected, loss of angular momentum is greater for orbits with higher

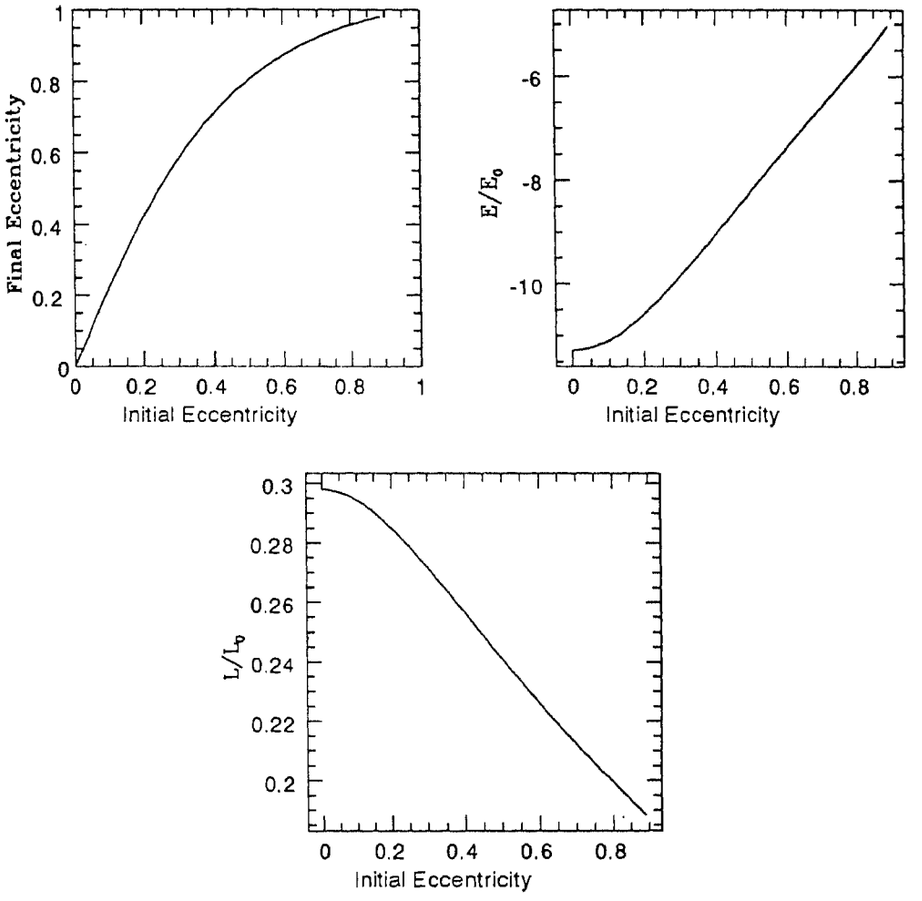

Figure 4.6: *For different initial eccentricities of an orbit with the same initial separation, the eccentricity, energy and angular momentum after a fixed interval of time are shown.*

eccentricity. The increase of eccentricity with time indicates that binary systems that have evolved in the presence of gas and hence suffered drag due to it, must lie on high–eccentricity orbits in general. While this may be so for orbits with long periods and hence larger separations, it need not hold for the shorter period binary systems. It is believed that almost all young protostars are accompanied by massive circumstellar disks, with typical extents of

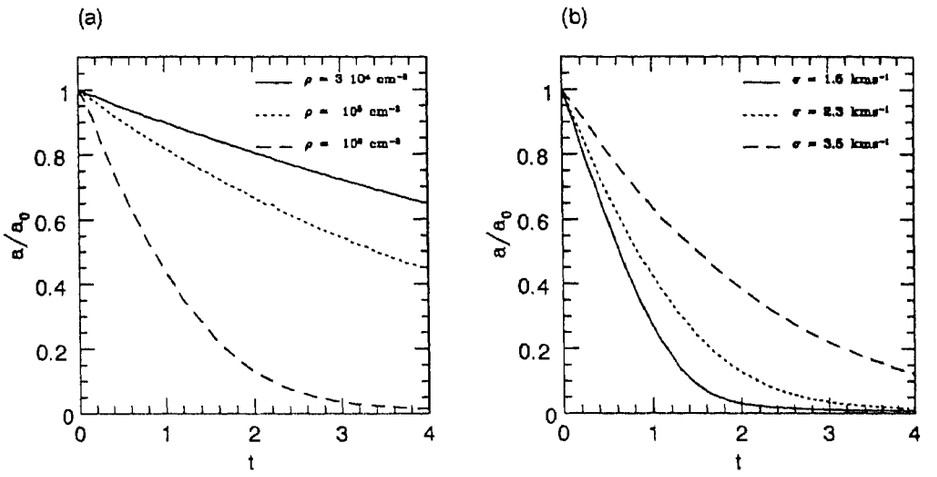

Figure 4.7: *Evolution of semi-major axis of a binary for different cloud densities (Panel (a)) and velocity dispersion of gas in the cloud (Panel (b)). Time is in units of* 10^6 *years.*

a $\sim$ 100 AU, (Strom et al 1993). Therefore, for separations much shorter than these, the presence of the disks has to be taken into account for a more realistic analysis. It is not clear how dissipation caused by disks affects the eccentricity of the orbit, though at very short periods, tidal forces may rapidly tend to make the orbits more circular (Clarke 1992). As circumstellar disks have not been included in our present analysis, we have not considered the evolution of short-period binaries, as we believe that the effects of disks on the binary orbit is probably more prominent at these separations. The effects of variation in cloud gas density can be assessed easily from equations 4.8,4.10 and 4.11. The relevant timescales vary inversely with density, and the evolution of semi-major axis for three different cloud densities is shown in Figure 4.7. The evolution for different gas velocity dispersions depends on the velocity of the binary and hence on the separation. Figure 4.7 also shows the semi-major axis plotted against time for different velocity dispersions. The cloud density has been kept constant at $\sim 10^6 cm^{-3}$. The drag force depends sensitively on the

velocity dispersion, and is greater for lower velocity dispersions. This implies that evolution of binaries subsequent to formation may, in general, be different for different clouds (with differing velocity dispersions or differing densities). There seems to be tentative observational evidence for differences in the frequency of short-period binaries in ρ Ophiuchus and Taurus-Auriga clouds. If the observed excess of closer binaries in ρ Ophiuchus is not because of a larger incidence of formation, evolution of PMS binaries in the presence of drag could be a possible explanation. ρ Ophiuchus has a lower velocity dispersion and a higher average gas density as compared to the Taurus-Auriga star forming region, and hence a drag force of greater magnitude. This implies that evolution to shorter orbital separations is faster in ρ Ophiuchus and it is more likely to contain short-period PMS binaries. It is to be noted that though only the dissipative effects of dynamical friction have been considered here, in principle, other forces could also drag the orbital evolution. For close binaries, disks and tidal torques provide active dissipative agents in addition to dynamical friction and are probably more important. Ram pressure due to the surrounding gas is another potential source of drag, and for self-gravitating objects like protostars, is similar in form to the dynamical friction term (in the limits of large velocity), except for being a factor of $\ln \Lambda$ lower in magnitude. The results derived here therefore apply equally well for ram pressure deceleration as well, but on longer timescales.

4.5 Statistical studies of PMS binaries

High-resolution techniques and better infra-red detectors have in recent times enabled the detection of large numbers of PMS binaries covering a wide range of periods. A comparison with observations of main-sequence (MS) binaries can thus be made and it is found that the fraction of PMS stars in binary systems is equal to or even larger than the frequency of MS binaries ($\sim 60 - 70\%$).

The periods of MS binaries form a smooth distribution in the range 0 < Log P(days)< 9, with a maximum at around 180 years (see Figure 4.1). The eccentricities span a wide range and only the shortest period orbits are circular. The masses of the primary and secondary are probably uncorrelated and are consistent with a random pairing from an initial mass function (Duquennoy & Mayor 1991). Periods of PMS binaries within the range observed appear to follow a similar distribution as that of the MS binaries. PMS binary orbits also have a range of eccentricities. Since drag affects the orbital evolution of a binary system as discussed above, it is to be expected that this will be manifest in the observed properties of PMS and MS binaries.

We consider a number of binary systems, which have a certain frequency distribution of periods (and hence separations), depending on their formation mechanism(s). These systems undergo dynamical evolution while they remain embedded in the molecular cloud, and evolve to shorter periods (and closer separations) due to the effects of dynamical friction. The drag being velocity dependent, is however, different for binaries with different orbital velocities. For example, if the initial distribution of periods were such that all binaries suffer a drag proportional to $1/v^2$, where v is the velocity, longer-period binaries suffer greater drag than the shorter-period ones. This would imply that the binaries in the longest period ranges, would have the shortest timescales for decay, with the timescale progressively increasing towards the shortest period binary systems. The number of binaries in the long-period range, would thus decrease rapidly with time, and at the same time populate the middle period ranges. The binaries here, however, decay on longer timescales and therefore do not evolve into short-period binaries rapidly enough. There is thus a build-up of the number of binaries at these periods (separations) and hence a peak is expected to form in the frequency distribution of periods with time. As the system evolves futher, the peak itself would slowly shift towards shorter periods. It is expected that the formation of the peak would also de-

pend on other parameters in the system, such as the eccentricity of the initial orbit, masses of the binary components, and also the initial distribution of periods. In order to investigate in detail, the effects of gas drag on the class of PMS binaries as a whole, statistical samples of binary systems are generated and evolved in time. The individual orbits are numerically evolved using the methods described earlier. The initial conditions and assumptions made are as follows:

1. The masses are determined from a Salpeter initial mass function ($dN/dM \propto M^{-2.35}$) within the range 0.5 $M_\odot$ to 5 $M_\odot$. Binaries are formed by randomly pairing two masses.

2. The eccentricities are random and constrained within the interval 0-0.8. Higher eccentricity orbits were not considered due to difficulties in maintaining the accuracy during numerical integration.

3. The separations (and hence periods) of the entire sample follow an assigned distribution. Two such initial distributions were considered, one where the number of binaries *per separation interval* are equal and another where the number of binaries are equal *per logarithmic separation interval.*

4. The separations (semi-major axes) are also randomly assigned to the binaries and lie between 100 AU and 10^4 AU. The lower limit has been somewhat arbitrarily chosen and corresponds to the typical size of a protostellar disk, beyond which the disk is expected to significantly influence the orbital evolution. The upper limit corresponds to an average expected separation for protostars in a clustered environment, beyond which the binary may not remain bound.

5. The binary is given a random position in the uniform density cloud (of density $10^6 cm^{-3}$ and velocity dispersion $2.3 kms^{-1}$) and assigned the local virial velocity with an arbitrary direction.

The sample consists of 100 binaries for the case with an equal number per separation interval (Case I) and 70 binaries for the case with equal number of binaries per logarithmic separation interval (Case II). Each binary orbit is integrated in time for about 5 10^6 years.

The frequency distribution as a function of period at different instances of time for Case I is shown in Figure 4.8. The initial distribution is constant with separation. As the drag force varies as the inverse square of the velocity, binaries with larger separations (and smaller velocities) suffer greater drag and lose energy at a faster rate as compared to the higher velocity binaries at shorter periods. The frequency distribution gradually gets altered and shifts towards shorter periods. A peak appears in the frequency-period distribution, which gets more pronounced at later times. The position of the peak slowly shifts towards shorter periods if the evolution is allowed to proceed for longer times. For an initial distribution that is constant in equal logarithmic intervals of separation, the frequency distribution also gets gradually altered as shown in Figure 4.9. A distinct peak in the frequency distribution appears at later times than in Case I probably because of the presence of a comparatively larger number of shorter period binaries which evolve more slowly.

The observed maximum in the frequency distribution with period can perhaps possibly be explained as an effect of gas drag (or other disipative forces) which determines the initial evolution of a binary while still embedded in the molecular cloud. The position of the maximum then depends mainly on the cloud parameters and partially on the duration of the embedded phase of a typical binary system. The observed peak in the MS binary distribution would then be representative of the typical or average cloud conditions in the Galactic star-forming environment.

The eccentricity of a binary acted upon by dynamical friction increases with time. This implies that binary orbits that have decayed to shorter periods are also more eccentric. Observations of MS binaries seem to show the reverse

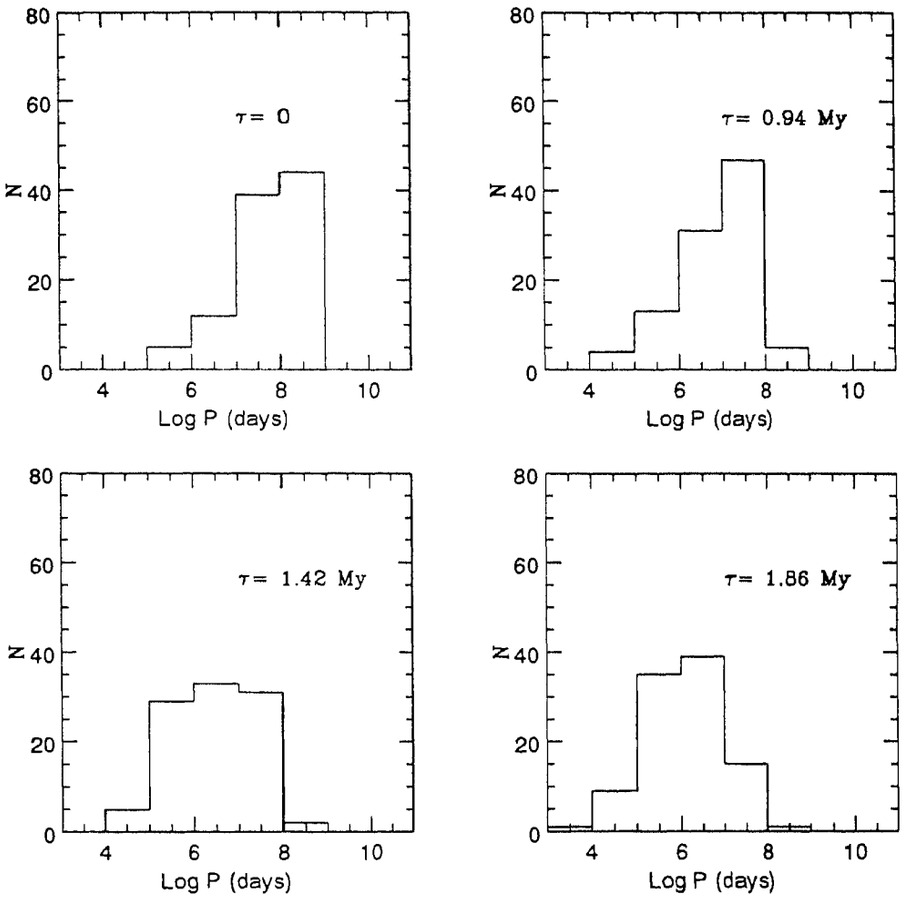

Figure 4.8: *Frequency distribution with period of binaries which are initially distributed equally in equal intervals of separation. (Case I)*

trend, with close binaries lying on nearly circular orbits. It is believed that for very close binaries, tidal forces rapidly tend to circularize the orbits (e.g., Mathieu 1994). The trend towards low eccentricities is however seen only for orbits with periods shorter than $\sim$ few 100 days, and our analysis does not extend to such short-period binaries. Figure 4.10 shows the observed eccentricities of MS binaries and those from the above samples, plotted against

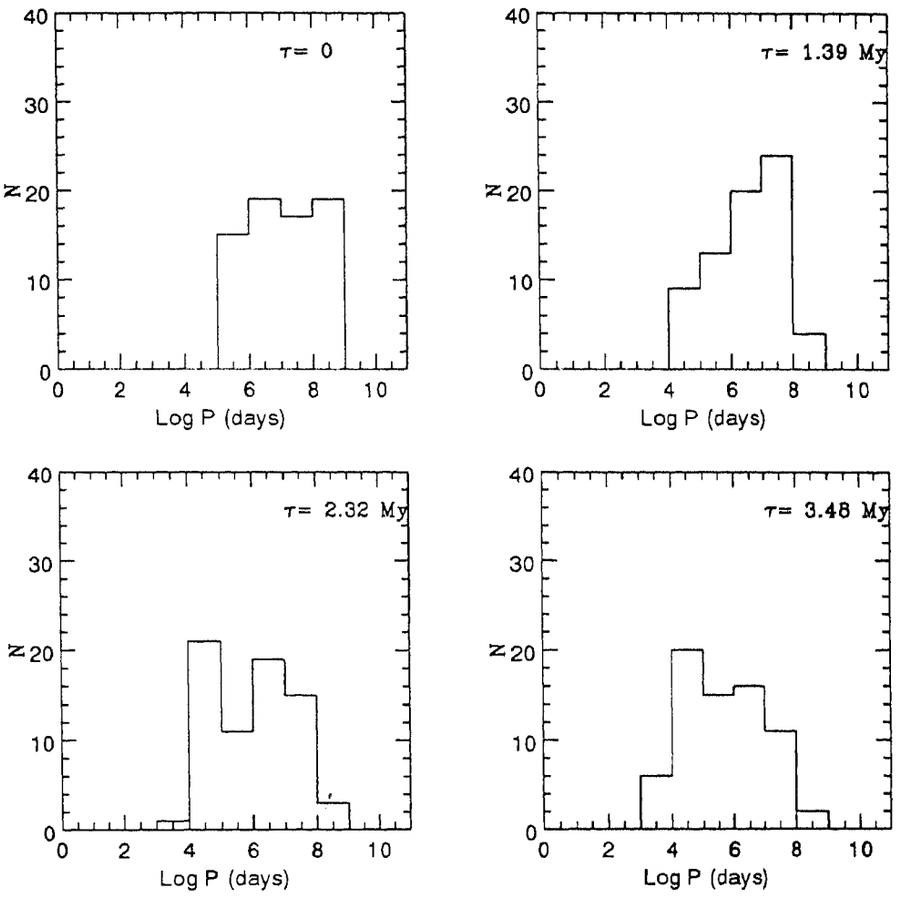

Figure 4.9: *Frequency distribution with period of binaries which are initially distributed equally in equal logarithmic intervals of separation. (Case II)*

the period of the orbit for the overlapping range of periods (3.5 < Log P (days) < 5). It is seen that within the range of periods observed, there is no contradiction between the results obtained here and observations.

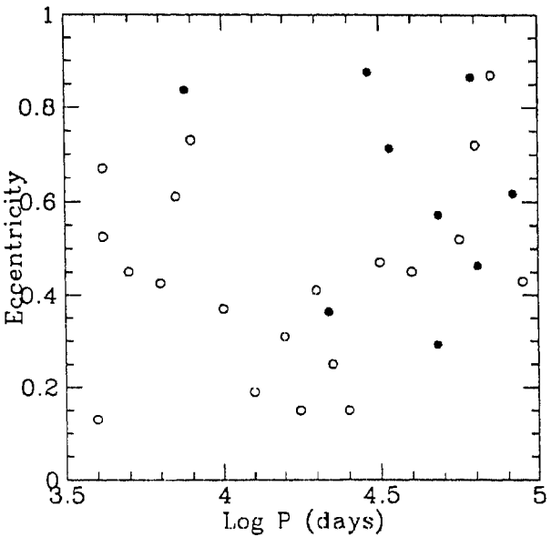

Figure 4.10: *The eccentricity-period distribution for MS binaries (open circles) (from Duquennoy & Mayor 1991) amd PMS binaries after* 1.8 10^6 *years (filled circles). (Plotted for Case I).*

4.6 Implications for binary formation

The presence of a peak in the frequency distribution with separation for MS and PMS binaries suggests the existence of a preferred lengthscale for the formation of binaries. Existing mechanisms for binary formation include fragmentation, fission, capture processes and instabilities in disks. Of these, fragmentation is currently believed to be the primary formation process (see reviews by Bodenheimer 1992, Pringle 1991, Boss 1992) where the protostar fragments during the isothermal collapse phase or alternatively where the binary is formed as a result of a hierarchical fragmentation process. The frequency distribution arising from fragmentation is not well-determined (Boss 1992), but formation of binaries with larger separations is easier or more favoured than the formation of close binaries (Bodenheimer 1992). Decay of the orbit due to dynamical friction can circumvent the problem of forming close binaries, as long-period

binaries get dragged and evolve to shorter periods.
If all (or any other) of the above mentioned mechanisms are equally important for the formation of binaries, there are intrinsically different lengthscales involved in each case. (e.g., the separation of a binary cannot be much larger than the extent of the disk if the binary forms by gravitational instabilities in a disk). It is then very unlikely for the initial frequency distribution to be a uniform function of period. In such a case, dissipation of energy due to drag may serve to smoothen out the irregularities, though the precise nature of the resultant frequency distribution would depend on the initial distribution.

4.7 Conclusions

The evolution of a protostellar binary system is investigated while it is embedded in its parent molecular cloud core, and is acted upon by gas drag due to dynamical friction. Approximate analytical results are obtained for the energy and angular momentum evolution of the orbit in the limiting cases, where the velocity is much smaller than, and much larger than the velocity dispersion of the gas. The general case is solved numerically. Dissipation causes a decay of the orbit to smaller separations and orbital eccentricity increases with time. For a protostellar binary embedded in a typical star-forming cloud core (of density $\sim 10^6$ cm^{-3} and velocity dispersion 2.3 kms^{-1}) the decay time for the semi-major axis of the orbit to half its initial value is about 10^{5-6} years. As a binary probably spends about a few 10^6 years embedded in the cloud, significant evolution of the orbit is expected before the dispersal of the cloud. Binary populations have been statistically generated and evolved for comparison with observations of MS and PMS binaries. Dynamical friction changes the initial frequency distribution with period of the binaries, which is shifted towards shorter periods. A maximum is obtained in the distribution as seen observationally. Two different initial distributions are considered, and the peak is

found to shift slowly towards shorter periods at later times. Decay of the orbit due to gas drag causes an evolution of long-period orbits to shorter periods and thus enables the formation of close binaries.

References

Abt, H.A., 1983, Ann. Rev. of Astron. Astrophys., 21, 343

Binney, J., Tremaine S., 1987, In "Galactic dynamics", Princeton University Press, Princeton, p.791

Bodenheimer, P., 1992, In "Star formation in Stellar systems", Cambridge University Press, Cambridge, p.1

Bodenheimer P., Tohline J.E., Black D.C., 1980, Astrophys.J, 242, 209

Boss A.P., 1992, In "Complementary approaches to double and multiple star research", IAU Coll. 135, p.195

Chandrasekhar S., 1943, Astrophys.J, 97, 255

Clarke C., 1992, In "Complementary approaches to double and multiple star research", IAU Coll. 135, p.176

Duquennoy A., Mayor M. 1991, Astron. Astrophys., 248, 485

Goldstein, H. 1977, In "Classical Mechanics", p.24

Gorti, U., Bhatt, H. C., 1996, MNRAS, in press

Hoffer, J., 1985, Astrophys. J., 289, 193

Hut P., Makino J., McMillan S., 1995, Astrophys. J. Lett., 443, L93

Lienert Ch., Weitzel N., Zinnecker H., Christou J, Ridgeway S, et al 1993, Astron. Astrophys., 278, 129

Mathieu, R.D., 1992, In "Complementary approaches to double and multiple star research", IAU Coll. 135, p.30

Mathieu, R.D., 1994, Ann Rev. of Astron. Astrophys., 32, 465

Pringle J., 1991, In "The physics of star formation and early stellar evolution", Kluwer, Dordrecht, p.437

Prosser C.F., Stauffer J.R., Hartmann L., Soderblom D.R., Jones B.F., Werner M.W., McCaughrean M.J., 1994, Astrophys.J., 421, 517

Reipurth B., Zinnecker H., 1993, Astron. Astrophys., 278, 81

Shu, F.H., Adams F.C., Lizano, S. 1987, Ann. Rev. of Astron. Astrophys, 25, 23

Strom S.E., Edwards S., Strutskie M., 1992, In "Protostars and Planets III", eds Levy E.H., Lunine J.I., Tucson:University of Arizona Press, p837

Chapter 5

Dust around Young Stellar Objects: Herbig Ae/Be stars

5.1 Introduction

The protostars, which form from the dense condensations or clumps in molecular clouds, collapse at a later stage to eventually form young stars. These stars burn hydrogen in their central regions, and arrive at the main sequence. Prior to this phase, the young stars pass through the pre-main-sequence evolutionary phase, wherein they are generally termed as Young Stellar Objects or YSOs. The collapse phase results in a central stellar object surrounded by a circumstellar disk, the latter being a result of the conservation of the angular momentum of the parent cloud core during the collapse process. The central star grows in mass by accreting through the surrounding disk, and during its early evolution also undergoes a mass outflow stage. The outflows from YSOs are usually bipolar, highly energetic and are often accompanied by well collimated jets. The accretion luminosity of the disk initially dominates the radiation from the system. As accretion through the disk slowly ceases, the disk radiates by reprocessing light from the central star, which is now the dominant source of radiation. The star and disk are often surrounded by an

envelope of dust and gas, which may be visible as a reflection nebula. The dust component of the circumstellar matter causes extinction and polarization of stellar radiation. The thermal emission from the dust is mostly in the infrared and the spectral energy distribution (SED) of the star provides an important diagnostic tool in the determination of the evolutionary status of the young star (see section 1.3). As the dust absorbs light from the shorter wavelengths and re-radiates at the longer wavelengths, the observed SED is largely determined by the properties of the circumstellar dust. We study here the dust in the environments of a class of YSOs, the Herbig Ae/Be stars.

Herbig Ae/Be stars are young, intermediate-mass pre-main-sequence stars and are often surrounded by reflection nebulosities. These stars have envelopes of circumstellar matter distributed in the form of massive disks and/or as extended shells. Their spectra show strong emission lines like in the low-mass T Tauri stars, and some stars show double-peaked emission in the infrared region. A list of 26 stars was first made by Herbig (1960) in an attempt to find high-mass counterparts to the low mass, pre-main-sequence T Tauri stars. This list was extended by Finkenzeller & Mundt (1984) to include 57 objects, and to the present day other observers (e.g., Hu et al 1989, Bergner et al. 1990) have added new candidates taking the catalogue to a total of more than 70 stars. Herbig Ae/Be stars show large near and far infrared excesses, attributed by various authors to thermal emission by dust distributed in circumstellar disks or shells (e.g., Tjin a djie & Thé 1978; Catala 1983; Yamashita et al. 1989). Spectroscopy in the infrared region has revealed characteristic dust emission features at 3.3 μm and 9.7 μm providing unmistakable evidence for the presence of dust grains in the circumstellar environments of these young stars (e.g., Cohen 1973; Whittet et al. 1983). The relatively large degree of polarization and its variation on short timescales, further indicates scattering dust in the close neighbourhood of these stars (e.g, Vrba et al. 1979; Grinin et al. 1991; Jain & Bhatt 1995). Low Resolution Spectra in the 9–21 μm

wavelength range obtained by the Infrared Astronomical Satellite (IRAS) show characteristic dust features, such as the 9.7 μm silicate band in absorption or emission and the 11.3 μm emission feature, for many of these stars.

Dust in the environment of young stars is found to differ from that in the general interstellar medium. It has been suggested by many authors that the dust around Herbig Ae/Be stars is anomalous (Thé et al. 1981; Steenman & Thé 1989; Yamashita et al. 1989; Sorell 1990; Bibo & Thé 1992). Large values of R, the ratio of total (A_V) to selective extinction (E(B−V)) have been deduced from the UBV data for some stars. Others have suggested the presence of dense clouds with large grains in a less dense envelope of small grains near the star to provide possible explanations for the variability among these stars (Voshchinnikov 1990; Bibo & Thé 1992; Bibo & Thé 1991; Grinnin et al. 1991). An observable effect of circumstellar dust is extinction and reddening of starlight. The wavelength dependence of extinction is determined by the dust grain composition and size distribution. If the circumstellar dust around Herbig Ae/Be stars is different from the mean interstellar dust, one may expect the wavelength dependence of the extinction by this dust to be different from the mean interstellar extinction law (Savage & Mathis 1979; Steenman & Thé 1989; Steenman & Thé 1991). The wavelength dependence of extinction to the star in the optical and near- infrared regions can be described by the colour excesses (e.g., E(B−V)= $(B-V)_{observed}-(B-V)_{intrinsic}$, where the intrinsic colours are those for an unreddened main sequence star) and the colour excess ratios E(U−B)/E(B−V), E(V−R)/E(B−V), E(V−I)/E(B−V) and E(V−I)/E(V−R). These colour excess ratios can be computed from stellar photometric measurements in the UBVRI bands. For the mean interstellar extinction law (Savage & Mathis 1979), they have the following values: E(U−B)/E(B−V) = 0.80, E(V−R)/E(B−V) = 0.78, E(V−I)/E(B−V) = 1.60 and E(V−I)/E(V−R) = 2.05. The variation of the colour excess ratios with the mean dust grain radius in the grain size distribution has been studied by

McMillan (1979) and Steenman & Thé (1991). McMillan (1979) computed the theoretical colour excess ratios for homogeneous spherical grains using the Mie theory. These ratios have been plotted by McMillan (1979) against grain size parameter a_o which is proportional to the mean grain size. All colour excess ratios E(V−λ)/E(B−V) with the wavelength λ longward of the V band, increase as the mean grain size increases. The ratio E(V−I)/E(V−R) is rather insensitive to variations in a_o and increases only marginally. E(U−B)/E(B−V) has a different behaviour and decreases with increasing mean grain size. Similar behaviour of the colour excess ratios is obtained from the analysis of Steenman & Thé (1991). They have studied the wavelength dependence of extinction with particular reference to Herbig Ae/Be stars, for different values of the lower grain size cutoff in a power law distribution of grain sizes ($dn(a) \propto a^{-3.5}da$). An increase in the value of the lower cutoff results in an increase in the mean grain size and indicates an absence of very small grains that cause extinction in the ultraviolet.

From the photometric data for the Herbig Ae/Be stars we can derive the values of these ratios and compare with those for mean interstellar extinction. In this chapter we present the results of such a study (Gorti & Bhatt 1993). Apart from the physical size of the dust grains, the chemical composition of circumstellar dust around Herbig Ae/Be stars is also investigated (Bhatt & Gorti 1993). The IRAS Low Resolution Spectra in the 9–21 μm wavelength range are examined for 17 stars.

5.2 Photometric data and analysis

Photometric data for the UBVRI bands has been taken from the literature for known and candidate Herbig Ae/Be stars and is listed in Table 5. 1. The R and I band data were converted from the Cousins system to the Johnson system, where necessary, by using the transformations given by Bessel (1979). Many

Table 5.1: *Photometric data for Herbig Ae/Be stars. J and C refer to R and I magnitudes in the Johnson and Cousins systems respectively.*

Star	Sp.type	ref.	U	B	V	R	I	ref.
BD +61 154	B8eq	(9)	10.70	10.96	10.38	9.92C	9.40C	(16)
RR Tau	A3–A5	(26)	11.79	11.52	11.07	10.75C	10.40C	(16)
LKHA 208	B5–B9e	(14)	12.32	12.05	11.62	11.33C	11.04C	(16)
LKHA 215	B7-B8e	(26)	10.88	186	10.36	9.94C	9.48C	(18)
HD 259431	B2e	(9)	8.42	8.96	8.67	8.34C	8.07C	(18)
R Mon	B0	(7)	12.43	12.80	12.18	11.58C	11.00C	(18)
LKHA 218	B6e	(7)	12.49	12.30	11.87	11.55C	11.26C	(18)
HD 53367	B0 IV	(9)	6.78	7.41	6.97	6.61C	6.19C	(18)
HD 76534	B2e	(9)	7.54	8.11	7.96	7.83C	7.70C	(27)
RCW 34	A0e	(9)	12.61	12.73	11.81	–	–	(15)
Herbst 28	B5e	(15)	12.20	12.00	11.28	–	–	(15)
HD 97048	B9e	(9)	9.03	8.79	8.44	8.20C	7.94C	(18)
HD 150193	A4e	(9)	9.69	9.33	8.80	8.41C	7.97C	(18)
KK Oph	A5–A7e	(9)	11.71	11.26	10.57	10.09C	9.52C	(16)
LKHA 118	B5:Vpe	(10)	11.77	12.09	11.13	–	–	(2)
MWC 297	O9	(3)	13.84	14.54	12.17	9.45J	8.39J	(2)
VV Ser	B1–B3e	(10)	13.20	12.78	11.87	11.21C	10.49C	(16)
MWC 300	B:	(30)	12.46	12.61	11.60	–	–	(14)
TY CrA	B9e	(14)	9.47	9.39	8.95	8.58C	8.52C	(18)
BD+40 4124	B3e	(9)	11.02	11.28	10.54	–	–	(25)
AS 442	B8e	(12)	11.84	11.50	10.87	10.38J	9.94J	(21)
LKHA 134	B8-Ae	(12)	12.23	12.03	11.40	10.88J	10.42J	(21)
V645 Cyg	A0	(11)	15.74	15.16	14.06	12.91J	–	(17)
BD+65 1637	B3	(9)	10.17	10.49	10.08	9.53J	9.26J	(24)
LKHA 234	B5–B7	(26)	12.63	12.79	11.90	10.90J	10.25J	(24)
HD 216629	B3e	(9)	9.82	10.01	9.29	–	–	(22)
BLJ 71	B0–B8e	(1)	11.75	11.38	10.57	–	–	(1)
HD 97300	B9 V	(28)	9.50	9.35	8.98	8.70C	8.33C	(18)
V517 Cyg	A3–A5	(21)	12.89	12.50	12.03	11.57C	–	(21)

References to Table 1

1. Assousa, Herbst, Turner, 1977
2. Bastian & Mundt, 1979
3. Bergner, Kozlov, Kritsov et al., 1988
4. Bergner et al., 1990
5. Breger, 1974
6. Cohen & Schwartz, 1976
7. Cohen & Kuhi, 1979
8. Dibai, 1969
9. Finkenzeler, 1985
10. Finkenzeller & Mundt, 1984
11. Goodrich, 1986
12. Herbig, 1958
13. Herbig, 1960
14. Herbig & Rao, 1972
15. Herbst, 1975
16. Hillenbrand, Strom, Vrba et al., 1992
17. Humphreys et al., 1980
18. Kilkenny, Whittet, Davies et al., 1985
19. Marraco & Rydgren, 1981
20. Mendoze, 1968
21. Petrova & Shevchenko, 1987
22. Racine, 1968
23. Reipurth, 1983
24. Shevchenko & Yakubov, 1989
25. Strom, Strom, Breger M. et al., 1972
26. Strom, Strom, Yost et al., 1972
27. Thé, Felenbok, Cuypers et al., 1985
28. Thé, Wesselius, Tjin a Djie et al., 1985
29. Tjin a Djie, Remijn & Thé, 1984
30. Wolf & Stahl, 1986

Herbig stars are known to be variables and therefore only simultaneous measurements have been considered. Very few Herbig Ae/Be stars have been monitored photometrically. When simultaneous measurements for a given star are

Table 5.2: *The* E(B−V) *colour excess and various colour excess ratios of stars with corresponding errors.*

Star	E(B−V)	E(U−B)/E(B−V)	E(V−R)/E(B−V)	E(V−I)/E(B−V)	E(V−I)/E(V−R)
BD +61 154	0.67±0.06	0.06± 0.22	1.03± 0.02	2.06 ± 0.05	2± 0.01
RR Tau	0.34±0.06	0.53± 0.05	1.03± 0.01	2.03 ± 0.12	1.97± 0.11
LKHA 208	0.55±0.08	1.25± 0.2	0.87± 0.02	1.66 ± 0.04	1.91± 0.01
LKHA 215	0.62±0.07	0.71± 0.21	1.06± 0.02	2.1 ± 0.08	1.98± 0.03
HD 259431	0.53±0.07	1.06± 0.2	1.06± 0.05	2.03 ± 0.12	1.92± 0.03
R Mon	0.92±0.07	1.1± 0.11	1.06± 0.03	2.09 ± 0.06	1.96± 0.01
LKHA 218	0.57±0.05	1.19± 0.07	0.95± 0.01	1.71 ± 0.04	1.81± 0.06
HD 53367	0.74±0.07	1.05± 0.28	0.91± 0.02	1.93 ± 0.06	2.12± 0.02
HD 76534	0.39±0.07	0.74± 0.33	0.82± 0.02	1.68 ± 0.1	2.05± 0.07
RCW 34	0.92±0.09	-0.13± 0.25	±	±	±
Herbst 28	0.88±0.05	0.86± 0.08	±	±	±
HD 97048	0.41±0.09	1.17± 0.32	0.88± 0.07	1.71 ± 0.15	1.94± 0.02
HD 150193	0.42±0.06	0.64± 0.03	1.06± 0.01	2.13 ± 0.11	2.01± 0.09
KK Oph	0.52±0.07	0.65± 0.03	1.00 ± 0.02	2.09 ± 0.09	2.1± 0.05
LKHA 118	1.03±0.05	0.32± 0.09	±	±	±
MWC 297	2.67±0.04	0.15± 0.02	1.07± 0.01	1.59 ± 0.01	1.48± 0.01
VV Ser	1.15±0.09	1.11± 0.07	0.91± 0.03	1.82 ± 0.07	2± 0.02
MWC 300	1.17±0.05	0.35± 0.08	±	±	±
TY CrA	0.5 ±0.09	0.65± 0.29	1.13± 0.1	2.2 ± 0.21	1.95± 0.01
BD +40 4124	0.94±0.06	0.48± 0.16	±	±	±
AS 442	0.72±0.06	0.89± 0.13	0.71± 0.01	1.46 ± 0.01	2.06± 0.03
LKHA 134	0.69±0.16	0.57± 0.29	0.75± 0.01	1.51 ± 0.02	2± 0.06
V645 Cyg	1.1 ±0.09	0.53± 0.16	1.03± 0.02	±	±
BD +65 1637	0.61±0.07	0.64± 0.22	1.03± 0.04	1.79 ± 0.07	1.73± 0.01
LKHA 234	1.03±0.07	0.32± 0.08	1.03± 0.02	1.79 ± 0.06	1.74± 0.03
HD 216629	0.92±0.07	0.57± 0.15	±	±	±
BLJ 71	0.99±0.14	1.02± 0.28	±	±	±
HD 97300	0.43±0.09	0.96± 0.04	0.97± 0.09	2.09 ± 0.23	2.16± 0.04
V517 Cyg	0.36±0.07	0.51± 0.02	0.91± 0.01	±	±

available at many epochs, we have considered measurements corresponding to the epoch of maximum visual brightness. As our interest lies in the properties of the dust in the vicinity of these objects, only those with a large colour excess have been considered so that the circumstellar dust contributes substantially to the observed extinction, relative to the interstellar component. We have restricted our analysis to stars showing an E(B−V) excess larger than 0.32, which corresponds to an extinction of about 1 magnitude in the visual band for an interstellar R, the ratio of total-to-selective extinction. Colour excesses E(U−B), E(B−V), E(V−R) and E(V−I) have been calculated by subtracting the intrinsic colours for the corresponding spectral type from the observed colours U−B, B−V, V−R and V−I. The intrinsic or unreddened colours of main sequence stars have been taken from Johnson (1966). Ratios of these

colour excesses viz., E(U−B)/E(B−V), E(V−R)/E(B−V), E(V−I)/E(B−V) and E(V−I)/E(V−R) have been computed and are listed in Table 5. 2 with their probable errors. The errors involved in the photometric magnitude determinations are usually of the order of 0.02 magnitudes or in some cases, lower. A conservative error of 0.02 magnitudes has been adopted for all the stars. There is also an uncertainty involved in the determination of spectral type, which would cause an error in the value of the colour excesses. In order to assess these errors, an uncertainty of one subclass in the determined spectral type is assumed, and where a spectral type range has been assigned by the authors the range has been used. The uncertainties in spectral classification have been converted into the corresponding uncertainties in intrinsic colours of these stars. Our analysis has not been extended to the near infrared JHK bands as there may be flux contamination by non-stellar sources such as *thermal dust emission, free-free* and *bound-free* emission. For the optical bands, UBVRI, the contribution from these sources is negligible. As Herbig stars are emission line stars, the photometric magnitudes measured may also be affected by the flux contained in the emission lines. An estimate can be made for the flux contribution by the Hα line to the R band, which is the strongest emission line observed. However, even for an equivalent width of 50 Å the contribution of the emission line flux to photometry is less than $\sim$ 0.03 magnitudes. Simple calculations show that the contributions of the free-free and free-bound processes are of the same order of magnitude as the emission line flux. The errors introduced in the photometric measurements in the optical bands is thereby small, and has been neglected. Contamination of the UBVRI bands by thermal emission from dust can be estimated by considering the spectral energy distributions of these stars (see for e.g. Hillenbrand et al. 1992). In general, the flux contribution of thermal emission by dust is negligible. However, there are a few stars viz., LKHA 198, V380 Ori, R CrA, T CrA, LKHA 233, MWC 1080, NX Pup and MWC 342, where there appears

to be some contamination and these have been excluded from the analysis. As we have considered only those stars with an E(B−V) colour excess greater than 0.32 magnitudes, the errors introduced in the values of the colour excess ratios due to flux contribution by these various sources in the UBVRI bands, are reduced.

5.3 Anomalous colour excess ratios

The colour excess ratios obtained for Herbig Ae/Be stars (Table 2) can be compared with their mean interstellar values. Our results show that the colour excess ratios for extinction towards these stars deviate from the normal interstellar values systematically. In Figure 5.1, they have been plotted against the effective temperature T_{eff} of the central star for the corresponding spectral type. It can be seen from the plots that the points representing the Herbig Ae/Be stars deviate from the interstellar values depicted by the dashed lines. In the following we discuss the behaviour of the different colour excess ratios in relation with the theoretical analyses by McMillan (1979) and Steenman & Thé (1991).

$E(V-I)/E(V-R)$ As predicted by the theoretical analyses of McMillan (1979) and Steenman & Thé (1991), this colour excess ratio is rather insensitive to grain size, increasing only slightly with increasing mean grain size. It can be seen from Figure 5.1 that most of the points lie close to the interstellar value and the scatter is very small. The mean for the dust around Hernig Ae/Be stars is 1.95 with a dispersion of 0.16. The small dispersion for this ratio and a mean value similar to that for interstellar extinction i.e., 2.05, indicates that the colour excesses observed are indeed due to extinction and that the flux contributions due to non-stellar sources like scattering, thermal dust emission, free-free and bound-free processes etc., are small.

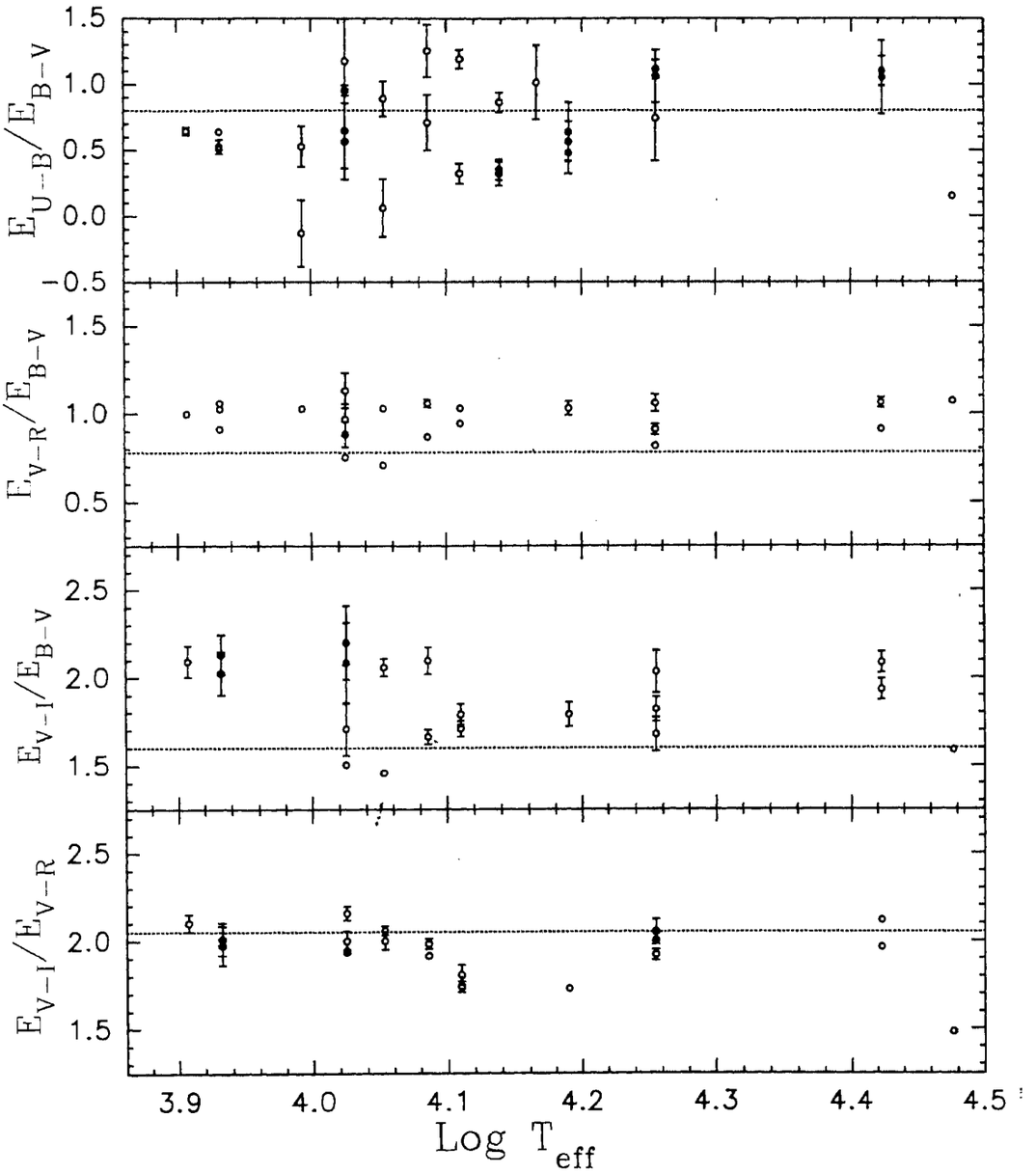

Figure 5.1: *Various colour excess ratios are plotted against Log T_{eff}. The dashed lines indicate the interstellar values for the different ratios. In some cases, the errors are too small to appear on the plot.*

$E(V-R)/E(B-V)$, $E(V-I)/E(B-V)$ These colour excess ratios have mean values that are larger than the interstellar, consistent with a large

dust grain population. The deviations from the interstellar value are large. E(V−R)/E(B−V) has a mean value of 0.97 compared to the interstellar 0.78. The mean of E(V−I)/E(B−V) is 1.87 whereas the interstellar ratio is 1.60.

$E(U-B)/E(B-V)$ The mean value for this ratio is 0.69 which is lower than 0.80, the number expected for normal interstellar extinction, and is interpreted as due to the presence of larger dust grains. There are some stars that lie above the interstellar value which would indicate that the mean grain size is smaller than the interstellar, but the other colour excess ratios for the same stars are inconsistent with such an explanation. There may possibly be two distinct populations of grains in the circumstellar regions of these stars, one with a larger mean dust grain size and the other a smaller mean grain size than the interstellar dust. The plot also shows one star (RCW 34), with a negative value of E(U−B), which may be due to a spectral type misclassification. The star may be of an earlier type than that given in the literature.

The mean colour excess ratios obtained for the dust causing extinction towards Herbig stars indicate a possibly different grain size distribution, with a larger mean grain size. This further implies that the ratio of total to selective extinction R given by $A_V/E(B-V)$ is larger towards these stars. The visual extinction A_v obtained for a star by assuming an interstellar R=3.1 is hence an underestimate. The photometric brightness of the star would therefore also be underestimated. It is to be noted that the extinction determined is the total extinction to the star which includes extinction by intervening interstellar dust grains along the line of sight. The colour excesses are therefore due to interstellar as well as circumstellar dust. To cause the large deviations observed in the colour excess ratios, the dust grains in the neighbourhood of Herbig Ae/Be stars must be significantly larger than the average interstellar dust grain. It should be noted here that for a given star, the characteristics of the dust grains inferred in this analysis corespond to the epoch of measurements. The photometric variability of Hernig Ae/Be stars is usually explained as due to an

obscuration of the central star caused by drifting dust clouds in its immediate neighbourhood. Thus, the anomaly in the dust grain characteristics can vary with the variability of the central star. An inference drawn from photometric measurements made at an epoch of decreased brightness, gives the characteristics of a dust grain population that includes the dust in the obscuring cloud. In any case, the values of colour excess ratios obtained imply the presence of an anomalous dust grain size distribution in the system, as a whole. If the grain size distribution in the circumstellar environment of Herbig Ae/Be stars is a power law similar to that for the interstellar dust ($dn(a) \propto a^{-3.5}da$), then the mean grain size can be increased by increasing the lower cutoff size in the distribution. The results presented here may thus indicate the depletion of very small dust grains around Herbig Ae/Be stars as suggested by Steenman & Thé (1991). Such a grain size distribution also explains the anomalously low extinction observed in the ultraviolet. The larger mean grain size in the circumstellar environments of Herbig Ae/Be stars, can also be attributed to a growth of dust grains in the high density regions of the disk, which may later lead to the formation of planetesimals.

5.4 IRAS Low Resolution Spectra

Low Resolution Spectra for the 9–21 μ range of the infrared region, are available for 17 Herbig Ae/Be stars in the IRAS LRS catalogue (Neugebauer et al 1986) and are presented in Figure 5. 2. Of these 6 stars show 10 μm emission, 4 stars show 10 μm absorption, 4 stars the 11.3 μm unidentified infrared feature and 3 show featureless spectra. The features seem to be correlated with the spectral type of the star and the E(B−V) colour excess towards the star. The spectral types of the stars have been adapted from Finkenzeller and Mundt (1984) and from Finkenzeller (1985). The colour excesses have been computed using intrinsic or unreddened colours of main sequence stars from

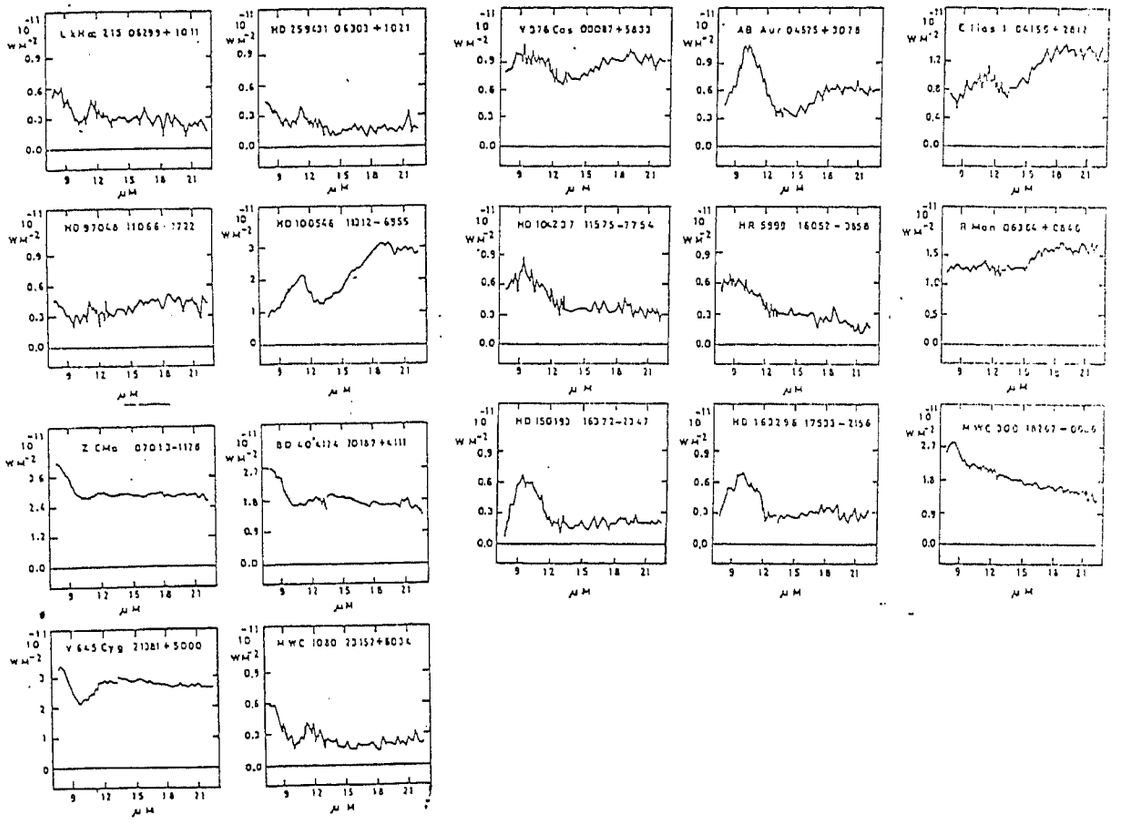

Figure 5.2: *IRAS Low Resolution Spectra in the 9-21 μm range for 17 Herbig Ae/Be stars*

Johnson (1966). The colour excesses, spectral types and IRAS LRS spectral classes of the stars are listed in Table 5. 3. A plot of colour excess, E(B−V) and spectral type of the stars places them into well separated categories, as can be seen in Figure 5.3.

Table 5.3: *Spectral type,* IRAS LRS *classes, and colour excess for the 17 stars*

Star	Spectral type	IRAS LRS classes	E(B−V)
V376 Cas	F0	63	0.64
Elias 1	A0	50	1.50
AB Aur	A0	69	0.14
LkHα 198	B7-B8	80	0.62
HD 259431	B2	80	0.50
R Mon	B0	50	1.38
Z CMa	B/A	31	1.20
HD 97048	B9	80	0.41
HR 5999	A7	23	0.12
HD 150193	A4	69	0.42
HD 163296	A7	69	0.01
MWC 300	B:	13	1.17
BD + 40 4124	B3	31	0.94
V645 Cyg	A0	32	1.10
MWC 1080	B0	72	1.70
HD 100546	B9	82	0.09
HD 104237	A0	25	0.27

- The 10 μm silicate band is seen in absorption *only* for stars with a spectral type earlier than $\sim$ B9-A0 *and* an E(B−V) colour excess $\geq$ 1.0.
- The 10 μm silicate emission band is observed *only* for stars of a spectral type later than $\sim$ A0 and with low colour excesses, i.e., E(B−V) $\leq$ 1.0.
- The 11.3 μm unidentified emission feature is present for early type stars with low colour excesses, (E(B−V) $\leq$ 1.0).
- Three early type stars show featureless spectra.

5.5 Chemical composition of dust

There seems to be a clear demarcation between the stars with different spectral types and colour excesses. A possible explanation may be suggested on the basis of the chemical composition of the dust around the stars as well as its spatial distribution. Spectra of earlier type stars do not show the 10 μm

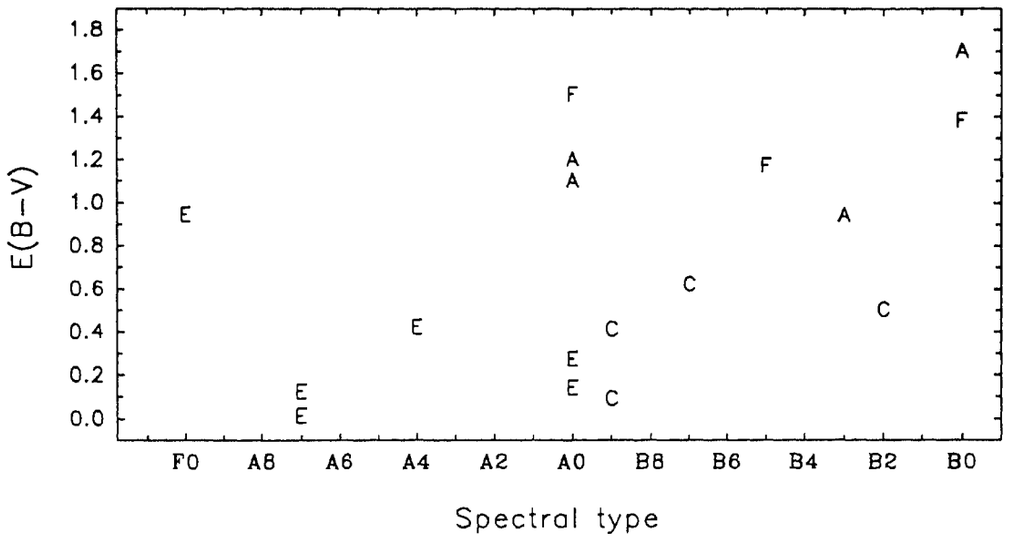

Figure 5.3: *The colour excess E(B−V) and spectral type of the stars are indicated in the figure. The symbols represent the spectral feature and have the folowing meaning — **A**: 10 μm absorption; **E** : 10 μm emission; **F**: featureless spectra and **C**: 11.3 μm feature.*

emission band, indicating the absence of hot dust in their close neighbourhood. The dust in their immediate vicinity is probably destroyed or blown away due to a higher radiation pressure and stronger winds. Thus along the line of sight towards these stars, only the cool outer dust is present which causes absorption at 10μm, against the continuum background. But however, the PAH (Polycyclic Aromatic Hydrocarbon) component of interstellar dust, is extremely stable and survives even under these harsh conditions. The 11.3 μm feature, seen in 4 early type stars with low extinction, is attributed to emission from PAHs. PAH emission is not seen in late type stars, as ultraviolet radiation is required for the excitation of the PAH molecules, which later deactivate through IR vibrational fluorescence (IRF). The 10 μm silicate band is in emission for late type stars, with a spectral type later than $\sim$ A0. This indicates the presence of optically thin, hot dust in the close environments of these stars, and probably implies that they do not effectively destroy the dust

in their immediate surroundings. It should be noted that there are no late type stars in the sample with large E(B−V) which may be a selection effect. Three early type stars with large excesses show featureless spectra. The spectra can be interpreted as continuum emission by an optically thick disk. The large E(B−V) may be caused by obscuring dust clouds along the line of sight to the star, which do not obscure the disk.

5.6 Conclusions

We have analysed photometric data in the optical bands for Herbig Ae/Be stars and obtained the colour excess ratios, in order to study the wavelength dependence of extinction towards these young stars. These values have been compared with the theoretically expected behaviour of the colour excess ratios as a function of grain size. The ratio E(V−I)/E(V−R) is fairly constant as expected which seems to indicate that the observed colour excesses are largely due to extinction. E(V−R)/E(B−V) and E(V−I)/E(B−V) are larger than that for the mean interstellar extinction law whereas E(U−B)/E(B−V) is lower, consistent with a grain size distribution having a large mean grain radius. Grain growth and depletion of small grains are two possible mechanisms that can lead to a large average grain size of a grain size distribution. The latter mechanism provides a possible explanation for the low extinction observed towards these stars in the ultraviolet region. Grain growth and aggregation in the high density environments of the circumstellar disks may possibly lead to the formation of planetesimals around stars.

The infrared spectra of Herbig Ae/Be stars show dust spectral characteristics which seem to depend on the spectral type of the central star. It is inferred that early type stars, i.e., stars with a spectral type earlier than $\sim$ A0, destroy the dust in their immediate neighbourhood and therefore do not show the 10 μm silicate band in emission. This band is seen in absorption

for those stars which have large E(B−V) colour excesses, and hence greater extinction, due to colder dust situated farther out from the stars. The PAHs being more stable are not destroyed and cause the 11.3 μm feature in early type stars with smaller E(B−V)s. The later spectral type stars do not destroy dust as effectively and their spectra have the 10 μm emission band.

References

Assousa G.E., Herbst W. & Turner K.C., 1977, ApJ, 218, L13

Bastian U. & Mundt R., 1979, A&AS, 36, 57

Bergner Y.K., Kozlov V.P., Krivtsov A.A. et al., 1988, SvA, 28, 313

Bergner Y.K. et al., 1990, Astrophysics, 32, 23

Bessel M.S., 1979, PASP, 91, 589

Bhatt H.C., Gorti U., 1993, BASI, 21, 541

Breger M., 1974, ApJ, 188, 53

Bibo E.A. & Thé P.S., 1990, A&A, 236, 155

Bibo E.A. & Thé P.S., 1991, A&AS, 89, 319

Bibo E.A. & Thé P.S., 1992, A&A, 260, 293

Catala C., 1983, A&A, 125, 313

Cohen M., 1973, MNRAS, 161, 105

Cohen M. & Schwartz R.D., 1976, MNRAS, 174, 137

Cohen M. & Kuhi L.V., 1979, ApJSS, 41, 373

Dibai E.A., 1969, Astrophysics, 5, 115

Finkenzeller U. & Mundt R., 1984, A&AS, 55, 109

Finkenzeller U., 1985, A&A, 151, 340

Goodrich R.W., 1986, ApJ, 311, 882

Gorti U., Bhatt H.C., 1993, A&A, 270, 426

Grinin V.P., Kiselev N.N., Minikulov N.Kh. et al., 1991, Ap&SS, 186, 283

Herbig G.H., 1958, ApJ, 128, 259

Herbig G.H., 1960, ApJSS, 4, 337

Herbig G.H. & Rao N.K., 1972, ApJ, 174, 401

Herbst W., 1975, AJ, 80, 212

Hillenbrand L.A., Strom S.E., Vrba F.J., et al. 1992, preprint

Hu J.Y., Thé P.S. & de Winter D., 1989, A&A, 208, 213

Humphreys et al., 1980, ApJ, 237, L17

Jain S.K., Bhatt H.C., 1995, A&AS, 104, 399

Johnson H.L., 1966, ARA&A, 4, 193

Kilkenny D., Whittet D.C.B., Davies J.K. et al., 1985, S. African Astron. Obs. Circ., 9, 55

Marraco H.G. & Rydgren A.E., 1981, AJ, 86, 62

McMillan R.S., 1979, ApJ, 225, 880

Mendoza E.E., 1968, ApJ, 151, 977

Neugebauer G. N. et al, 1986, A&ASS, 65, 607

Petrova N.N. & Shevchenko V.S., 1987, SvA Lett., 13, 289

Racine R., 1968, AJ, 73, 233

Reipurth B., 1983, A&A, 117, 183

Savage B.D. & Mathis J.S., 1979, ARA&A, 17, 73

Shevchenko V.S. & Yakubov S.D., 1989, SvA, 33, 270

Sorell W.H., 1990, ApJ, 361, 150

Steenman & Thé P.S., 1989, Ap&SS, 161, 99

Steenman & Thé P.S., 1991, Ap&SS, 184, 9

Strom K.M., Strom S.E., Breger M. et al., 1972, ApJ, 173, L65

Strom S.E., Strom K.M., Yost J. et al., 1972, ApJ, 173, 353

Thé P.S., Tjin a Djie H.R.E., Bakker R., et al., 1981, A&AS, 44, 451

Thé P.S., Felenbok P., Cuypers H. & Tjin a Djie H.R.E., 1985, A&A, 149, 429

Tjin a Djie H.R.E & Thé P.S., 1978, A&A, 70, 311

Tjin a Djie H.R.E., Remijn L., & Thé P.S., 1984, A&A, 134, 273

Voshchinnikov N.V., 1990, Astrophysics, 30, 313

Vrba F.J., Schmidt G.D. & Hintzen P.M., 1979, ApJ, 227, 185

Whittet, D.C.B. et al., 1983, A&A, 123, 301

Wolf & Stahl, 1986, IAU Symp.116, 248

Yamashita T., Sato S., Nagata T. et al., 1989, ApJ, 336, 832

Chapter 6

Conclusions

The previous chapters have detailed the research carried out within the scope of this thesis work. The thesis has dealt with a study of interactions between ambient cloud material and protostars in star-forming regions. Star formation in molecular clouds is the result of a complex interplay among various physical processes, with the physical state of the system being continually re-defined through a host of interactions between the clouds and newly formed stars. Young stars play a major role in the evolution of the cloud, primarily through their radiative activity and in the form of stellar winds and outflows. Massive stars explode as supernovae while still embedded in the cloud, injecting huge amounts of energy which may even disrupt the cloud. The formation of the first generation of stars in a cloud alters the initial conditions in the cloud. It affects subsequent star-forming activity by both *inhibiting* further star formation through injection of kinetic energy, and *promoting* it via shock compression of gas through outflows and winds which act as triggering mechanisms. Protostellar effects on cloud gas also influence molecular cloud structure, driving holes, shells and possibly filamentary structures in the gas. Most of these interactions are radiative in nature, and have been studied in considerable detail so far. The effects of the cloud gas on the young stars have, on the other hand, received relatively less attention, though they are probably equally important.

Star-cloud interactions have formed the base of this thesis, with more emphasis laid on an investigation of the effects of the star-forming environment on the dynamical evolution of protostellar systems. Dynamical effects of the ambient cloud gas on protostellar clumps and protostar clusters have been analysed. Binary systems consisting of protostars remain embedded in the cloud, prior to gas dispersal, for $\sim 10^{5-6}$ years. Early dynamical evolution of the orbital parameters of protostellar binaries due to the molecular cloud gas is studied. Finally, some properties of circumstellar dust around the young, pre-main-sequence Herbig Ae/Be stars are inferred from observational data. The results of the above analyses and the conclusions drawn are summarized below.

Gas drag due to dynamical friction by the surrounding medium on clumpy structures in molecular clouds significantly affects their motion. Molecular clouds have a hierarchical structure, down to the scale of nearly stellar-mass clumps, that are the direct percursors to young stars when star formation sets in. The dynamics of these protostellar clumps have been studied in the presence of the ambient gas which provides a source of gravitational potential, and impedes the motion of the clumps through drag forces. Dynamical friction and accretion-induced drag provide the agents of dissipation in our cloud model, with the former being more dominant. The deceleration caused is proportional to the mass of the moving object and this results in more massive clumps being subjected to greater drag. Lower mass clumps are also decelerated by a force that is smaller in magnitude in proportion to their mass. The acceleration due to gravity, being independent of mass, the difference in dynamical evolution of clumps with differing masses is determined by the difference in the drag forces acting on them. Higher mass clumps lose energy and angular momentum at a higher rate and spiral in towards the centre of the cloud on lower-energy orbits. Less massive clumps occupy average radial positions further away from the centre of the cloud. Thus, a spatial segregation of mass is established in the clouds, with the more massive clumps near the centre of the cloud and lower

mass clumps distributed throughout. The mass segregation caused by the effects of dynamical friction is established much earlier than that by equipartition in N-body systems, for parameters typical of star-forming molecular clouds. The timescale for mass segregation due to drag is found to be of the order of ~ 1 Myr, whereas relaxation timescales are of the order of a few tens of Myrs. Mass segregation is more pronounced and faster in denser clouds, as the drag is directly proportional to the density of the cloud. Variations in clumps mass spectra and the density profile of the interclump gas have little effect on the dynamics, and do not affect the timescale of segregation in the cloud system. The total cloud mass is distributed in the clumps and the ICM, and the relative fractions of mass in the two components to some extent influences the dynamics. The timescales for mass segregation, however, do not significantly change, within the ranges considered in this analysis. Along with spatial segregation of mass, some velocity segregation of mass is also observed, though it is not as pronounced. The results obtained provide a possible explanation for the mass segregation observed in many young open clusters. These clusters are often found to be too young to have dynamically relaxed and for equipartition of energy to have taken place. Examples of young clusters that show evidence for mass or luminosity segregation are NGC 2071, the Trapezium cluster and NGC 2024. The mass segregation observed can be explained as the result of the dynamical evolution of the protostellar clumps that formed the cluster. Star-forming clouds are thus expected to form their most massive stars at the centre of the cloud, assuming that more massive protostellar clumps give rise to the more massive protostars in a cluster.

The protostellar clumps in the cloud, become gravitationally unstable and collapse to form a protostar cluster at a later stage of evolution. The early dynamical evolution of a proto-star cluster while it is still embedded in the molecular cloud was investigated numerically. The star formation process, being intrinsically inefficient, is expected to leave behind remnant clumps. These

clumps have either failed to form stars, or are clumps whose protostars have drifted out or been ejected by dynamical encounters. The dynamical evolution of a protostar cluster in the presence of these massive clumps has been studied, and it is found that the dynamics of the massive clumps influences the motion of the lower mass protostars. The massive clumps segregate to the centre of the cloud under the influence of dynamical friction drag as seen earlier, and this causes an accelerated relaxation of the entire system. The formation of a dense central region results in a scattering of the protostellar orbits, some of which gain enough energy during encounters to be ejected out of the system. The overall effect on the system is to form a dense core of clumps, and an expanded halo of low mass objects. The formation of a bound open cluster from a protostellar cluster, is determined by the relative fraction of mass in stars and gas, in the region local to the star-cluster. The expansion of the protostar system during its early evolution, may thus have implications for the formation of bound clusters. The ejection of low-mass stars is proposed as an explanation of the observations of T Tauri stars that appear to be far from active star-forming sites in a cloud, and are in regions devoid of dense gas. ROSAT observations of star-forming regions have revealed the presence of large extended halos of low-mass stars around molecular clouds, as also obtained in our simulations of the dynamics of embedded protoclusters.

Ambient gas continues to exert an influence even at later stages of protostellar evolution. The formation of binary and multiple systems appears to be the more common outcome of star formation than single stars, and dynamical friction in binary systems was next studied. Protostellar binaries are surrounded by the parent molecular cloud gas for a significant fraction of their early evolutionary phase, before the gas is dispersed. The gas drives orbital evolution of the binary system, through dynamical friction and this has been investigated in considerable detail. The general effect of drag on protostellar binaries is the loss of orbital angular momentum and energy. The orbits evolve to those of

higher binding energies, as the component protostars lose energy due to drag and spiral inwards. The evolution of orbits is, therefore, towards shorter separations and also higher eccentricities. The co-efficient of the dissipative drag is velocity dependent, decreasing for higher velocities. The angular momentum loss rate is lower than that of energy, which tends to make the orbits more eccentric with time. Formation theories for binaries tend to produce those with large separations more easily than short-period systems. The decay of orbits to shorter periods is proposed as an alternative mechanism for the formation of close binaries, from initially longer period binaries. Drag due to ambient gas has further implications for binary orbit evolution, due to its velocity dependent nature. Close binaries have higher orbital velocities and hence are dragged down on much longer timescales than the lower velocity long period systems. The evolution of a group of binaries with a distribution of separations, thus has different members evolving on different timescales depending on their separations. Statistically generated samples of binary systems were evolved with two functional forms for the initial distribution, and it is found that a peak in the frequency distribution with period is obtained in both cases, as seen observationally.

Finally, dust in the circumstellar environments of a class og young stellar objects, the Herbig Ae/Be stars, was studied using available photometric and spectroscopic data in literature. The results indicate that the dust in these environments differs in its properties from the average interstellar dust. The colour excess ratios in different photometric bands were found to be anomalous, and imply a larger mean size for the dust grain in the neighbourhood of these stars. This could be due to a depletion of small dust grains near these stars, and may also indicate the growth of dust grains in the high density environments of circumstellar disks. Low Resolution Spectra in the 9–21 μm wavelength range obtained by the Infrared Astronomical Satellite were examined where available to determine the nature of the dust grains. The infrared spectra of the Herbig

Ae/Be stars show dust spectral characteristics which appear to depend on the spectral type of the central star. Early-type stars are inferred to destroy the dust in their immediate environments, whereas later spectral type stars are not as effective in dust grain destruction.

This thesis has thus dealt with some molecular cloud-protostar interactions. The dust grain characteristics in circumstellar environments were inferred from the radiated stellar energy at different wavelength bands and features in the infrared spectra of pre-main-sequence stars, with a view to understand the effects of young stars on their immediate environment. The dynamical effects of the molecular cloud gas on various stages of protostellar evolution were studied during the course of this thesis. The forming star remains embedded in the cloud for about $\sim$ few 10^6 years and is expected to be significantly affected by the presence of the surrounding gas. Interactions of a diverse nature are likely between protostars and the cloud. The predominant influence of the cloud is probably its gravity, as it is typically orders of magnitude more massive than the young stars. The dynamics of protostars are therefore governed by the cloud potential, and we have studied mainly the gravitational aspects of the cloud-star interactions. Dynamical friction is a drag force that is gravitational in origin and is seen to affect the evolution of protostars both at the protostellar clump stage and at the pre-main-sequence stage of evolution. Apart from the drag due to the smooth component of cloud gas, the gravitational interactions between the clumps and young stars was also studied. The models considered during the analyses were, however, restricted in nature. Though the description was adequate for an understanding of the predominant physical effects, more realistic studies are required for a complete picture. Principally, collisions between clumps need to be taken into account in the N-body analyses, and magnetic fields are perhaps important in governing the dynamics in clouds. A more refined analysis of the orbital decay of protostellar binaries, has to consider the fact that protostars are mostly formed in clustered

environments and encounters with other stars and clumps may affect their orbital evolution. Other possible improvements include a self-consistent analysis of the entire system, where the ambient gas, considered static here, is also subject to dynamical evolution.

The environment and its prevailing physical conditions during the early stages of a star are thus seen to have a profound impact on its evolution. The processes studied here are by no means exhaustive, even if interactions exclusively of a gravitational origin are considered. To acquire a comprehensive view of the consequences of cloud-star interactions, and to assess the importance of the various physical processes in furthering present-day understanding of star formation, more in-depth analyses on these and other aspects of environmental influences on young stars need to be made. Ram pressure due to gas acting on protostars and their circumstellar disks, accretion processes, collisional encounters between clumps with embedded protostars, dynamical evolution of protostellar disks in a cloud containing massive clumps, are a few other interactions that are possible, notwithstanding those that are mediated by magnetic fields, shocks, turbulence and other physical processes. Studying interactions between young stars and the ambient gas and the factors determining their evolution is perhaps critical towards an understanding of the star formation process.